Chapter 1 Introduction

1.1 General Background

The ancient port of Ostia, near Rome, was established in 620 BC by King Ancus Marcius. All the wealth of the Roman conquest was sent to Ostia, and legions of Roman soldiers were dispatched overseas from this invaluable port. The city, which in its peak was one of the most important in the Roman Empire, became a virtual ghost town during the fifth and sixth centuries AD because the Tiber River filled with too much silt to allow heavy ship traffic.

Although the above represents one of the more historically spectacular consequences of sedimentation, today's ports rely heavily on dredging activities. A recent report by the U.S. Army Corps of Engineers calculates that a total of 268,465,100 cubic yards of sediment was dredged under the Corp's jurisdiction in the year 2001, at a total cost of $867,760,200[1]. During the same year in England and Wales, capital and maintenance dredging led respectively to the licensing for ocean disposal of 2,827,146 tonnes and 15,692,561 tonnes of dredged material[2]. This equates to roughly 16,148,574 cubic yards in total. A much larger quantity of material is dredged about one year per decade. In 1999 for instance roughly 29 million cubic yards were licensed for disposal at sea, at costs running over 100 million pounds. These quantities do not include material which has been disposed without a license, or that which has been disposed of on land, the latter of which includes nearly all of the material dredged from the Thames River and its tributaries.

Clearly, any reduction in the amount of dredging required could reduce costs to governments and port authorities. As a result there have been several multinational and cross disciplinary projects to understand and model the siltation patterns in natural estuaries. It has been found that aggregation, or flocculation, of particles by electrostatic

[1]http://www.iwr.usace.army.mil/ndc/dredge/dd01cos2.htm. These data include all costs associated with dredging: engineering and design, surveys, placement, by the Corps. They do not include private projects. Pers comm. M.R. Pointon, USACE.

[2]Tim Hanham, Marine Consents & Environment Unit. DEFRAS, UK.

interactions has consequential relationships with sedimentation and consolidation processes. For example turbidity maxima and shoals in estuaries are both formed where flocculation leads to increased settlement of suspended material (Nichols and Biggs 1985). Indeed, it is generally accepted that there would be very little deposition and accumulation of fine-grained material, if the suspended fine sediment particles were not coagulated as flocs or aggregates.

A recent and one of the largest projects aimed at predicting sedimentation patterns is the European funded MAST III COSINUS project. The models produced by this project required both field testing and lab testing to determine the behaviour of natural sediment. Of utmost importance to the models is the ability to take into account both the flocculation process and the development of strength in a consolidating bed. The suspended flocs, it is suggested, may have an effect on the bed structure, which will have have an effect on the consolidation, the erodibility and the resuspension of sediment. According to Partheniades (1965) the bed in an estuary ranges from a loose honeycomb state to a dense compact one. Evidence for floc structures in soil samples has been obtained using scanning electron microscopy (eg. Bennett *et al.* 1991). However, quantitative research into the influences that flocculation conditions have on the strength and structural properties of the bed is scarce.

Along with understanding natural estuarine sedimentation patterns, a specific need for research comes from the disposal of dredged material in subaqueous disposal facilities. A "scow"cubic yard is a yard of dredged material as it sits in a scow after being removed from the bottom. It can be from one-fifth to one-third more than a "survey" cubic yard by the time it is processed. Furthermore, when this material is pumped into a subaqueous confined disposal facility the particles will flocculate as they settle which may influence the behaviour of the bed they form. It may take years for the material to even approximate its original consistency, affecting capitalization costs of these projects. There is a clear need for understanding and predicting the volume that disposed material will occupy.

There are also other industrial applications which require an understanding of how flocculation affects bed properties. In the sewage treatment and water purification industries the 'dirty' water is stirred to enhance flocculation, allowing the large aggregates to settle to a sludge cake and be taken away to landfills or used as fertiliser. Here it is important to create both large flocs for efficient settling, and to create compact beds for efficient removal. In the ceramics industry, aggregation in moulding clays leads to flaws in the articles that are being formed (green bodies), thus there is considerable interest in stemming aggregation. On the other hand, there is also a growing effort in manufacturing industries toward the possibility of precisely controlling the flocculation of ceramic particles so that these green bodies can be manufactured directly from sedimentation with different sedimentation conditions leading to a precise variation in their structure and density (Lewis 2000). Other areas in which flocculation and consolidation play a significant role include the extraction of metals from ores, and the bulking of the surface of paper with clay to enhance its quality.

Although flocculation and consolidation have been studied extensively in the above fields as separate processes, very few studies have been conducted to relate the processes of flocculation to the strength and structure of the beds (sludges, filter cakes, green bodies, etc) which are formed by the flocs, particularly with natural sediment. Van Leussen (1988) and references cited therein, recognizes that the seabed is formed mainly by deposition of aggregates and its properties must therefore be governed by the structure of the settled aggregates, their intergrain cohesive strength and their susceptibility to crushing or particle rearrangement with depth of overburden. In other words, the aggregation process may determine the erosional and structural properties of the consolidating bed.

The aim of the research described in the following pages is to provide data and interpretations regarding the relationships between flocculation conditions and bed properties. Much of the data from this research has been supplied in a practical form to the EU MAST III COSINUS project for modelling the sedimentation, consolidation and erosion of estuarine sediments. It is freely available to participants of that project, and to

interested parties. In this thesis the data is closely examined in terms of sizes, shapes, concentrations, settling velocities, densities and fractal dimensions of the flocs; and densities, void ratios, effective stresses, intrinsic properties, and strengths of the soil beds.

1.2 Thesis Outline

Chapter 1 introduces the subject, discusses the relevance and areas of application of the research and defines the deficiencies that exist in the current knowledge. A significant portion of Chapter 1 is devoted to literature reviews of flocculation and consolidation processes.

Chapter 2 describes in detail the equipment that has been designed or modified specifically for the research. This equipment includes a video imaging and online analysis system, a computer controlled sedimentation system and bender element shear wave measurement apparatus, the ISIS bed erosion device and a pore pressure measuring system. Other existing equipment that has been used, such as an x-ray for density measurements, is also described in Chapter 2.

Chapter 3 reports on the sediment properties and the experimental programmes. The sediment has come from four sources. Mud from the Tamar Estuary has been used in most of the experiments since it was simultaneously being studied in detail by the COSINUS project (see for example Dyer (1999)). Other muds used are from Dibden Bay, Weston-Super-Mare and Combwich, which had all previously been used in experiments at Oxford. The experiments mainly consisted of altering the concentrations of mud in the settling columns, however some experiments also tested the effects of salinity and turbulence.

Chapter 4 discusses the results of the floc measurements. The flocs are described in terms of their shapes, sizes and other characteristics under different conditions. Focus is placed on the development of floc size distributions with increasing column concentrations. Results of particle velocity analyses are then used to describe the possible onset of hindered settling.

Chapters 5 and 6 discuss the results of the external and internal bed measurements. Specifically, Chapter 5 reports on the visible properties of the bed and the settlement of the

bed water interface. Chapter 6 reports the results of the x-ray density, pore pressure, bender element and shear strength tests. These chapters report wherever possible the observations made about the beds that relate specifically to their formation by flocs. Chapter 6 concentrates on effective stress - void ratio relationships, and on creep processes.

Chapter 7 takes the experiments one step closer to the *in situ* conditions by investigating the erosion properties of the beds, combined with their biological properties. A combination of x-ray measurements and imaging techniques are used to describe how the top surface of the bed is influenced by biological factors.

Chapter 8 then brings together the results of the three previous chapters to discuss the effect that floc properties have on bed properties. Several mechanisms are looked at which help to address observations made in Chapters 5 and 6 about the structure of the beds. There is a section on how deposition conditions affect the beds in terms of intrinsic properties of the sediment, and a further section on how calculations for both flocs and beds compare.

Chapter 9 outlines the main findings and makes recommendations for further research.

1.3 Literature Reviews

In order to cover adequately the processes taking place between flocculation and consolidation both of these topics are reviewed. Features of flocculation which are examined include the forces leading to flocculation, collision mechanisms, the floc structure types, and the influences of environmental conditions. Consolidation is reviewed in terms of the current theories of effective stress, creep, and bed stiffness and strength.

1.4 Flocculation review

A half century ago Suzuki and Kato (1953) reported on their observations from a submersible of what they termed ‘marine snow’. Since then many scientists have noted that particles suspended in oceans are nearly entirely in the form of clustered primary particles of biogenic, terrigenous, anthropogenic and other sources (Alldredge and Gotschalk 1988; Droppo 2001). These clusters are referred to as flocs, floccules, pellets,

agglomerates, aggregates, marine snow, streamers and stringers. These clusters are herein referred to as flocs or aggregates.

Much of the current knowledge about flocculation comes from the water treatment industry. The efficiency of the whole water treatment plant lies in its ability to cause the particles to flocculate effectively, and to create a compact sludge for removal. Normally this is achieved by adding coagulants (flocculants) and through aggressive mixing. These conditions can not be equated to natural estuarine conditions, nonetheless the research methods and information provided by these studies are extremely useful. Reviews regarding flocculation in estuaries are given by Dyer (1985) and van Leussen (1988)

DVLO Theory

In order to understand the geochemistry of the flocculation process, it is necessary to understand the composition and structure of clay minerals. Two basic crystalline units form clay minerals; silicon-oxygen tetrahedra (Figure 1.1a), and aluminum or magnesium octahedra (Figure 1.1b). The silicon oxygen tetrahedra combine to form a 'silica' sheet. The aluminium or magnesium octahedra combine to form a second sheet, if the central metal is aluminium then the sheet is a gibbsite sheet, if the central metal is magnesium then it is a brucite sheet. The balance of valences in the silica sheet require that the tip of each tetrahedron is connected to a negatively charged atom, which is conveniently the hydroxyl of the octahedron.

A series of these sheets make up a clay 'platelet'. Each of these groupings is held together by ions, potassium in the case of illite (Figure 1.2b) and water in the case of montmorillonite (Figure 1.2c). On the face of each platelet there is normally a negative charge due to the exposed oxygen atoms in the broken bonds of the crystal lattice. Additionally, negative charges will result from isomorphic substitution of positively charged cations of a low valency within the lattice for other principal structural cations of a higher valency. At the particle edge the charge is generally positive due to protonation of the broken bonds of the silica tetrahedra (Dyer, 1985). The unsatisfied charges, on both

face and edge, will be balanced by the sorption of ions. These ions are the potential-determining ions from the surrounding fluid (pore water), which determine the surface charge on clay minerals.

The overall particle charge is normally negative for clay minerals. Because of this a series of negatively charged layers is built up around individual clay particles (Figure 1.3). Gouy and Chapman independently described the distribution of charge and potential in the solution as a function of distance from the surface. Their unified theory is based on a number of simplifying assumptions (eg. Shaw, 1980). The negative charge induced by the clay particle attracts positive ions, particularly to layers near the particle surface. Stern improved the Gouy-Chapman theory by accounting for the finite size of ions and the specific adsorption of ions to the clay surface, in what is now termed the Stern layer.

Water is a polar compound due to the distribution of H^+ ions and electrons on opposite ends of the molecule from one another. Water is electrically attracted toward the surface of clay particles by three methods: 1) attraction between the negatively charged faces of clay particles and the positive dipoles of water; 2) attraction between cations (positive ions) surrounding the negative clay surface and the negatively charged water dipoles; and 3) hydrogen bonding between the hydrogen atoms shared by oxygen atoms in the clay and the oxygen atoms in water.

The electrically attracted water that surrounds the clay particles, including the attracted positive ions, comprises the electrical double layer (EDL). This is the area contained within the concentric circles in Figure 1.3. The plastic properties of clayey soils are due to the existence of double-layer water. Yariv and Cross (1979) give a detailed description of the structural complexities of water in the space between clay platelets. The outer layer of the EDL is the diffuse layer in which positive ions are attracted to the negative platelet faces, and negative ions are attracted to the positive platelet edges, but as the platelets hold a net negative charge the attraction of positive ions (cations) is the dominant process.

Derjaguin and Landau, and Verey and Overbeek, in 1948, independently developed a quantitative theory for the stability of lyophobic colloids[3], known as the DVLO theory. A concise review of this theory is given by Schramm (1996). It was developed to account for the observation that colloids coagulate quickly at high electrolyte (salt) concentrations, and slowly at low concentration, with the transition from one to the other known as the critical coagulation concentration. The DVLO theory accounts for the energy changes that take place when two particles approach each other and involves estimating the potential energy of attraction versus interparticle distance, and the potential energy of repulsion versus distance. These quantities are shown in Figure 1.4 and described below.

When clay particles are close to and parallel to each other, and their electrical double layers overlap, the negative-negative repulsion (V_R) between their surfaces decreases with the inverse of distance (Figure 1.4 top curve). There is a very slight counter-force on the ions attracted to the clay surfaces, which is the osmotic force, or the tendency of ions to diffuse randomly throughout the solution owing to their thermal energy. This force is considered unimportant for the flocculation of clay particles.

In addition to the repulsive force, there is an attractive force, which is largely attributed to Van der Waal's forces. The attractive force between two flat parallel surfaces decreases with the inverse cube of distance (Figure 1.4 bottom curve). This force is also dependent upon the chemistry of the pore fluid, but for water generally does not change with minor changes in the water constituents.

The forces of attraction and repulsion between the particles vary at different rates with respect to the distance of separation, leading to a net force as shown in Figure 1.4 (middle curve). Where the particles become close enough the net force between them is attractive and the particles will form aggregates, or flocs.

---

[3] The term colloid, used correctly, refers to nanometre sized particles in a dispersion, but colloid theories are commonly applied to larger particles such as clay platelets.

The ionic composition of the porewater is very important. An increase of counter ion concentration or an increase of counter ion valence (ie. salt concentration or composition) in the double layer both act to neutralize the negative particle surfaces close to the particle. Therefore the double layer shown in Figure 1.3 is depressed, so that the repulsive potential decreases according to the Gouy-Chapman theory. This shifts the repulsion curve in Figure 1.4 downward, and allows clay particles to be attracted to one another more strongly and at further separation distances.

Collision Kinetics

Two principal factors determine the rate of aggregation of particles in a suspension: the frequency of particle encounters and the probability that the particles adhere to one another after these encounters.

The number of combined collisions occurring per unit time and per unit volume between two size classes is given by (van Leussen 1988):

$$N_{ij} = a \cdot K(d_i, d_j) n_i n_j \tag{1.1}$$

where d_i and d_j are the diameters of the two size classes i and j, n_i and n_j are the number concentrations (volume^{-1}) of the two size classes, $K(d_i,d_j)$ is the collision frequency function, and *a* is a stability factor

The collision frequency function $K(d_i,d_j)$ is specific for a particular mechanism and depends on the sizes of the colliding particles and on properties of the system such as temperature and pressure. The stability factor, *a*, gives the percentage of effective collisions, that is the percentage of collisions in which two units form a single unit. Rapid flocculation occurs in a completely 'destabilized' suspension, which has a stability factor of 1. Increasing the salinity from 0 to only a few ppt tends to destabilise natural mud suspensions by the DVLO theory described above, so that flocculation occurs.

Equation 1.1 simplifies the flocculation process by making use of two factors, the rate at

which particles collide, and the rate at which they adhere to one another upon collision. The collision process can be further broken down into at least four different mechanisms (Dyer 1985; van Leussen 1988). These are Brownian motion (perikinetic flocculation), velocity gradients within the suspension liquid (orthokinetic flocculation), differential settling of the suspended particles, and inertial encounters. Each of these processes leads to different floc structures, and three are reviewed here.

Brownian motion (perikinetic flocculation)

Perikenetic flocculation is caused by bombardment of the flocs by the thermally agitated water molecules, which can cause the flocs to come into close proximity. Perikinetic flocculation, caused by Brownian motion, is only effective at very high particle concentrations and for particle sizes less than about 0.5 ：m to 2 ：m (Dyer 1985). Aggregates formed by Brownian motion have a ragged structure, are weak and easily dispersed by shearing or easily crushed in a deposit.

Velocity Gradients (orthokinetic flocculation)

Orthokinetic flocculation due to a water column velocity gradient will occur if particles are spaced less than the sum of their radii in zones of the liquid having shear layers. For flocs formed under orthokinetic conditions, there is a critical shear value above which they are torn apart leading to a maximum floc size. The flocs have relatively higher strength than other types of flocs and tend to be spherical. Orthokinetic flocs are large under low shear conditions, and small under high shear conditions (Dyer 1985). Orthokinetic flocculation is perhaps the most important in the mixing zones of estuaries. Van Leussen (1988) and references therein make calculations with the collision frequency factors for the various types of flocculation. For grainsizes larger than 0.5 to 2 ：m, orthokinetic flocculation becomes more important than perikinetic flocculation, and at a particle diameter of 10 ：m orthokinetic flocculation is already over 100 times greater than perikinetic flocculation.

Differential Settling

Differential settling rates of large particles as compared to smaller particles leads to these

larger particles growing as they sweep past smaller ones. Differential settling is effective during low current velocity, and with large particles (Dyer 1985). There is little stress on aggregates forming under conditions of differential settling and therefore the aggregates are ragged, weak and have low density. In estuaries, differential settling becomes dominant in slack water conditions (van Leussen 1988).

It is clear from equations representing each of the flocculation processes given by Dyer (1985) and Van Leussen (1988) that the number concentration of particles, n, is an important parameter affecting the frequency of particle encounters. Also important are the system energy and the particle size.

Floc characteristics with consequences to the bed

Floc Composition and Ordered Structure

The floc framework is constructed of a combination of minerals and organic matter. According to Bache *et al.* (1997) the floc interior appears to be filled with a gel promoted by a high concentration of particles derived from the free precipitate. These gel particles form weak coagulation structures which contribute to the overall cohesion of the floc. In nature the framework and interior may also contain its own living microcosm. Because flocs are often found under conditions of agitation the most probable floc shape is a sphere (or elongated spheroid), the shape most capable of resisting deformation by surface forces.

An important aspect of the aggregate is the ordered structure illustrated in Figure 1.5. These orders were first proposed by Michaels and Bolger (1962), and result in properties at several levels. A terminology for these orders was has been developed which includes, in increasing order, primary particle - particle aggregate (pa) - particle aggregate aggregate - particle aggregate aggregate aggregate and so on (Firth and Hunter 1976; van de Ven and Hunter 1977; Krone 1986). The particle aggregates, otherwise known as flocculi, are the basic structures and formed under the highest shear rate at which the system was ever subjected. The average number of flocculi in a floc depends on the shear rate. With increasing aggregate order the densities diminish rapidly toward the density of the liquid,

and the shear strengths decrease rapidly. Generally flocs are restricted to four orders of aggregate structure.

It has been mentioned that clay particles are plate-shaped and can carry both positive and negative charges at the same time, on different parts of the particle (edges and faces). This heterogeneous charge distribution leads to various modes of clay platelet orientations. Figures 1.6a to d show that, even at the primary aggregate level, there are several modes of aggregation. At higher orders the different modes can be combined in different ways to form variations of the high order structures. Figures 1.6e to g show some combinations of the face-face tactoids of Figure 1.6b. The various modes and tactoid configurations depend on the clay mineralogy, solution pH, solution ionic composition, and solution ionic strength. These geochemical properties affect the interaction of clay platelets, the number of platelets per tactoid and the overall structure of tactoid aggregation.

Floc density

As briefly mentioned above, the density of the flocs decreases rapidly with increasing aggregate order, or floc size. This has very important practical consequences, particularly if mass transfer rates of sediment are to be calculated based on floc size data. The dependancy of density on size had been observed long ago in the water treatment industries (Lagvankar and Gemmell 1968; Tambo and Watanabe 1979) and was closely examined for estuarine flocs a decade later (eg. Krone 1978). Gregory (1997) gives a concise review of the fundamental factors which influence floc density.

Fractal Structure

Several decades after the observations on the ordered structures were made, theories of fractal geometry were applied to flocs (Meaken 1988; Li and Ganczarczyk 1989; Huang 1993; Huang 1994; Gregory and Chung 1995; Bache *et al.* 1997). According to these authors fractal geometry is suitable for describing flocs as they are porous structures in which the effective density decreases as the size increases.

The fractal dimension is a measurement of the effectiveness of the flocs to fill space as a function of the floc size. Kranenburg (1994) and Huang (1994) present equations to show that the fractal dimension n_f of the aggregates may be calculated from settling velocity and size data. These are discussed in Chapter 7. The larger the fractal dimension, the more uniform the floc structure. The maximum fractal dimension is 3, which is the Euclidean dimension for a three dimensional object and corresponds to a porous structure whose porosity or effective density is not a function of size (Huang 1994). For mud flocs the fractal dimension may be considerably lower, generally varying between 1.4 for large fragile flocs and 2.2 for strong estuarine flocs.

The ordered structure, and therefore the fractal dimension, of the flocs vary depending on the flocculation mechanisms involved and the geochemical conditions. As discussed earlier, there are several mechanisms which bring particles close enough together so that they coalesce. Many studies have established a relationship between porosity (or effective density) and size for flocs formed by fluid shear (Magara *et al.* 1976; Tambo and Watanabe 1979; Gibbs 1985a; Gibbs 1985b; Huang 1993; Huang 1994). These studies show that flocs formed in shearing conditions (orthokinetic flocs) have definite fractal properties. Fewer studies examine the fractal structure of flocs formed by differential settling (Alldredge and Gotschalk 1988; Huang 1994). Huang (1994) compared the fractal properties of flocs formed by fluid shear and differential settling and concluded that flocs formed by differential settling do not exhibit simple scaling behaviour and cannot be considered using the fractal concept, whereas those formed by fluid shear can be considered as fractal structures. Merckelbach (2000) has recently extended the study of floc fractal theory into a consolidating bed following the work of Kranenburg (1994).

Floc strength

Direct measurements and discussions regarding aggregate strength are found in Migniot (1968), Faas (1984), Williams (1986), Verreet and Berlamont (1987), Firth and Hunter (1976), van de Ven and Hunter (1977), Al Ani *et al.* (1991) and Bache *et al.* (1997). Most researchers report that large, less dense flocs are less strong, and break apart easily under

shear. The increase in void ratio (decrease in density) as floc diameter increases means there is an alteration in the number of particle bonds per unit floc volume. Shear strength per particle bond is found to decrease with increasing floc size. The research by Al Ani *et al.* (1991) is exceptional in that it indicates that larger flocs require a larger stress to break them apart, which is attributed to the more elastic nature of the larger flocs.

1.5 Video imagery and analysis of flocs

In many studies laboratory analysis of single flocs has provided valuable information about particle composition and size of constituent mineral grains. However studies have shown that the overwhelming majority of these flocs have been destroyed by conventional sampling and analysis techniques, thus their physical dimensions cannot be measured adequately (Johnson and Wankersky 1985; Eisma 1986; Milligan and Hill 1998). Particle size analysis using particle sizers in the laboratory have returned median diameters an order of magnitude smaller than the diameters measured with the same techniques in situ (Law *et al.* 1997) and Quisset and Fipiwitu settling tubes appear to break up flocs to a greater extent. This illustrates the fragile nature of estuarine suspended particles. Some techniques developed for field particle size analysis depend on the deployment and retrieval of a sample bottle followed by on board analysis (eg. use of the Owen tube), however this clearly disturbs the sample. Other traditional methods of suspended particulate matter analysis (sedigraph, Coulter counter, microscope, Atterberg cylinder etc.) all depend on sampling which results in considerable damage, or alteration to the flocs. Laser and light technologies describe the flocs as a number of counts during a certain time frame, but do not allow direct observation of flocs.

Within the past two decades photographic systems have been developed to capture flocs in situ. Silhouette photography was first used in a laboratory setting to identify active biological samples (Edgerton 1979; Ortner *et al.* 1979). These systems have been modified with video equipment and computer imaging technology to provide more accurate and more efficient data analysis. Table 1.1 summarizes the video techniques which have been developed for measurements of flocs. Video systems have an important advantage over

other techniques in that they do not disturb the flocs. Also, as opposed to settling tube techniques, they give absolute settling velocities, size and shape rather than being derived (sometimes inadequately) from concentration or settling rates. Videography has the added advantage that direction of movement is captured, so that calculations of settling velocity can properly account for residual currents and porewater expulsion at the bed. Some results of the use of these techniques are given in Table 1.2.

Table 1.1 Photographic and videographic instruments developed for floc observations.

Acronym	Name of Equipment	Institute	See reference
VMSS	Video Multi Sensor System	Institute of Biogeochemistry and Marine Chemistry, University of Hamburg	Pfeiffer (1996)
INSSEV	In Situ Settling Velocity Instrument	Institute of Marine Studies, University of Plymouth	Fennessy *et al*. (1994)
STRAT	Part of STRATAFORM research programme	School of Oceanography, University of Washington	Sternberg *et al*. (1996)
AGCFCA	Atlantic Geoscience Center Floc Camera Assembly	Geological Survey of Canada, Beford institute of Oceanography	Syvitski *et al*. (1995)
BIOPROBE	Part of BIOPROBE water sampling system	GEOMAR, Kiel, Germany	Thompsen and Ritzrau (1996)
NIOZ	Netherlands Institute for Sea Research in situ suspended matter camera	Netherlands Institute for Sea Research	Eisma and Kalf (1996)
BENTHOS 373	BENTHOS 373 Plankton Silhouette camera	Habitat Ecology Section, Bedford Institute of Oceanography	Milligan (1996)
ENDO	Endoscopic system	ERGRENE, ENPC-ENGREF Cedex, France	Maldiney and Mouchel (1996)
VIS	Video in situ	Rijkswaterstaat	Van Leussen and Cornelisse (1996)
HRW	Video Imaging in Owen tube	Hydraulics Research, Wallingford	Dearnaley (1996)
ISAAC	In Situ Aggregate Analysis Camera	Institute of Marine Sciences, University of North Carolina	Knowles and Wells (1996)

Table 1.2 Floc properties in natural conditions.

Location	measurement technique	median floc size, esd* (μm)	floc concentration (mg/dm^3)	median settling velocity (mm/s)	Reference
River Tamar	videography	20 - 600	-	-	Fennesy *et al*. (1994)
Elbe Estuary	various techniques	40 - 980	0 - 1600	0.2 - 3	Dyer *et al*. (1996) Eisma *et al*. (1996)
Ems Estuary	photography	140 - 350	80 -200	-	Eisma and Kalf (1996)
California shelf	videography	20 - 600	-	0.1 - 2.2	Sternberg *et al*. (1996)
Halifax Inlet	photography	50 - 2000	0 - 0.2	0.01 - 2.31	Syvitski *et al*. (1995)

* esd - equivalent spherical diameter is the diameter of the sphere which contains the same volume as the floc image

1.6 Variation in flocs

There are a variety of parameters which are known to cause some degree of change in the flocculation process, and therefore possibly the subsequent consolidation processes. The influences some of these parameters is expected to have on floc structure or development are explained below.

Organic content

Because the availability of surface-active organic matter is generally sufficient (Hunter 1980), organic coatings are suspected to be present on suspended particles in almost all estuaries. Indeed, Loeb and Neihof (1977) found that particles naturally form organic coatings within 1 hour of exposure to seawater, and conclude that uncoated particles are not expected in natural estuaries.

Observations on the effect of organic matter on the flocculation process have given varied and complex results. Dyer (1985) reports that organic material on the particles, such as mucal films secreted by bacterial activity and organics adsorbed from suspension enhance flocculation. On the contrary, Gibbs (1983) measured the effect that natural organic coatings have on the coagulation process of natural particles from tests in cuvette and blade-type reactors. The results showed that natural, coated material coagulates significantly slower than samples with the coatings removed. Whitehouse *et al*. (1960; cited in Dyer, 1996) found that the presence of complex carbohydrates in concentrations between 0.0005 to 1 g/l increased floc size, but more proteins decreased their size.

All three of these authors amongst others (Wilkenson *et al.* (1997), Kretzschmar *et al.* (1993)), attribute the increased or decreased flocculation to changes in net particle charge. Despite the discrepancies in the above papers, it is generally believed, regardless of charge, that organic material aids in the aggregation process through the formation of bridges between particles.

Turbulence/shear

Eisma (1991) and Eisma *et al*. (1991) studied several European estuaries and came to the conclusion that in situ floc size is variable, and is not related to changes in salinity, the content of organic matter, or the concentration of suspended matter. Instead they suggest that the rapid variations in turbulence and bottom shear are the most important factors controlling floc size and character. Others researchers agree that fluid shear is the main mechanism for floc formation in the natural environment (eg. Tsai *et al.* 1987; Drapeau *et al.* 1994).

Turbulence influences the floc size in two opposing ways: aggregation and disaggregation. Most studies on flocculation have focussed on the aggregation process, and floc disaggregation due to turbulence remains poorly understood. An increase in turbulence (from none) results in an increase of the number of collisions per unit time in orthokinetic flocculation and thus in larger flocs. When the turbulent pressure differences are larger than

the strength of the flocs, the flocs will be broken down. Van Leussen (1988) gives a limited review of the relationship between the size of turbulent eddies and the disaggregation of flocs. Other researchers who have made significant contributions include Parker *et al*. (1972), Firth and Hunter (1976), van de Ven and Hunter (1977).

As well as their role in determining floc size, the history of shear conditions is important regarding the structure of flocs. Francois and Van-Haute (1985), Broadway (1978), Matsuo and Vonnol (1981), Glasgow and Hsu (1983) have dealt with the problem pertaining to the floc structure in relation to the mixing conditions of the liquid phase. Kusuda (1981) found that when a clay suspension was subjected to a high shear followed by a period of low shear, the flocs were less dense than those formed under a low shear only. The floc density is reduced as the difference between the two shear rates is increased.

Concentration

The exact effect of particle concentration on maximum floc size is unclear, but it is generally considered an important, if not the most important, factor controlling floc size. Many researchers in the lab and field have found a strong positive correlation between concentration and floc size. Milligan and Hill (1998) report that concentration has an important effect on aggregate rate in the initial stages of flocculation, particularly under very low shear rates. In similar experiments Tsai *et al.* (1987) found that while there was a positive correlation in very low concentrations, the equilibrium floc size actually decreased with increasing sediment concentrations from 50 mg/l to 800 mg/l and concluded that under conditions of high shear the dominant process of flocculation switches from concentration to shear forces. According to Van Leussen (1988), smaller and denser flocs will be formed at higher sediment concentrations.

Salinity

The effect of salinity on the flocculation process is discussed earlier in this Chapter. The repulsive forces between mud platelets depend on the concentration of positive ions in the water. In saline water where the double layer is depressed the flocs are more likely to come

into close contact and adhere to one another. The work of Krone (1962) clearly shows the increased flocculation caused by increasing the salinity. Owen's work on Avonmouth mud in the laboratory confirmed the flocculating effect of salinity (Owen 1970). In this saline flocculation the dominant attractive force is the Van der Waals which leads to mud platelets adhering parallel to one another. In less saline water the Van der Waals forces are overshadowed by electrostatic forces of attraction. The positive charges at the edge of clay particles are attracted to the negative charges of the face, leading to a perpendicular array of particles constituting a floc cardhouse structure.

Various studies have been conducted to determine the concentration where salt flocculation predominates. Krone (1962) reported that increasing the salinities above a certain threshold did not show any appreciable increase in settling velocity (ie. floc size). According to Einstein and Krone (1962) a collision between fine sediment particles in a solution of more than 1 ‰ salinity always results in coagulation. In practice Whitehouse *et al*. (1960) obtained an abrupt flocculation at salinity contents of 1 ‰ to 7 ‰. Drake (1976) suggested a salinity concentration of 2 ‰ as a point of flocculation (discussed in van Leussen 1988). For kaolinite and illite salinity contents above 2 ‰ did not produce an increase in the flocculation, for montmorillonite there was an increase in flocculation at higher salt concentrations. Krone (1962), Allersma *et al*. (1967) and Migniot (1968) showed similar laboratory results that up to a certain salinity flocculation was enhanced and the settling velocities increased.

Unlike in laboratory experiments, measurements in situ show that varying salinity has no observable effect on particle size, actually measured by settling velocities (Burt 1994). According to Burt, salinity does not affect the ultimate floc size, but it does affect the speed with which flocs form. In nature material is held in suspension long enough for a much greater degree of flocculation to occur regardless of the salinity.

1.7 Consolidation and bed processes

In quiescent estuarine water a relatively dilute flocculated suspension settles to a more

concentrated suspension followed by a fluid mud and eventually reaches the state of consolidation. The transition between these stages is not well defined.

The first study specific to the settling of flocculated slurries is attributed to Coe and Clevenger (1916). These authors describe the concentration zones which exist in a slurry suspension. Further work has revealed that when flocs in suspension reach a concentration of approximately 10 g/l they block the displacement of water from below. This is termed hindered settling, where the settling of flocs is hindered by the displaced water. Hindered settling is generally reported as a decrease in floc settling velocity. As settling and consolidation continue the void spaces decrease leading to a further reduction in the permeability of the sediment to escaping water. The volume of the hindered sediment is linearly related to the initial suspended concentrations above approximately 10 g/l. Krone (1962) found that the structure of the hindered phase was constant from 10 g/l to above 40 g/l.

Kynch (1952) published a 'theory of sedimentation', in which he closely examines the development of the concentration zones. His basic assumption was that the settling rate of a slurry at a point depends only on the local concentration of the slurry. Layers of solids concentrations grow upward from the base of the column at constant rates. The plot shown in Figure 1.8 illustrates the settlement over time of the slurry - water interface, and of the bed - slurry interface. A zone of flocculation was added to this figure by Imai (1981). Many researchers are still using the Kynch theory as a basis for more complicated models. Bürger and Wendland (2001) provide a tribute and thorough review of Kynch-related work.

Michaels and Bolger (1962) conducted a classic suite of carefully planned experiments in which kaolin slurries were mixed at different concentrations and with different pore water salinities and pH values. The model they proposed is based on the premise that flocs cluster together to form aggregates, and these aggregates join together to form extended networks. It is these networks that determine the settling properties of flocculated suspensions. Their experiments were based solely on the height of the sediment water interface versus time in

glass settling columns with ID 6.5 cm. However they make observations about work done by Fuerstenau (1960), who examined the internal development of flocculated CaO beds using an x-ray technique. More will be said about these observations shortly.

Been and Sills (1981) and Sills (1998) have advanced an x-ray technique similar to that of Fuerstenau (1960) to examine the sequence of settling, deposition and consolidation of natural marine sediment in still water. Normally for these experiments a perspex column is filled with a slurry of known density. The x-ray source and receiver are traversed up and down the column, and the x-ray countrate at the receiver is converted to bulk density throughout the bed. More detailed information about this apparatus is given in Chapter 2. Surface settlement is initially rapid, followed by a slower settlement, such as that seen in Figure 1.8. Internally, the density of the soil is characterised by the presence of two density steps, one marking the transition between overlying water and the mud beneath, and the other marking the development of a denser layer upwards from the base of the settling column (Figure 1.7a). It is at the meeting between the rising dense layer and the settling mud/water interface that the mud/water interface settles less rapidly.

It is noticeable on the Figure 1.7a that the dense layer moving upward from the bottom has a rounded shape. It is a similar rounded shape in the density profiles made by Fuerstenau (1960) that Michaels and Bolger (1962) had made observations. They describe a model that the flocs do not settle on the bed into a closest-packed geometry, but rather their placement is dictated by random adhesions to flocs in the bed. It is only after the overburden weight is sufficient that these flocs are forced into their closest-packed array. Therefore the size of the curved surface on the upward moving high density layer is an indication of the height of overburden soil that creates enough force for the flocs to rearrange in the bed. The model proposed by Michaels and Bolger (1962) was lacking in thorough data and warrants further investigation, not least since the techniques of x-ray density measurements have been improved, but also to apply the model to real seabed mud where the floc conditions can be measured, rather than chemically flocculated kaolinite slurries in which the flocculation conditions are supposed.

A simple mechanism to explain consolidation theory in soils was first proposed by Terzaghi (1936). In his theories about one-dimensional consolidation he makes use of an imaginary stress called effective stress, F' which is defined as the difference between the total stress, F, and the pore water pressure, u:

$$\sigma' = \sigma - u \tag{1.2}$$

Consolidation is the process whereby the load is gradually transferred from the fluid phase of the soil to the developing soil frame, thus the pore pressure decreases leading to an increase in effective stress.

Good reviews of the progression of consolidation theories from Terzaghi's initial thoughts are presented in Been (1980) and Schiffman *et al*. (1985). Terzaghi's theory is based on a number of assumptions, which have since been proven inadequate (Craig 1974). For instance, Terzaghi suggested that the structure and behaviour of a soil is uniquely associated with the effective stress conditions. This assumption works adequately in some situations, such as those described in the following paragraphs, but it does not account for the creep behaviour of clays.

Been (1980) and Been and Sills (1981), along with many subsequent papers, use the definition of effective stress as a framework for analysis. A density profile may be integrated to produce a total vertical stress profile. Excess total vertical stress may then be calculated by subtracting the hydrostatic pressure at all heights. Excess pore pressure is likewise calculated by subtracting the hydrostatic pressure from the measured pore water pressure. In Figure 1.7b the vertical stress is compared with the corresponding pore pressure (both of these are reported as excess, that is above hydrostatic pressure). By definition the excess pore pressure in the clear water above the sediment bed is zero. Where the density is that of a fluid supported mud the excess pore pressure and excess total stress are nearly indistinguishable. When the bed is more dense the pore pressures drop significantly below the total stress as some of the vertical stress is carried by the soil

particles. In a slurry experiment, which has constant mass through time, the total vertical stress remains the same, the pore pressures drop and thus an effective stress is apparent (Figure 1.7, Equation 1.2). In this manner the onset of effective stress has been used to identify the transition to a soft consolidating structured mud from an overlying suspension. The density at which this structure develops has been termed the structural density since it represents a structural framework in the bed[4]. For example the structural density of the experiment shown in Figure 1.7 is between 1.2 and 1.23 Mg/m^3.

Creep

Terzaghi suggested that effective stress uniquely defines the state of a soil's structure. Sills (1998) And references therein examine this suggestion by comparing changes in structure to changes in effective stress over time. The parameter void ratio, e, is used to represent the soil structure. These researchers show that there is not necessarily a straight forward correlation, especially at low effective stresses. Rather, at constant effective stress the void ratio continues to decrease.

This phenomenon known as creep, secondary compression, or perhaps inappropriately as secondary consolidation[5], is the consolidation which continues to take place after excess pore pressures have dissipated. This is now a commonly reported phenomena in clays (eg. Leroueil *et al.* 1985; Sills 1995), yet its causes are still a matter of debate.

Not all laboratory experiments exhibit creep behaviour, and it seems to vary with the type of soil and with the stress history, such as initial density, sedimentation rate and depth of bed (Sills 1998). The effect of sedimentation rate is described by Sills and Elder (1984), who quote data collected by Sills and Thomas (1984). Sills and Elder report that altering

[4]Structural density is equivalent to the term gelling concentration used in chemical engineering literature

[5]Secondary consolidation develops in a state of almost constant effective stress, indicating a soil restructuring rather than consolidation process. Some engineers assert that secondary *compression* is a more appropriate term.

the sedimentation rate leads to a different structural density. When the structural phase develops at a suitably low floc concentration (ie. low settling rates) there appears to be no suspension phase, and the structured phase (onset of effective stress) occurs at a lower concentration (as low as 80g/l or 1.05 Mg/m^3). When the structural phase develops at such a low concentration the surface density continues to increase quite rapidly with time. This density increase probably corresponds to an increase in strength and resistance to shear. Slowly sedimenting mud has more time to strengthen before arrival and loading of additional flocs, leading to an open structure, which is subject to collapse upon further loading (see also Sills 1995). More quickly sedimented beds do not have time to strengthen before being bombarded and loaded by additional flocs. In fact, the same mass of soil can lead to a bed that is twice as high, under conditions of suitable low sedimentation rates. This phenomenon, of collapsing flocs, has been termed the flocculated creep model. Evidence to support it is found in Sills and Thomas (1984), although neither the collapse nor the flocs were observed directly.

Kuenen (1965) also reports that a less dense bed forms under low slurry concentrations, and a more dense bed forms under slurries of higher concentrations. In fact, Kuenen reports it is possible to have the same mass concentration in a mobile slurry in one experiment, as in a consolidating bed in another experiment. But rather than attributing this to flocculated creep taking place in the bed, Kuenen suggests that it is due to collisions taking place in the highly concentrated suspension that lead to higher density flocs forming the bed.

On discovering that sedimentation rate plays a significant role in the consolidation properties of the bed, these and similar papers have left some unexamined questions. First, sedimentation has been achieved by either depositing a slurry into a column, or by a simple peristaltic pump arrangement. The deposition rate under these conditions is still significantly higher than would normally be expected in an estuary. It remains unanswered (to the author's knowledge) as to how very slow deposition rates, comparable to those in most estuaries, would affect the bed properties. Second, it has not been possible to validate either the flocculated creep model, or the suggestion made by Kuenen (1965) of high

density disaggregated flocs, since the flocs have not been directly observed in either case. Finally, a question remains unanswered as to the survival of flocculated beds under a significantly increasing pressure, such as those encountered in typical seabed engineering applications.

Allain *et al* (1995) have partially addressed the first of these questions and described the time evolution of the floc structure at very low and at intermediate concentrations of $CaCO_3$ suspensions. At low concentrations they observed cluster deposition. Aggregates of varying sizes form from the initially dispersed sediment, and settle at different rates. The larger aggregates 'sweep up' particles due to differential settling. Gradually the turbidity of the fluid decreases. The well defined clusters settle to produce a voluminous bed which undergoes slow compaction. At higher initial concentrations, aggregates no longer settle separately. Instead they form a network immediately which collapses and settles under its own momentum. The volume fraction separating cluster deposition from network collapse is reported as $3x10^{-3}$. This corresponds to a bulk density around D . 1.047 Mg/m^3, assuming the $CaCO_3$ had a laboratory standard specific gravity of 2.55. This almost certainly coincides with the lower limit of the structural densities reported by Sills and Thomas (1984). Thus there seems to be a different mode of deposition for very dilute (though flocculated) versus slurry experiments. Since the work by Alain et al is mainly descriptive, this process requires a more quantitative investigation.

Intrinsic vs. Natural Sediment Properties

Burland (1990) discusses the significance of the state of a soil relative to the intrinsic compression line (ICL) and the sedimentation compression line (SCL), particularly in the response of a soil to the application of a load. Compression curves for various reconstituted clays[6] (intrinsic compression curves) are a function of void ratio. Burland normalises these compression curves with respect to the void ratio to produce a unique line describing all

[6] Reconstituted Clay is that which has been collected and re-mixed in the laboratory at a higher water content of one and a half to two times the liquid limit of the original sample.

clays on a plot of Intrinsic Void Index (the normalized void ratio) vs. total pressure. This line is termed the Intrinsic Compression Line (ICL). The ICL is insensitive to experimental conditions, thus it provides a frame of reference for assessing the properties of a natural clay, whose compression curve usually lies well above the ICL, and a method of predicting these natural properties from the results of laboratory experiments on reconstituted clays.

The deposition conditions profoundly affect the position of the sediment compression curves with respect to the ICL, indicating an effect on the fabric of the sediment. Slow deposition in still water leads to an open random fabric (high void index). Rapid deposition from a dense suspension or sediment deposited in a current gives rise to a more oriented fabric with a lower void index, thus the compression curve is shifted downward towards the ICL. Similarly, the application of a load reduces the void index and shifts the compression curve downward towards the ICL (Burland 1990).

Previous work at Oxford confirms that the conditions under which a sediment is deposited can have a significant effect on its state (Sills and Thomas 1984), as can the process of creep (Sills 1995), both of which alter its position relative to the ICL. It appears that a high rate of increase of effective stress can cause a collapse, thus influencing whether the state of a soil moves quickly towards the SCL or remains above it (Sills 1997).

Development of Bed Stiffness and Strength

In traditional soil mechanics the level of effective stress is the factor controlling the shear strength of the sediment. Factors which affect the stiffness and strength (apart from effective stress) include cementation, biological effects, and perhaps the rearrangement of flocs. Soil stiffness and strengths are often measured using triaxial and oedometer apparatus. However in soft soils, and lower stress situations, techniques of particular interest are shear vane tests, bender element tests, and erosion tests.

Shear vanes have been used to monitor the development of structure in soft soils, alongside measurements of effective stress, by Elder (1985) and Bowden (1988), and references cited

therein. Bowden reports nearly linear relationships between the strength measured by shear vane and the effective stress in soft soils, for both peak shear strength and residual shear strength. Elder found only the residual shear strength gave this correlation. Typically the experiments contained a maximum effective stresses of around 0.8 kPa, which resulted in a peak shear strength of 0.4 kPa and a residual shear strength of around 0.08 kPa. The ratios of strength to effective stress, s_u/F'_v, are higher for soft soils than they are for normally consolidated stiffer soils. The clear disadvantage with shear vane tests is the absolute destruction of the soil sample, making the shear vane useful only at the end of experiments.

An alternative, and non destructive, technique is found in the use of bender elements. These are biceramic plates, which vibrate (a fraction of a millimetre) when subjected to a voltage. As a result a shear wave is created at their tip which propagates through the soil. The shear wave velocity can be related to the density, and therefore to the development of a soil. As the development of the bender element in the research of soft soils is still very much underway, the methods section in Chapter 2 refers to the most appropriate literature on the subject.

Many factors affect the erosional properties of cohesive sediment, including its grainsize, maturation time, aerial exposure, biostabilisation, changes in sedimentation rate and bioturbation rate. Of particular interest here are the effects of consolidation time and biological activity, together termed maturation, in sedimentation experiments.

A longer consolidation time may be expected to lead to increased resistance to erosion, due to structural collapse of the aggregates and due to bed cementation, or gelling. Krone (1999), for instance, reviews papers by Roberts *et al.* (1998) and Zreik (1998), both of which show that resistance to erosion is directly related to bed density, where the changes in density occur through time with structural alteration of aggregates.

Biological activity is also generally thought to lead to increased resistance of the beds to erosion. Stabilisation by biofilm (mainly diatom) exudates has been suggested for many

years, but was first experimentally examined by Holland *et al.* (1974). Burrows of benthic organisms were traditionally thought to increase bed strength; however this is still a topic of debate, since evidence to the contrary has been found. An excellent review of biological effects on sediment stability is given by Paterson and Black (1999), in which the authors propose theories to explain why these organisms would require that they decrease the stability of the beds.

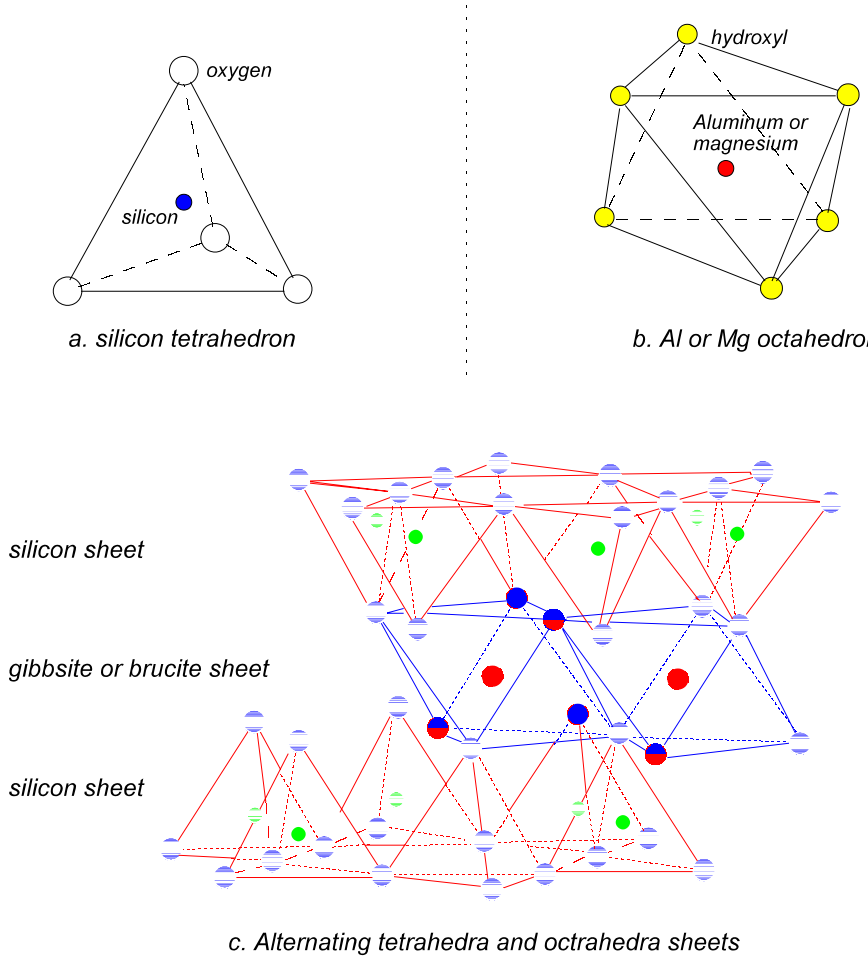

Figure 1.1 Kaolinite consists of alternating silica terahedral sheets and aluminium octahedra (gibbsite) sheets.

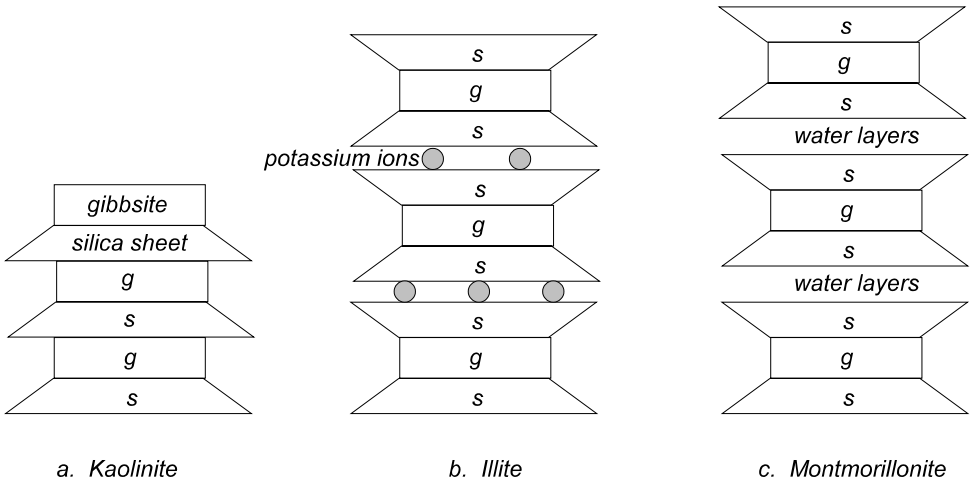

Figure 1.2 Symbolic structures for common two layer and three layer clays.

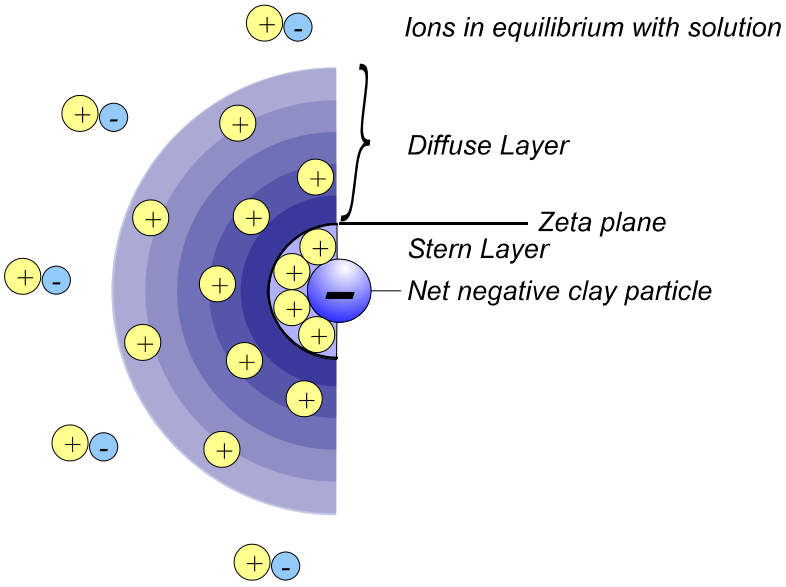

Figure 1.3 Negatively charged layers in the double layer attract positive ions. The concentration of these positive ions increases towards the negatively charged clay surface.

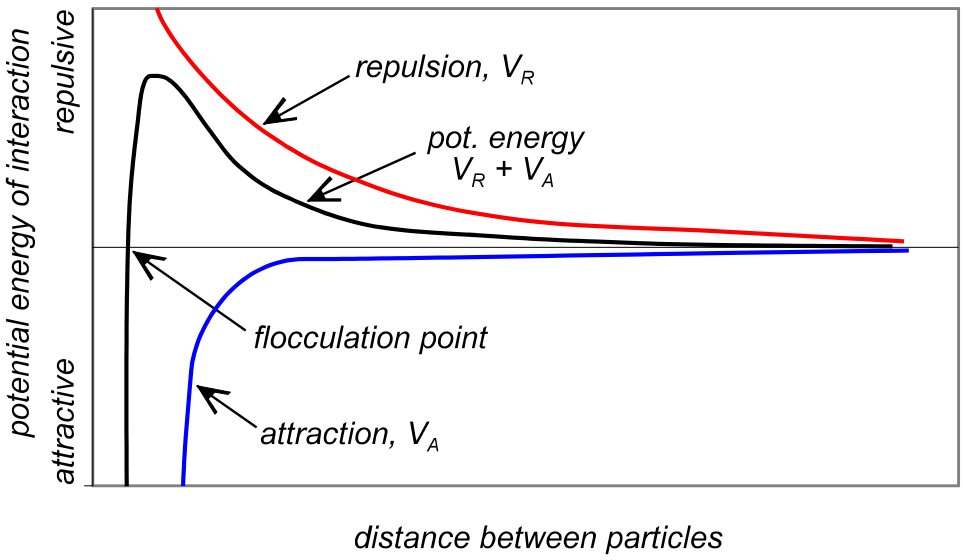

Figure 1.4 DVLO energy theory. The combined attractive and repulsive forces lead to aggregation at small interparticle distances.

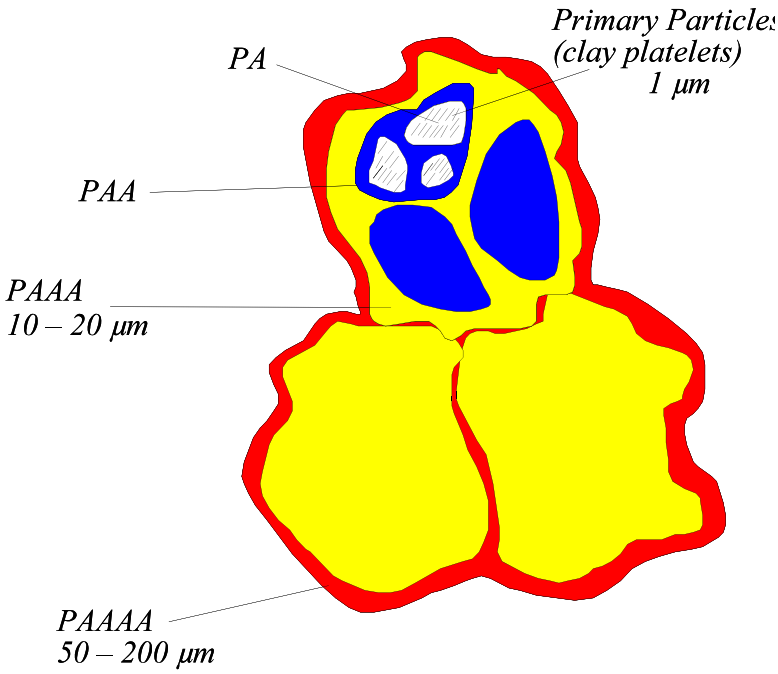

Figure 1.5 Schematic drawing of the ordered floc structure with typical sizes.

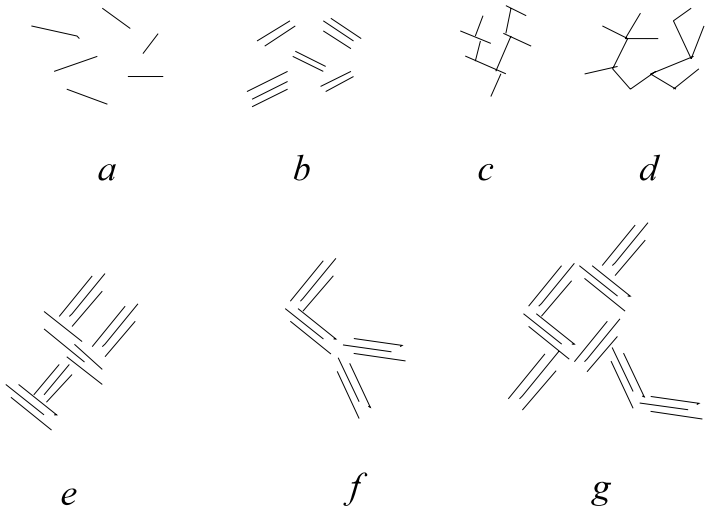

Figure 1.6 Possible modes of clay particle association. A. Dispersed, B. Coagulated into tactoids (face-face), C. and D. Flocculated primary particles (edge-face and edge-edge), G. Coagulated and flocculated particles

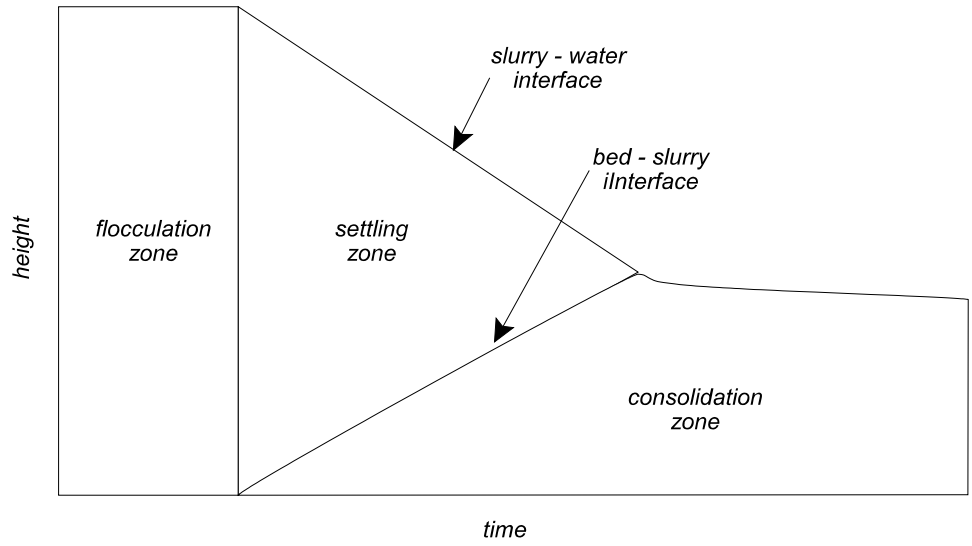

Figure 1.8 The mud/water interface height through time for a typical slurry experiment.

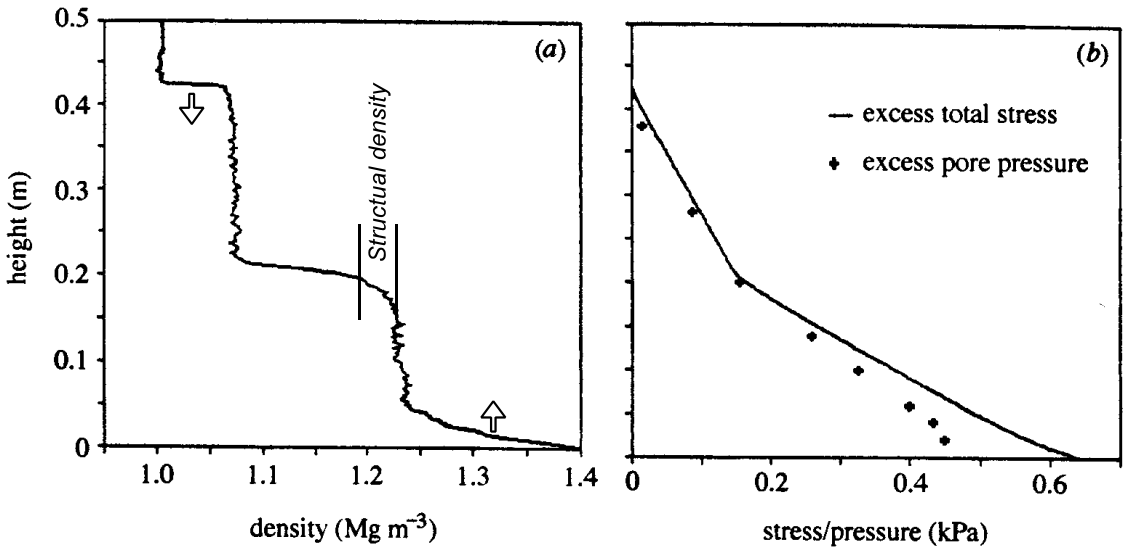

Figure 1.7 Experiment REDMO5 from Sills (1998) showing a) a typical density profile and b) the calculation of effective stress as the difference between excess total stress and excess pore pressure.

Chapter 2 Methods and Equipment

The experimental setup and methods described here follow many years of settling column tests at Oxford. Most often, in previous tests, the columns have been filled with a slurry of known density and the slurry properties are measured as it settles and consolidates. In natural estuaries, the concentration of mud is usually lower than in slurry column experiments, and the individual mud particles have more freedom of movement. The following equipment has been designed to allow low concentrations of mud particles to flocculate freely in the water column and to settle at realistic natural estuarine settling rates. A laboratory setup, complete from sedimentation source, through the development of flocs, to settlement and long-term consolidation allows all processes to be viewed without disturbance. Immediate analysis of flocs in a laboratory sediment column eliminates floc destruction, and allows accurate observation of floc properties. Measurements are made on the flocs in the water column, and on the structure and strength of the beds.

2.1 Settling column apparatus

Several columns have been designed to incorporate a number of measuring devices, which are described throughout this chapter, and some of which are shown in Figure 2.1. For slowly deposited experiment mud is introduced to the top of the column. A vyon filter prevents the solid particles from escaping, while allowing added water to flow through to overflow ports. The columns have pressure ports throughout their heights. Bender element ports for measurement of shear stiffness are placed near the base of the column. There are two overflow ports at the top of each column. Glass viewing ports for video analysis have been placed at heights of 30 and 69 cm. The columns are segmented so that after sedimentation is complete the top segment, containing the water column, may be removed giving easier access to the beds for such measurements as erosion and shear strength. The maximum height of the columns is 1.5 m, between the gravity fed sedimentation entering the column and the lower reach of the x-ray traverse limit.

Experiments in the past have shown that processes in laboratory columns, particularly settling and consolidation, can be influenced by the diameter of the columns. The results of

several studies showed that consolidation in a column with smaller diameters is slower (Migniot 1987). However, Michaels and Bolger (1962) showed that the study of flocculated suspensions of kaolin could be carried out in columns of 48 mm diameter without fear of edge effects. Furthermore Van Goethem *et al*. (1985) found no difference in the relative residual height between columns with 100 mm diameter and those with 1 m diameter, with mud from Dutch Harbours. Research in the University of Oxford x-ray laboratory has shown that 100 mm columns provide accurate and reliable results for consolidation experiments on a range of natural estuarine soils, thus the equipment in this lab has been designed and calibrated for 100 mm columns.

2.2 X-ray density measurements

Density is indirectly measured using a non-destructive x-ray technique developed by Been (1980) and used in many studies at Oxford. The arrangement is shown schematically in Figure 2.2. A highly collimated beam of x-rays is directed through the column to a sodium iodide crystal and photomultiplier assembly, producing a count rate N which can be related to the density D through the equation:

$$N=N_0 e^{-k\rho} \tag{2.1}$$

N_0 and k are calculated by using calibration samples of known density. These samples are enclosed in sections of perspex column taken from the main sedimentation column. The calibration samples are made with the same soil used in the experiments, as k depends on atomic numbers of the elements in the sample. The x-ray and counting assembly is traversed vertically allowing measurements to be made along the entire column height with a vertical resolution better than 1 mm. A second method of calibration involves the use of calculated masses, rather than calibration samples. In a slurry experiment, where a slurry of known density is deposited at the outset of the experiment, the total mass in the column is known. This mass is conserved throughout the experiment, allowing the density profiles to be adjusted to match this mass over the volume of the slurry. A similar method is sometimes used for slowly sedimented experiments, where the quantity of mass in the bed

is estimated from the volume of slurry of known density that has been removed from the overhead slurry basin of the sedimentation system. Due to variations in the sedimentation rate this latter method may be less accurate than the other methods.

A typical x-ray session consists of an upward followed by a downward sweep of the column. The data of each sweep can be compared to determine whether there were any unwanted shifts in x-ray output voltage during the test. The x-ray profile in Figure 2.2 shows the water in the upper column at a density of just above 1 Mg/m^3, and a much more dense layer building up from the bottom, with an intermediate density between the two. Small variations in the count rate, by comparison to those caused by bed density changes, are due to both fluctuations in the x-ray output and photomultiplier assembly, and to variations in the column density (these small variations are not shown in the schematic). The accuracy of measurement depends on the traverse speed of the x-ray and on the density of the sample, given the exponential nature of the calibration. For example, a soil density of 1.22 Mg/m^3 is measured with the accuracy of ±0.002 Mg/m^3, whereas the accuracy of a soil of density 1.33 Mg/m^3 is better than ±0.004 Mg/m^3 (the units Mg/m^3 scale to g/cm^3). The x-ray technique, as well as its accuracies, are described in detail in numerous reports (Been 1980; Been 1981; Sills 1997) and will not be repeated here.

2.3 Porewater pressure

Pore water pressures are measured using a technique and apparatus originally developed by Bowden (1988) and shown in Figure 2.3. A single transducer is connected in turn to ports at different heights on the column wall (a) through a multiplexer (b) described in detail by Bowden. A plastic Vyon filter is placed in each port, allowing the transmission of water pressure without allowing the sedimenting soil to escape. The multiplexer consists of a top disc, holding the transducer, and a bottom disc into which the pore pressure lines feed. Each of the pressure inputs can be connected to the transducer in turn by rotating the top disc relative to the bottom disc.

One of the pressure inputs to the multiplexer is connected to a calibration tank. Starting at a

base position (relative 0) this tank is raised to a height of 1 metre, at 10 cm intervals, and then lowered again at 10 cm intervals from 95 to 5 cm (Figure 2.3c). A line equation and regression coefficients are calculated for the voltage versus the height of the calibration tank. A calibration may be made of the pressures observed in the column to those in the calibration tank by assuming that the slope of the voltage vs. height curve will be the same in both circumstances. Accuracies are of the order of ±0.01 kPa, or a 1 mm head of water.

Initially the multiplexer was turned by hand. However for this research the multiplexer has been automated, so that pore pressure measurements could be made by a computer throughout the length of an experiment. A stepper motor is used to turn the multiplexer, and at each step the computer monitors for a sudden jump in pressure which indicates that a pressure port is aligned to the transducer. At this point the computer waits for the pressure to become steady and then makes a measurement before moving on to the next port.

It is assumed that a straight line pressure-height relationship exists between the pore pressure ports. Figure 2.4 shows a measurement of excess pore pressures made near the end of an experiment on Dibden Bay Mud, about which more will be said in later chapters. This experiment has been subjected to a hydraulic gradient, causing the excess pore pressures to become negative. The solid curve represents a straight line interpolation between the pore pressure measurements, whereas the dotted line is a curve which has been smoothed automatically by Excel through the data. The difference between the two curves is nearly indistinguishable. These straight line interpolations were chosen as the preferred method to create pore pressure profiles, since the actual shape of the curve is unknown and may differ between experiments.

As pointed out by Sills (1998) and fundamental to this research, a distinction exists between voids within flocs (intrafloc) and those between them (interfloc). The measurements made using the pore pressure apparatus described above indicate the interfloc pore pressure only.

2.4 Hydraulic Gradient

Since the height of a bed in a column is rarely over 1 m, the maximum effective stress which can be achieved in a self-weight settlement column is in the order 5-10 kPa. In very slowly sedimented experiments, time constraints do not permit the beds to achieve such heights, and the effective stress is likely to be below 1kPa.

The effective stress is increased using a hydraulic gradient which is produced by draining water from the bottom of the column. Figure 2.5a represents the final condition at the end of self-weight consolidation when the pore water pressure and the hydrostatic pressure are equal, $u = u_h$. If drainage is permitted at the base of the bed, that is, if it is opened to atmospheric pressure, then the pressure at the point of drainage becomes zero (Figure 2.5b). Since the pore water pressure drops in a gradient towards zero the effective stress is increased. If the drainage outlet is lowered then the pressure is atmospheric at the outlet below the base of the soil. Since water exists in the tube leading to the outlet, the pressure follows a hydrostatic gradient up to the soil base, producing a negative pore pressure there and allowing a larger effective stress to develop. The hydraulic head is maintained using a Mariotte bottle, which allows a volume of water to be added to the top of the column equal to the volume that is drained. The water used in the Mariotte bottle has the same properties as the initial column water.

Experience with this device has shown that there is a limit to the hydraulic gradient that can be applied. If the gradient is too large then the suction developed in the water pulls the soil away from the walls and water begins to slip between the column walls and the soil. It was found in the present research that this method could increase the effective stress in the beds from around 1 to a few kPa, to a maximum of 12 to 18 kPa, before this slipping occurred.

2.5 Steady sedimentation system

Most settling column experiments conducted at Oxford and elsewhere start from sediment slurries of initial bulk density up to about 1.2 Mg/m^3. These slurries are often poured into

the column, and therefore represent events such as dredging excavation or the disposal of waste slurries. In this study, as previously mentioned, to represent natural estuarine and coastal conditions the mud is introduced at much lower concentrations giving flocs appropriate time and conditions to develop through the water column before they settle to the bed.

The sedimentation system used for the present experiments consists of computer controlled valves, pumps and stirrers. These are powered by a solid state relay device controller, which is in turn controlled by a pc through a Computerboards CIODIO48 digital input-output card. The system is described below and illustrated in Figure 2.6. The present system has gone through several generations of development. Originally Sills and Thomas (1984) used a simple peristaltic pump to deposit sediment steadily into columns. This was later developed by Gonzalez and Sills (1997), so that it included a seawater source, a mixing basin and was partially computer controlled. Considerable modifications have been made during this research, including the ability for sediment to be deposited to three columns simultaneously, and a safer, more controllable operation. These and other modifications are described below.

A known mass and density of clay is stored and kept stirred in a large mixing basin (A). This clay is very slowly and accurately pumped into a smaller basin, using a peristaltic pump (B). At the same time water from a reservoir (C) is allowed through a pinch valve (D) for a specified amount of time and mixed with the mud in the mixing basin. This small basin is kept stirred using a magnetic stirrer (E), at a specified speed. The mud is released at intervals from this basin via a pinch valve (F) through a narrow tube into the sediment column. This tube is made of hydrophobic rubber, which allows less frictional passage of the flocculated water. Meanwhile the water reservoir automatically refills itself from a larger source (G). An important feature of this system is that a known quantity of mud can initially be placed in the large mixing basin, and it can be steady diluted over several days to weeks while maintaining a constant input concentration to the column, rather than having to refill the mud source frequently.

Modifications have been made to allow the 250V electrical components to be used safely with openly flowing water unsupervised for weeks at a time. There are overflow outlets which allow water to escape when slurry is added, and backup overflow outlets in case the first become blocked. A vyon filter stops the flocs (or solid content) from escaping through these outlets. There are also infrared liquid level sensing devices throughout the apparatus that will stop the pumps and valves from working if blockage or equipment failures occur.

Also, since the system is computer controlled, precautions had to be made for the case of a power failure or computer crash. The hardware and software both require detection of a 'watchdog' signal. This is a TTL signal sent between the computer and device controller every few seconds. If this signal fails then the power to the devices is cut, and a warning message is displayed.

A program has been written which allows the user to set the sedimentation conditions and to monitor the progress of sedimentation. A log file includes a tally of sedimentation progress with messages such as '15-Apr-2002 15:35, Magnetic stirrer full, input paused, drainage permitted'.

There are four stages in which aggregates are believed to form in the sedimentation system: During the storage and mixing of the mud in the slurry basin, during the mixing of mud and water in the magnetic stirrer, during transport of flocs from the magnetic stirrer through small diameter pipes, and during the settling stage in the column. It is not believed that the scale of the shearing regime nor of the settling distance is large enough for flocs to reach their natural steady state properties[7]. However, it is believed that the control on sedimentation conditions is fine enough to create accurate and reproducible conditions.

Given these stages it may be possible to make some assumptions about the properties of the flocs formed in the system. Increasing the shearing rate in the magnetic stirrer should lead, on average, to smaller but stronger flocs as shearing forces are responsible for

[7]Discussed at a COSINUS participants meeting, Grenoble.

orthokinetic flocculation. Increasing the concentration will certainly affect floc characteristics in the stirrer. Increasing the concentration may also lead to larger flocs in the stirrer, in the tubes and in the settling column. It is difficult to predict the floc strength in this case, as the tumbling which takes place in the tube would lead to tough flocs, whereas the differential settling in the column would lead to weak, low density aggregates. There is not expected to be much perikinetic flocculation taking place (due to Brownian motion) as the majority of primary particles in the samples are larger than 2 ：m.

2.6 Video System

The development of floc video imaging technology and computerised analysis system is the key to understanding the nature of flocs under varying environmental conditions. The flocculation camera system developed is shown in Figure 2.7.

Video camera

In the initial experiments a relatively low resolution JVC310 monochrome camera was used. In addition to having low resolution this camera had several drawbacks. The camera supported interlaced data transfer only. Interlacing is the method by which most cameras transfer large amounts of data. It makes use of two horizontal grids each capturing alternate lines of video. The first grid is exposed a fraction of a second before the second. Thus in cases where particles are moving quickly they are captured as two particles. This is shown in Figure 2.7 where flocs eroded from the bed using a blade mixer clearly comprise two floc images. The analysis software would calculate the large 'double' floc in the bottom centre of the figure as a single horizontally elongated floc. This figure is an extreme case with the flocs moving very quickly under shear, the floc settling velocities are sufficiently low in most cases that the interlacing did not affect the floc images. Another drawback is that the camera had autoexposure dependant on light conditions. This feature is convenient for some applications, however where the images must be binarized it is important to keep the exposure time, and thus the light levels of the background, constant. This problem has been dealt with by an automated software binarising method described later.

A new JAI-CV1O was purchased which addresses each of these problems. In addition the camera has a much higher resolution of 948 x 576 pixels. The exposure time is manually set to a wide variety of settings through dip switches on the back panel, The sensitivity of the CCD can also be altered to match the exposure time. Most importantly for particle image analysis, the JAI is a progressive scan, or non-interlaced, camera, that is the entire image is sent to the capture board as one package of data, so there is no time delay between the first grid 'sweep' and the second. Both cameras were required throughout this research.

The theoretical resolution of the video system is the size represented by one pixel detected by the camera (since the video capture card has a much higher resolution capability). However, the practical resolution limit in terms of image analysis pragmatics and statistical meaning is larger. Since a floc is defined in Matlab as being a set of interconnected pixels, a floc has to be at least two pixels in size. For the JAI camera the smallest detectable floc is the number of pixels that define a floc multiplied by the length (height or width) of the imaged area divided by the number of pixels across that length:
2 pixels * 6400 μm / 768 pixels = 16.7 μm in width, and
2 pixels * 4600 μm / 574 pixels = 16.0 μm in height
For the JVC camera the smallest detectable floc is:
2 pixels * 7700 μm / 576 pixels = 26.7 μm in width, and
2 pixels * 5800 μm / 378 pixels = 30.7 μm in height

This is considerably smaller than those that would be distinguishable on the video monitors by eye. Various image analysis techniques described below (particularly dilation) decrease this resolution slightly.

PC frame grabber

Major consideration was given to the method of recording video images. It was decided that computer technology had progressed significantly that the camera could be operated, and the images captured, directly from/to a frame grabber board. A high end Imagraph I-50 series image processing board is used for this purpose. This board allows the capture of

monochrome images of 2000 x 2000 pixel resolution at 30 frames per second. Normally for this research the images were restricted to 768 x 574 pixels or to 576 x 378 pixels, by the JAI and JVC cameras respectively.

Illumination

The lighting setup has proved to be more crucial than the type of camera used, and testing of different methods lead to significantly larger variations in floc properties than different methods of image analysis. Several types of lighting have been tried, including ambient room light on a light background, ambient room light on a dark background, projector illumination, collimated Light Emitting Diode and laser sheets. Collimation of the light source eliminates the imaging of out of focus flocs and knowing the exact volume of illumination allows the concentration of flocs to be calculated. If out of focus flocs were included in the analysis, as they are using ambient light, then the software (and human eye) calculates these as having larger areas than focussed particles. The laser was chosen as the preferred method. It was found that the laser lighting was capable of penetrating the column at much higher floc concentration than the LED and ambient lights. Originally a HeNe visible red laser was used, which was replaced by more modern laser diode modules. The laser diodes were custom manufactured with several specifications important to this research. Each diode includes a cylindrical lens, which spreads the beam into a two dimensional fan, allowing only the particles within the plane of focus to be illuminated. The diode emits light in that portion of the ER spectrum (visible red) to which the video cameras are most sensitive. It was found that the original HeNe laser illuminated the particles too brightly, causing their reflections to affect the camera and images adversely. Therefore each diode is fitted with a potentiometer, which allows the light intensity to be altered. Each diode has also been fitted with a digital modulation device, which allows it to be strobed extremely quickly (at a rate faster than one frame exposure) for very fast moving particles, or conveniently powered on and off at specified time intervals by a computer TTL signal. The main drawback of using laser is that the light recorded by the camera is a reflection of the high intensity and highly directional laser beam, only showing when the particle surface is in such an orientation that it reflects from the laser source directly into

the camera. This leads to some 'twinkling' of the flocs as they rotate.

Software

Software has been written to allow the user to set capture times and rates. For each image the software powers the laser, captures the image, displays it on the screen and saves it to a specified directory. Initially it was hoped that two consecutive images at one second intervals would provide enough information to calculate the floc characteristics and their movements. However in more concentrated suspensions it has proved extremely difficult to track the movement of a single floc based only on two images. A minimum of three or four images must be taken sequentially in order to get accurate settling data. One such sequence is taken every 5 to 30 minutes during the sedimentation, although this time can be altered if necessary. Alternatively a short movie clip can be taken. However each photograph or movie frame requires approximately 1.2 Mbytes, thus a movie at regular frame speed (30 frames per second) requires 36 Mbytes per second. The memory requirements of the computerised image capture necessitated the use of a large and fast Ultrawide SCSI 3 hard disk.

Analysis using the Matlab Image Analysis Toolbox

A number of prepackaged Image Analysis Software packages have been tested for their suitability in this research. These include HLImage^{++}, Optimas and Image Pro Plus. However, because these are preprogrammed packages it was found that the manipulation of images and files, and the types of analysis which could be made, were limited. Matlab was chosen as the most flexible package. Matlab allowed an efficient method of analysing the images as well as storage and retreival of the datafiles, although considerable effort had to be made on writing software. A user interface has been written to allow the image capture conditions to be set and the data to be sent either to Excel or Matlab to be analysed in real time. Some of the more important image analysis techniques developed are described below.

Removal of non-uniform illumination

Figure 2.9a shows a typical floc image from experiment dbd3. Figure 2.9b shows the image negative since negatives are much easier to examine in printed form. The laser light source in this case is located to the left of the image, therefore the overall image illumination is non uniform, decreasing from left to right. This is not always obvious from looking at the image itself, but is clearly shown in a contour plot of the grayscale levels of the image (Figure 2.9c). In this plot the contours representing flocs have been removed leaving only the contours of the background. The left hand side of the plot shows a much higher overall illumination than the right hand side. The background can be removed by the following method. First, determine the general contours of the background illumination. Second, apply a filter that is based on this contour data, so that different parts of the image are darkened by a calculated quantity. Finally, brighten the whole image to counteract the dark filter that has been applied. The result, which is not shown, is indistinguishable to the eye from Figure 2.9b, but it aids in the ability for the software to distinguish clearly the flocs from the background on all parts of the image.

Autothresholding

Image processing techniques work most efficiently on binarised images, that is images made up of zeros for the background pixels and ones for illuminated floc pixels. Each pixel in the original floc image has a grey level between 0 (black) and 255 (white). These grayscale images are converted to a binarized image using a specified threshold value, above which particles will appear white and the background will appear black. As an example, Figure 2.10 uses the same image as in Figure 2.9. If the threshold level is chosen incorrectly then the software may detect no flocs at all, or alternatively it may detect tens of thousands of random noise pixels as flocs. In Figures 2.10a and b values of 10% and 40% have been chosen as thresholds, and the result is quite different for each. Because of variations in the laboratory ambient lighting, it is not possible to select a single threshold throughout the length of an experiment. This is also true of in situ studies where researchers report that grey levels defining the flocs may differ from the background by only a few units and that background grey levels in situ can vary, in themselves, by a few units (Bill Roberts, HR Wallingford, personal communication). Fortunately, due to the

high intensity of the laser lighting in the lab system, the flocs show as very bright reflections regardless of whether there are low light or no light conditions in the lab, making their definition more straight forward. Even so, when the laboratory is brightly lit the flocs are less distinguishable, especially at high concentrations.

An iterative method has been developed to automatically select a threshold. The method essentially looks for a specified rate of change in the number of illuminated pixels with increasing threshold values. It selects the threshold at which this rate is maximum, that is the threshold at which flocs are beginning to appear separated from the background. In Figure 2.11 the value used for thresholding is plotted against the average brightness of the thresholded image, the latter in effect being the number and/or size of flocs that are extracted from the original image at the given threshold (number of white pixels on black background). This has been done for every 20^{th} image out of 2729 images available for experiment, dbd2, an experiment using sediment from Dibden Bay. This figure shows that choosing a wrong threshold value (even slightly) will have a large effect on the number and/or size of flocs in the thresholded image (ie. the overall brightness), particularly at threshold values between 0.1 and 0.4. It also shows that each image leads to an individual curve- there is no unique threshold value that will yield roughly the same number or size of flocs from one image to the next. By the iterative method, the threshold point on the horizontal axis is chosen for each curve (each image) as the point where the change in brightness of the thresholded image per unit change in threshold value goes higher than one percent ( ) B/) T > 0.01), an arbitrary value, starting from the bottom right. The range of thresholds chosen within this single experiment is between 0.15 and 0.5. The automated method leads to less variation in floc size and number than a constant threshold. Overall, the automated method, which is based on a repeatable quantity, leads to improved analysis.

Dilation and Erosion

Other useful image analysis methods for the analysis of flocs are dilate and erode (see Figure 2.12). This simply means that pixels are added and then removed from the outside edge of each floc. This, for instance, can be useful in reconstructing faint flocs such as that

circled in Figure 2.10, which would otherwise be measured as many very small flocs.

Settling velocities

Two methods are used to calculate settling velocities of the flocs. Both methods make use of sequences of floc images, generally taken at one second intervals, or as movies. The first method makes use of a graphical user interface programmed in Matlab in which three images in the sequence are overlayed in different colours (Figure 2.14). The flocs are manually selected at the start of the sequence, and at the end of the sequence. The features of these flocs are calculated and returned, along with the calibrated vertical and horizontal distances travelled per unit time. As this method is interactive there is very little chance of errors being made in the determination of the floc paths.

In the second method the floc paths are determined using tracking algorithms developed in the IDL programming environment by J.C. Crocker and E.R. Weeks, University of Pennsylvania, and modified for the present research. Essentially the software calculates the possible tracks between each floc centroid and each of the other floc centroids in subsequent images. It begins to drop tracks as it becomes apparent that these tracks are not likely. That is, they are dropped if the possible tracks for a centroid in the most recent image do not follow one of the possible vectors that that centroid had been travelling previously. The floc properties, including centroid information were calculated using Matlab, the centroid information was sent to IDL for particle tracking, and then returned to Matlab where it was matched to the original floc properties. Three important parameters are sent to the programs with the Centroid data files: 1. In how many frames a floc must be present for the path to be valid; 2. In how many sequential frames may a floc be missing from the calculated path; and 3. What is the maximum displacement expected for any floc. Due to the high quality of the floc images and relatively simple floc paths the first two of the these could be set so that the flocs must appear in all of the sequential images. To determine the maximum expected displacement a series of tests was made at different values. The histogram shown in Figure 2.13 indicates that the number of pixels travelled per frame for all flocs in experiment dbd1 smoothly approaches a value less than 20 pixels.

In this case, very few flocs, if any, are expected to travel more than 20 pixels per frame interval, or 260 ：m per second. This histogram also provides evidence that the automated tracking is working well to represent the floc paths. If this were not the case then the histogram would take a staggered form and would not decrease steadily to zero. Most of the results in Chapter 4 use this automated method for calculating floc settling characteristics.

As mentioned above, a floc's illuminated surface area is changing as it spirals and tumbles through the water column. For both types of settling velocity analysis techniques the floc features are retained from the image in which the floc shows its largest surface area. The floc could conceivably be larger than that reported, but certainly could not be smaller.

Bender elements, Stiffness

Shear wave velocity, together with soil bulk density is used to calculate the shear stiffness of the soil at small strains (<0.001%). This gives an indication of the development of the soil structure. Methods of shear wave propagation in soft soils, using bender elements, were initially developed and described by Shirley and Hampton (1978). Since then bender elements have been used in many studies, generally in triaxial testing chambers, and with sand or silt. The equipment designed for the present research follows on the work of Ian McDermott (1992) which is one of few works devoted to very soft muds. The bender element testing apparatus developed for the research presented in this thesis is outlined in Figure 2.15, and the placement of the bender element transducers is shown in Figure 2.1.

Bender element transducers comprise two transverse expander plates of lead zirconate titanate (PZT4). These are bonded together in a fashion such that when a voltage is applied to the element one plate elongates and the other contracts, resulting in a bending displacement. With the bender element clamped at one end (ie. as a cantilever) the free end vibrates when energised. A small strain amplitude shear wave is generated at the vibrating end and propagates through the soil medium in a plane at right angles to the soil movement.

As shear waves do not travel through fluids, their efficient propagation through the sediment bed is dependent on the soil having a continuous structure. Weak soil structures, such as those in newly sedimented soils, will quickly attenuate shear waves (Shirley and Hampton 1978). Increasing the strength of the shear waves could easily lead to destructuring of the weak soil frame. Therefore a relatively weak signal must be transmitted (10 to 20 volts), and the received signal must be filtered and amplified.

A typical development of a shear wave signal from an initial column slurry, as observed by McDermott, is shown in Figure 2.16. This experiment, IM05, was conducted on a clayey silt collected off the coast of Isle of Man in the Irish Sea. Unlike tests in kaolinite and coarse materials, shear waves did not appear immediately in these soft mud tests. It was not until 50 hours had elapsed that the first shear waves were observed, and they were of very low amplitude, having velocities between 1 - 2 m/s which, according to McDermott, corresponds to a density of 1244 kg/m^3 and voids ratio 5.5. The high frequency signal recorded in the initial part of each trace was believed to be the compression wave generated by the shear wave transducer, and travelling both in the sediment and in the column frame. McDermott found that during the early stages of an experiment the shear wave often diminished and even disappeared altogether with no apparent explanation.

Before the bender elements could be used it was necessary to waterproof them for two reasons: to stop electrical short circuits and to protect them from sharp edged grains. Waterproofing has been accomplished by coating the elements with a two component epoxy in an aluminium mould. Araldite CY1301 resin and Araldite HY1300 hardener are used at a ratio of 5 to 1.65, as this method has been successfully used to encapsulate the elements at City University, London (Mr. L. Martyka, City University, personal communication). The mould has been designed so that the cantilevered end of the element is clamped, leaving a 1 mm space around the entire free end. This is similar to the design used by Goodman (1995), who made improvements over other designs. The epoxy is

injected into this space using a syringe. There is no need to waterproof the cantilevered end as it is separated from the column water by the element housing. A silicon spray was used as a release agent in the mould. According to Schultheiss (1983) and McDermott (1992) the resonant frequency is increased (mathematically and experimentally) to near 900 Hz by encapsulating the bender element in epoxy resin. This makes the element suitable for soft soil research as there seems to be little dispersion in shear waves propagating in clays and silts at frequencies between 600 Hz and 1.5 kHz (Shirley and Bell 1978).

After a period of experimentation using a variety of oscilloscopes and signal generators, the method adopted was to use a sine wave generator triggered by a pc at intervals set by the investigator. The materials required, and difficulties encountered, during the setup of the bender elements are documented in Lintern (2000) .

The bender elements emit both shear waves and compression waves, which travel both around the column (frame waves) and through the soil to the receiving element. For example, Figure 2.16 shows examples of shear waves collected by McDermott (1992). In this case the shear waves are not obscured by the initial compression or frame waves, but it can be imagined that the latter sometimes encroach on the arrival of the shear waves, particularly if the shear waves are moving very quickly, or if the frame waves are reverberating around the column. In order to minimise the effect of these frame waves the elements have been housed in epoxy resin which fits a receptor port on the column wall, and is completely sealed via “O” rings. In addition to the frame waves, it was found that electromagnetic and physical disturbances in the lab, even as little as the presence of the observer or a colleague working in an adjacent room, were enough to upset the test results. This was particularly problematic when the pumps or stirrers of the sedimentation system were operating. The random noise was largely overcome by averaging the incoming shear wave signal over as many as 75 samples.

By the averaging method, the frame wave reverberation was enhanced, along with the shear wave signal. Figure 2.17 shows the arrival of a shear wave in a comparatively dense mud

that was not confined in a column. This appears to be of very low frequency (around 80 Hz), and further tests showed that the frequency of the shear wave could normally be expected to be well below 1000 Hz, whereas the ambient frequency in the column and that of the compression waves could be expected to be considerably higher. A software lowpass filter was designed to keep only the components of interest in the received signal. For this, the Matlab Signal Processing Tool GUI was used to design a lowpass Chebyshev Type II filter with a passband of 0 to 1245 Hz and a cutoff band of 3271 Hz (Figure 2.18). Several other filter types were tried, but the Chebyshev gave the shortest transition band (rolloff), which became important where the column reverberation was similar in frequency to the bender element response, as was apparent in initial tests using clay samples within and without a column. The tradeoff is that the gain in the passband is not constant, however since the amplitude of the shear wave is of little interest this type of filter is well-suited to the task.

Shear wave velocities, V_s, are calculated for the soil by dividing the distance travelled across the column by time taken. This distance of approximately 65 mm can be measured accurately within 0.5 mm, which gives an accuracy for the velocity better than ±1%. From this an estimate of small strain shear stiffness may be calculated using bulk density, ρ, by the following equation:

$$V_s = \left(\frac{G_{max}}{\rho} \right)^{0.5} \tag{2.2}$$

Sands typically have velocities ranging from 40 - 100 m/s (Sculthеiss, 1983, Shirley and Bell, 1978); soft soil silts typically have velocities in the range 10 - 40 m/s (Shirley and Bell, 1978; Briggs, 1991); soft soil clays have velocities ranging from 1 - 40 m/s (Shirley and Hampton, 1978; McDermott, 1992).

In the present research a testing system has been designed to take advantage of modern computer data acquisition and control. A high speed Computerboards data acquisition card

is used to trigger, receive and filter the signal through a Matlab Data Aquisition script and a Visual Basic user interface.

2.7 Data Manipulation

Early in the work it became apparent that data storage, processing and analysis would be one of the chief obstacles. Over 100 Gigabytes of data has been collected, and some of the more complex image analysis methods require many continuous days of work for the most modern computers available. X-ray, pore pressure and erosion data were dealt with efficiently by using Visual Basic Macros. However, to reduce the size of, and improve access to, the image and bender element data, Matlab structures have been created. For instance, an image was first binarised using the automatic thresholding technique, and each of the flocs in that image was labelled with a number. A data structure for a single image contains all of the needed information for each floc. Table 2.0 presents each of the calibrated measurements, along with its units and its Matlab structure name. This use of data structures minimised the need to repeatedly do the heavy image processing.

Table 2-1 Calculations made for flocs, and the associated Matlab structure name.

Description	Units	Structure name
Distance travelled per frame	pixels/frame	XYPixPerFrame
Centroid positions of the flocs, relative to the lower left corner in the first and last images of a sequence	: m	FirstXCentroid, LastXCentroid, FirstYCentroid, LastYCentroid
Floc **Areas**, based on no. pixels.	: m^2	Area
Equivalent spherical diameter, calculated from Area	: m	EquivDiameter
Major axis length	: m	MajorAxisLength
Minor axis length	: m	MinorAxisLength
Eccentricity (elongation)	none	Eccentricity
Orientation	degrees	Orientation
Convex Area of the smallest convex polygon that can contain the floc	: m^2	ConvexArea
Filled Area of the bounding rectangle for each floc.	: m^2	FilledArea
Euler Number, number of objects minus number of holes in objects	none	EulerNumber
Solidity = convex area / filled area	none	Solidity
Extent = Area / filled Area	none	Extent
Frame Velocity in the **Y** direction	: m/frame	YDistperFrame
Frame Velocity in the **X** direction	: m/frame	XDistperFrame
Settling direction	degrees	SettlingDirection
Frame Interval	s	frameinterval
Settling Velocity (Y direction)	: m/s	SettlingVelocity
Velocity in **X** direction	: m/frame	XVelocity
Effective Density of flocs	Mg/m^3	EffectiveDensity

Description	Units	Structure name
Fractal Dimension	none	FractalDimension
Filename image number	none	filenum
Matlab encoded **Date**	none	datenum
Elapsed Time from start	hours	elapsedtime
Porosity	none	Porosity
Void Ratio	none	VoidRatio
Floc volume fraction = Solid volume over floc volume	none	FlocVolumeFraction
Floc Solids Volume	m^3	FlocSolidsVolume
Image volume fraction = volume of flocs over volume of image	none	ImageVolumeFraction
Permeability of flocs	m^3/s	Permeability
Threshold for binarising image	none	Threshold
Overall **brightness** of image, by summing all grey levels	unknown	Brightness
Minimum floc velocity (usually upwards)	: m/s	MinVelocity
Minimum Distance between each of the flocs.	: m	MinimumDistance

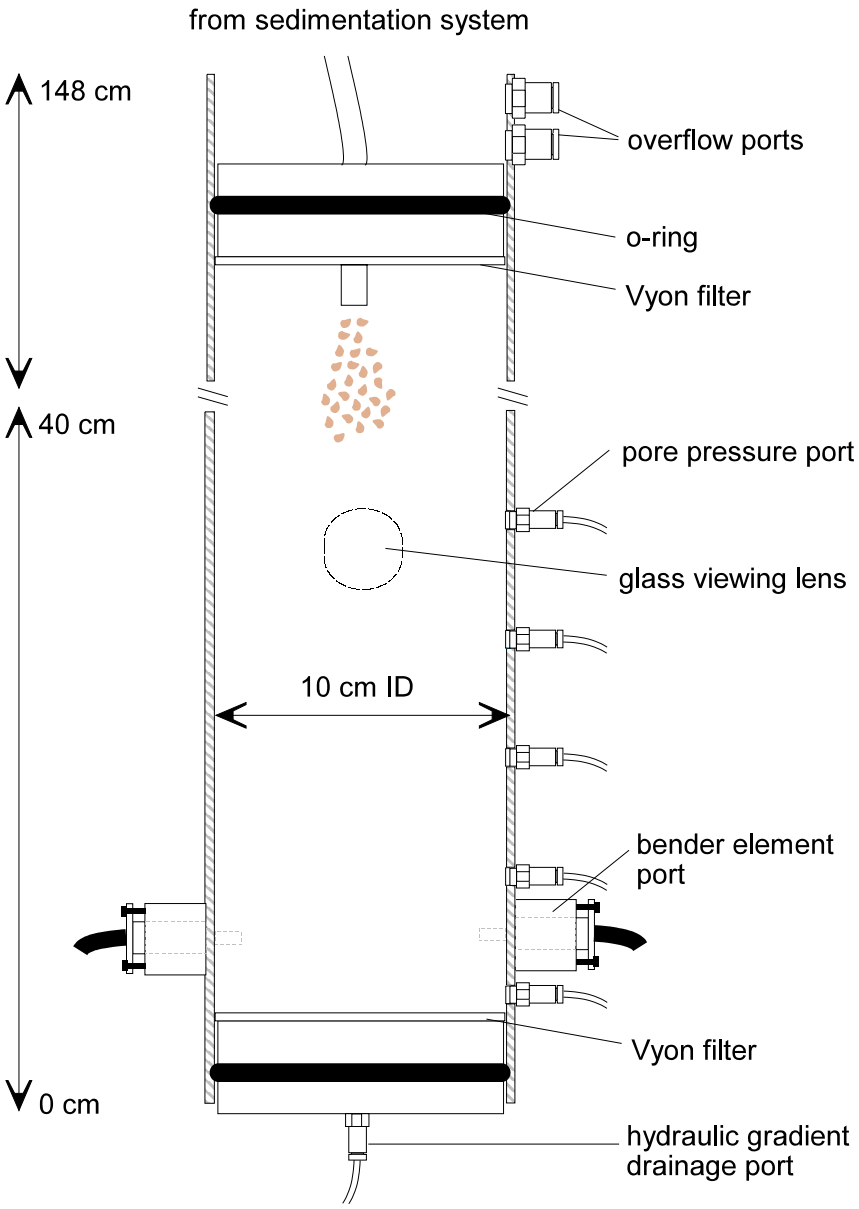

Figure 2.1 Schematic of the column setup. The break in the column walls in the figure represents where the column can be separated for easier access to the soil beds at the completion of the experiment, as well as indicating a portion of the column that is not shown in the figure.

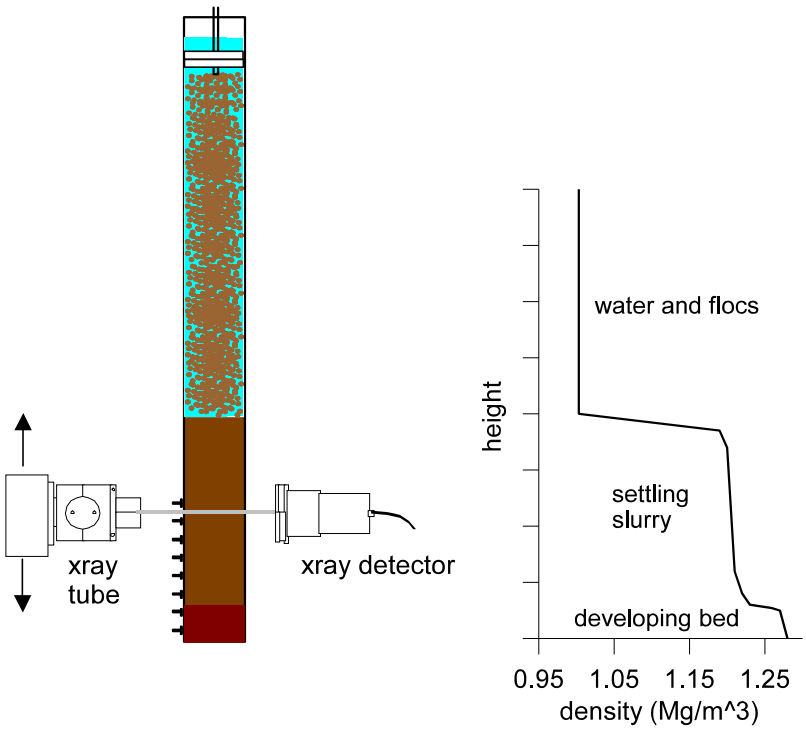

Figure 2.2 Schematic of the x-ray apparatus, showing a typical density profile to match the developing bed, the sedimenting slurry and the water in the column.

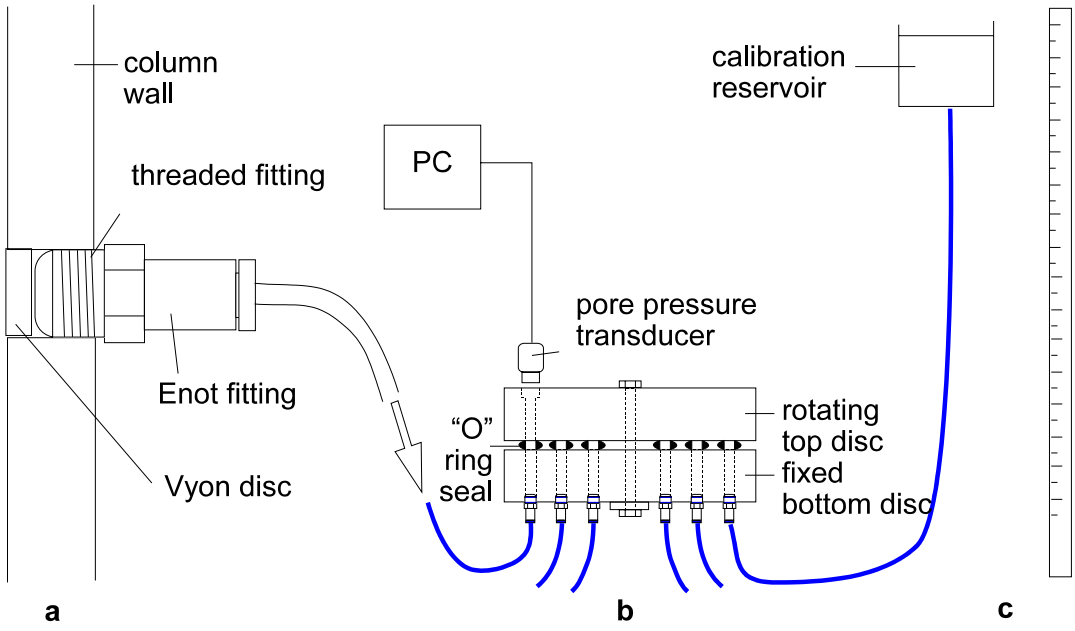

Figure 2.3 Measurement of pore pressure in the column (a), through a multiplexor to a single transducer (b). Calibration is made with a raising and lowering a head of water through a known distance (c).

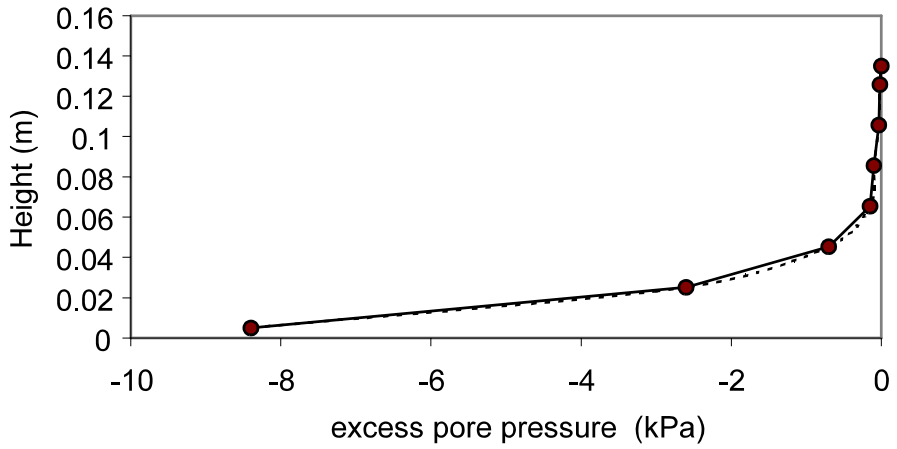

Figure 2.4 Experiment dbd2 excess pore pressures, showing a smooth fit and a linear interpolation.

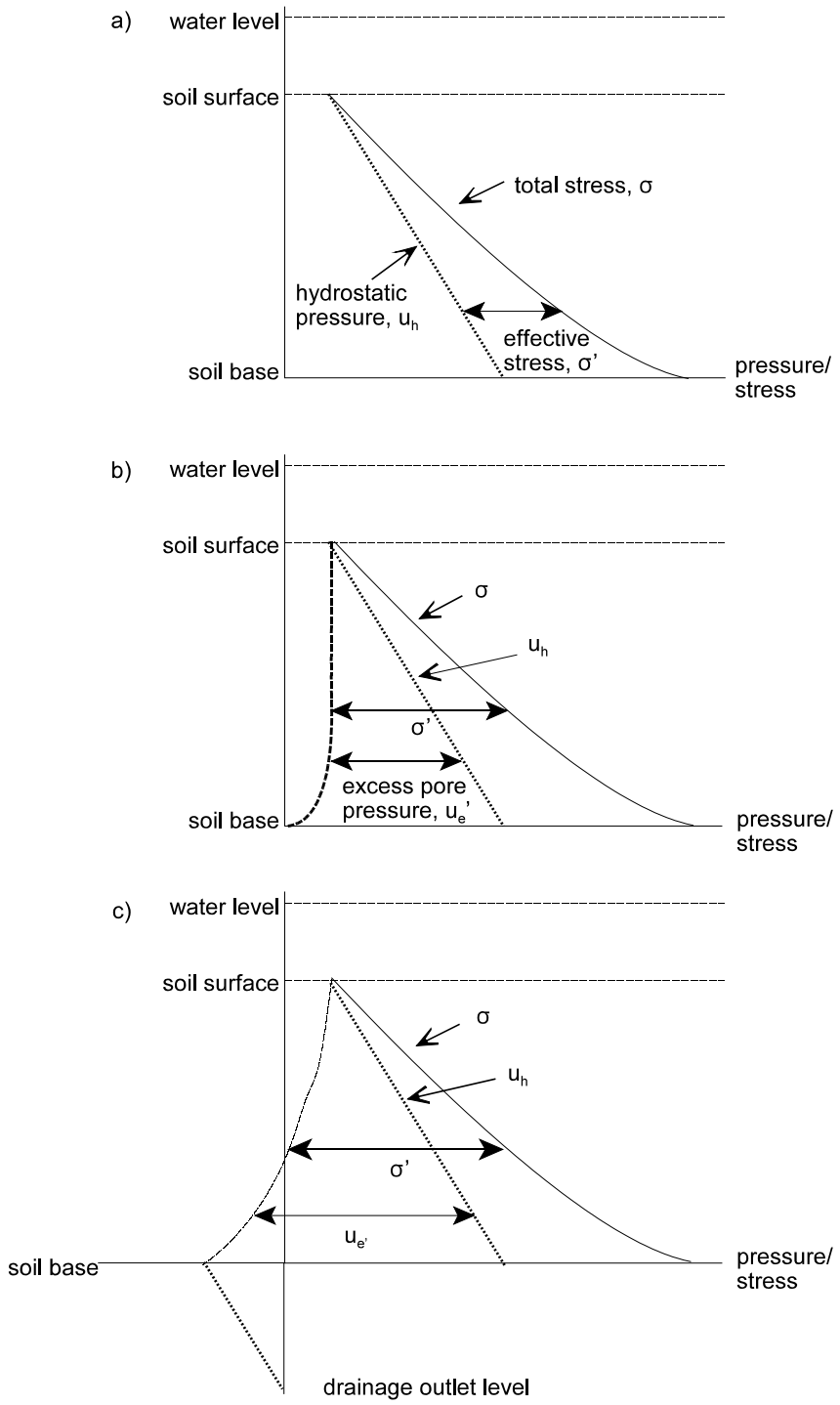

Figure 2.5 Development of effective stress by the application of a hydraulic gradient. A description is given in the text.

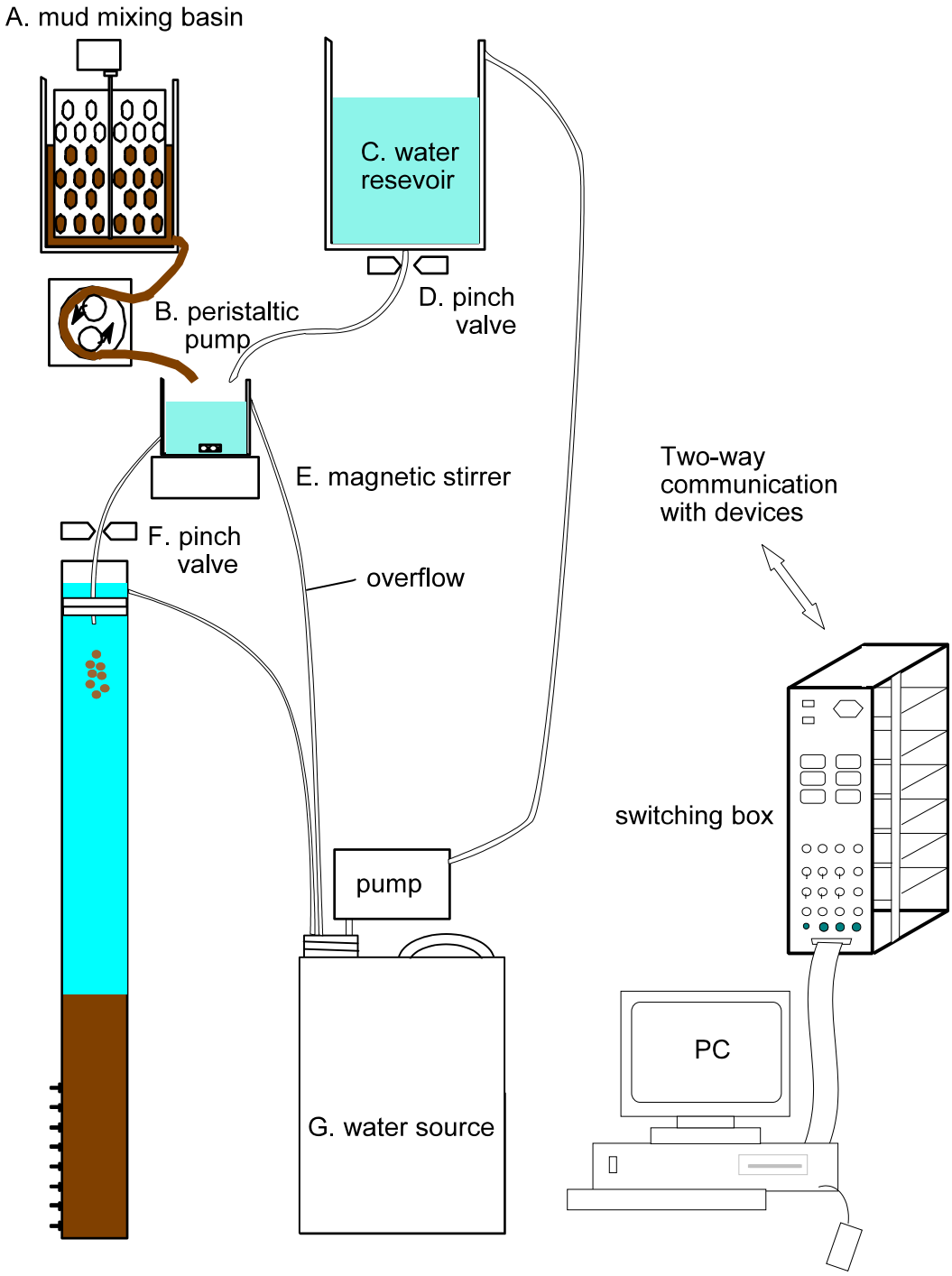

Figure 2.6 The sedimentation system. Each of the pumps and valves is operated by a computer through a switching box. Built in safety features are described in the text. Components of the video and x-ray systems are also shown.

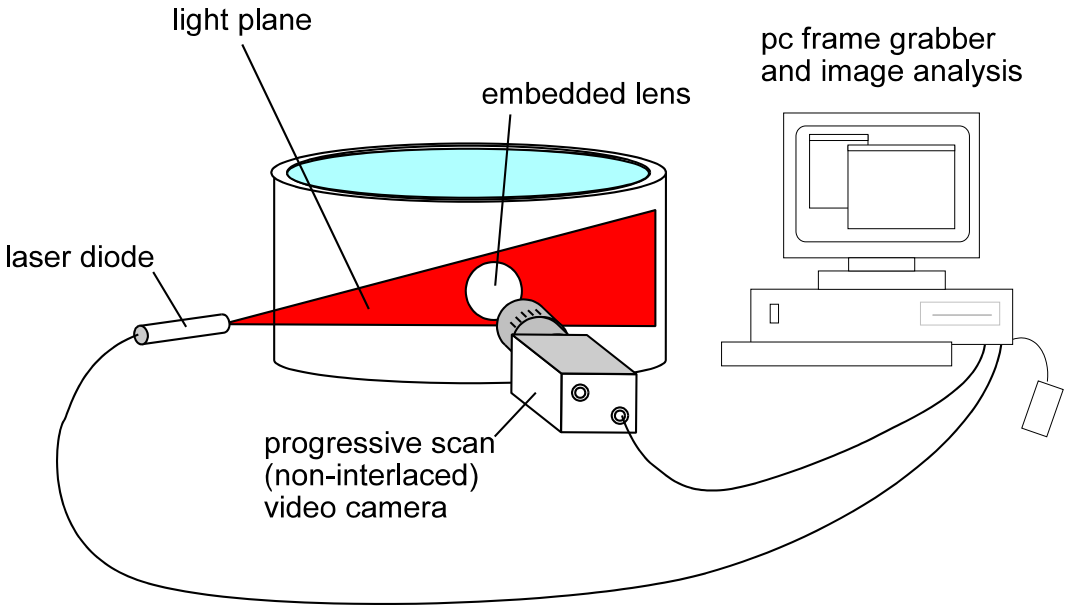

Figure 2.7 Schematic of the image acquisition and analysis hardware.

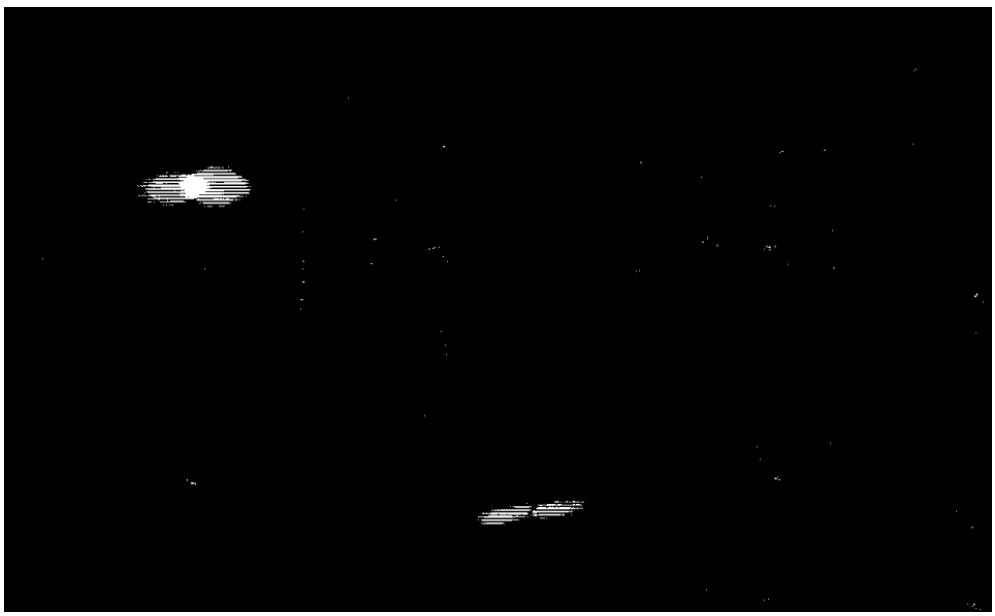

Figure 2.8 Image taken with interlaced camera double exposes fast moving flocs

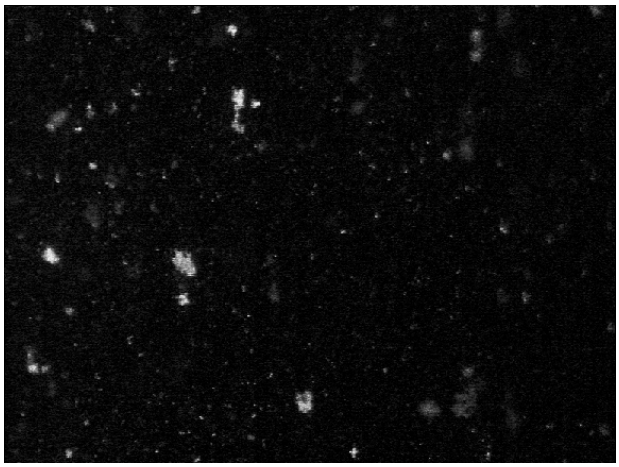

a) dbd3floc_0196A.bmp

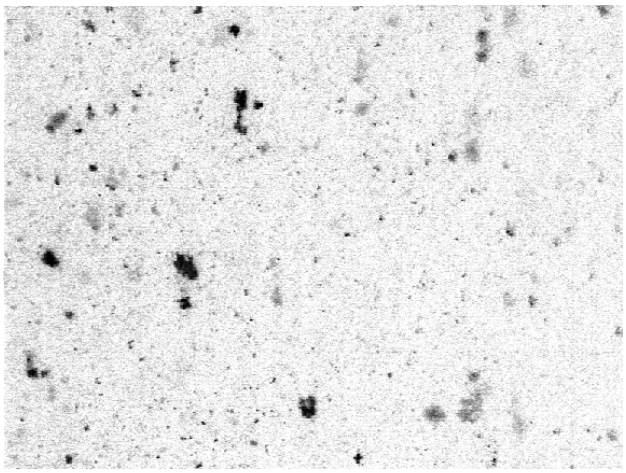

b) negative image

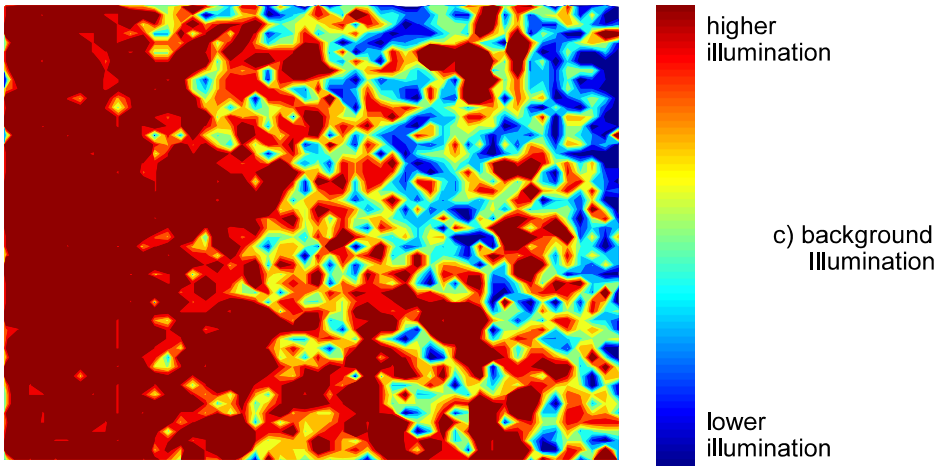

Figure 2.9 Determination of non-uniform background illumination.

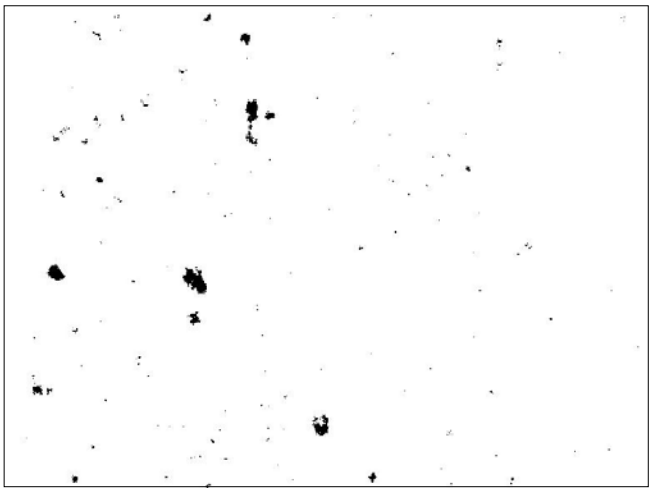

A) dbd3floc_0196A.bmp binarised at 0.10

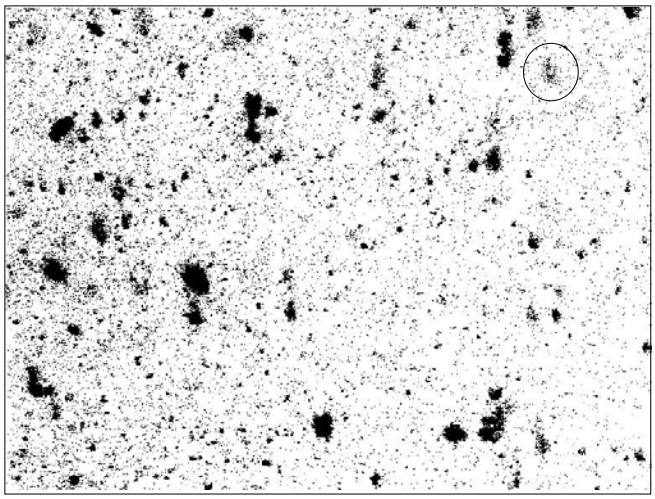

B) dbd3floc_0196A.bmp binarised at 0.40

Figure 2.10 Effect of different threshold values.

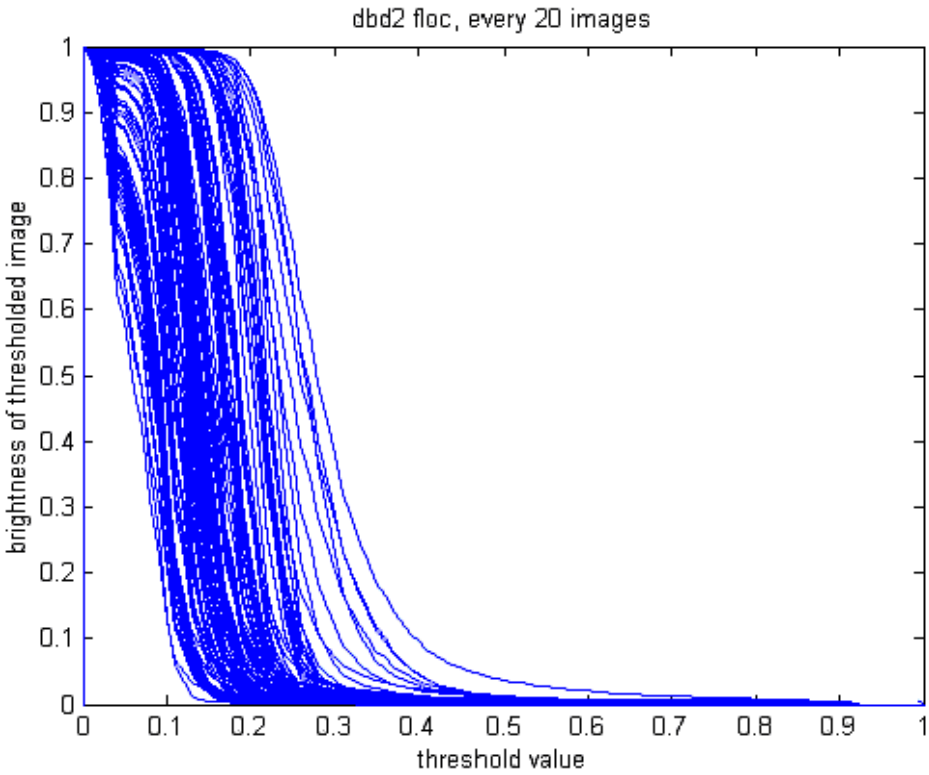

Figure 2.11 Effect of changing threshold on the brightness of the binarised image, and its variation throughout an experiment.

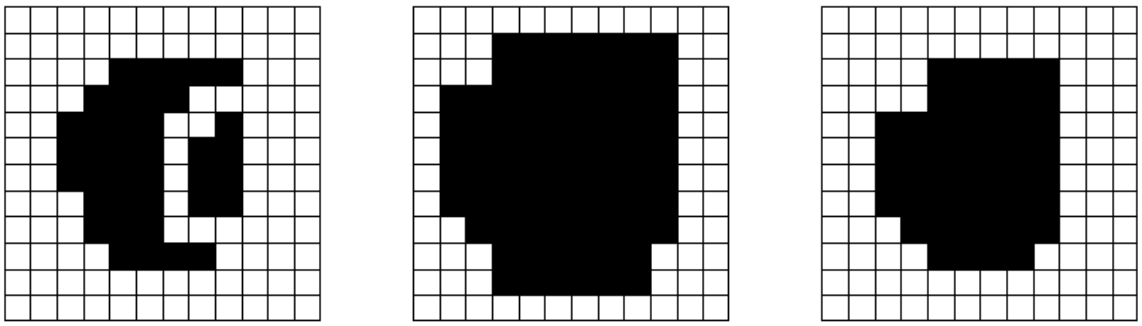

A. Binarizing may cause a faint floc to appear in two sections.

B. Dilate adds an outer layer of pixels to each floc, combining the two.

C. Erode removes the outer layer, making the size and shape more comparable to the original floc

Figure 2.12 Erode and dilate image processing techniques to enhance floc images

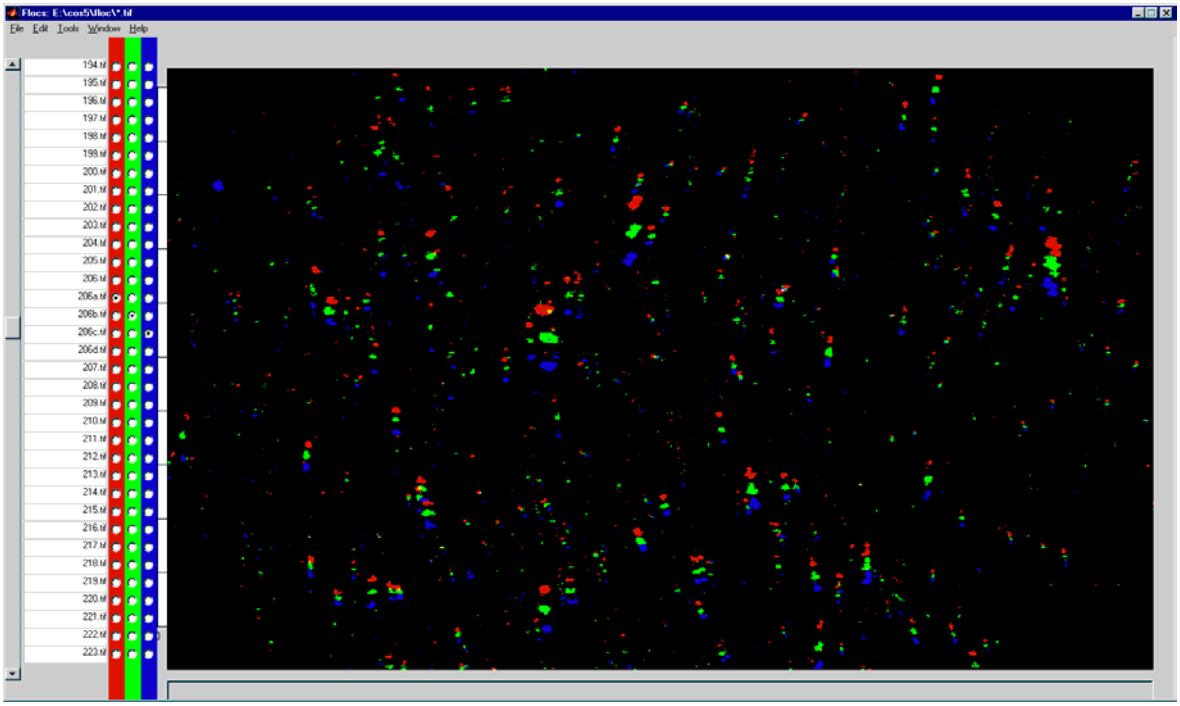

Figure 2.14 Graphical user interface programmed in Matlab to choose a sequence of files, calculate settling velocity by pointing to a floc in the first and last frame.

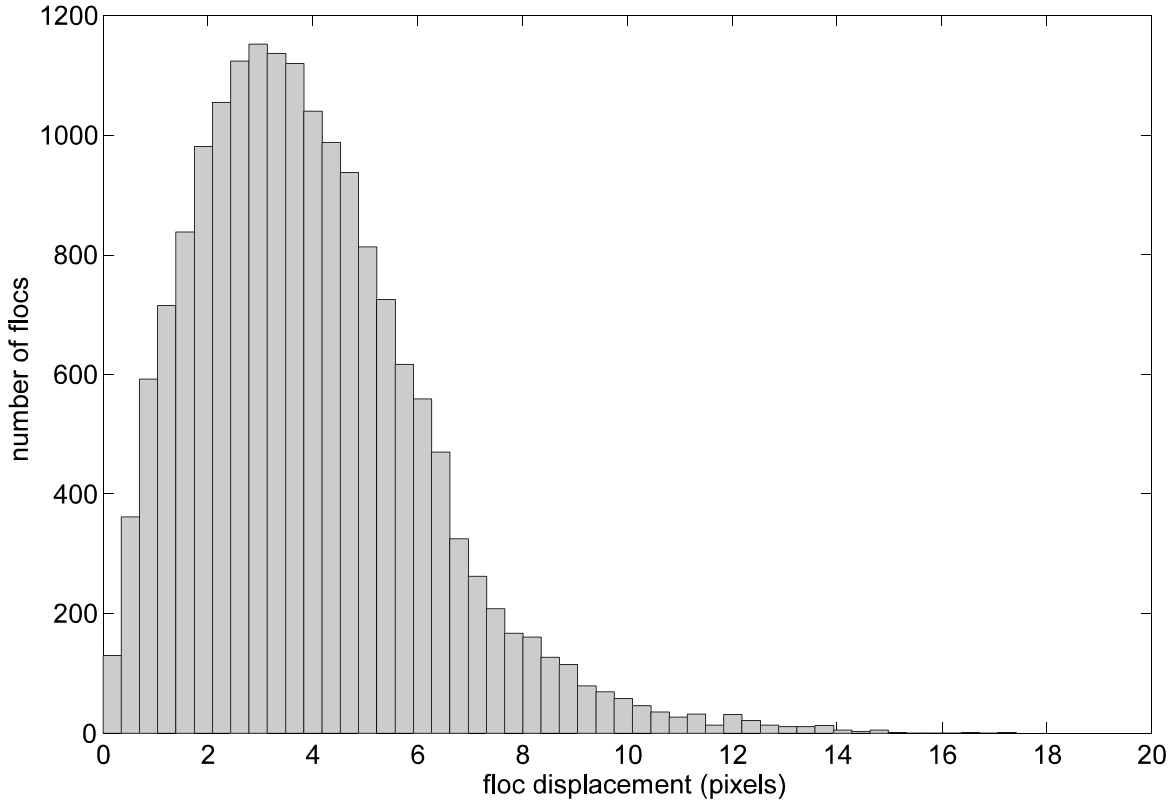

Figure 2.13 Histogram of floc velocities measured by automated tracking software.

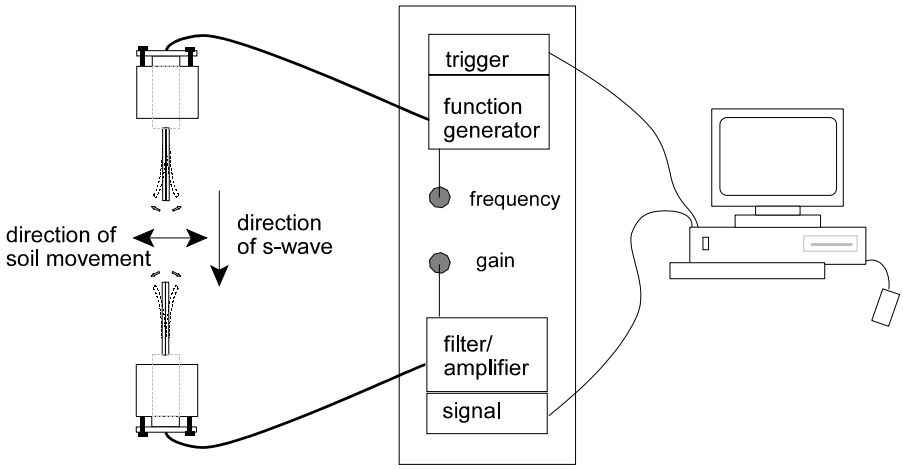

Figure 2.15 Schematic of bender element shear wave measurement apparatus.

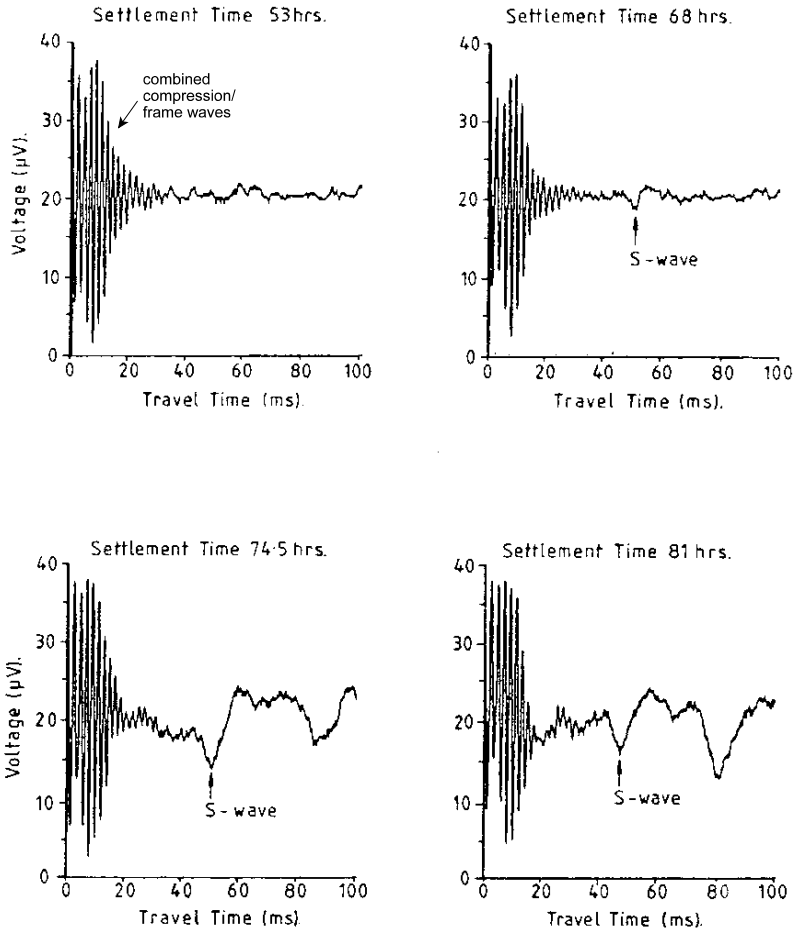

Figure 2.16 Development of a shear wave in a soft sediment. After McDermott, 1992.

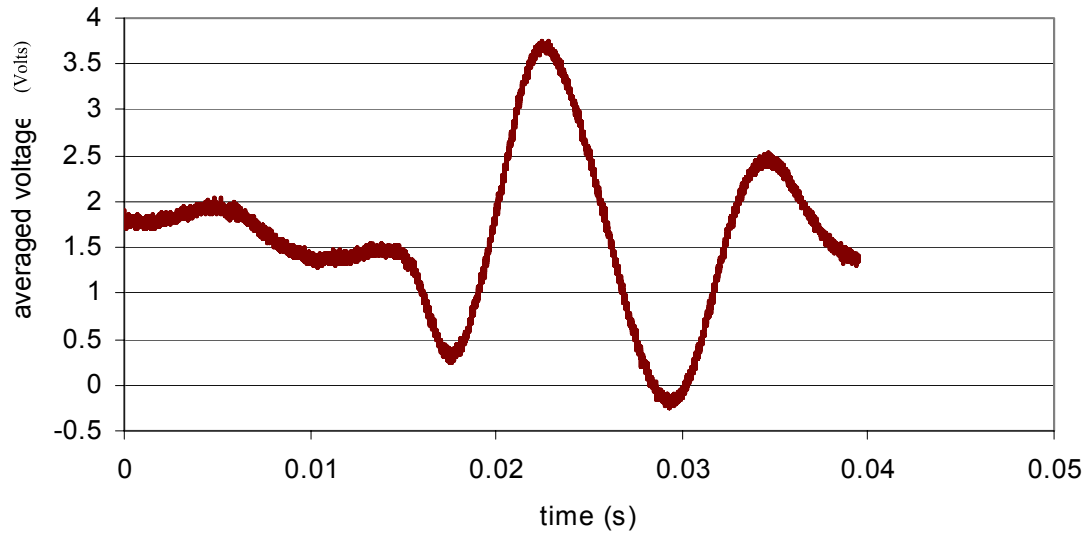

Figure 2.17 Shear signal received through clay with no containing frame. The received signal has a frequency of approximately 80 Htz.

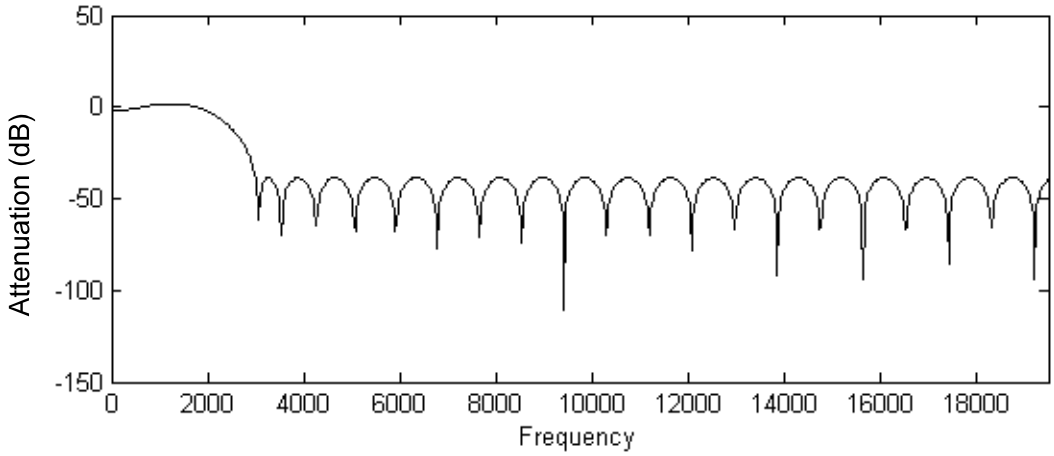

Figure 2.18 Lowpass Chebyshev Type II filter designed for processing of bender element signals.

Chapter 3 Soil Properties and Experiments

3.1 Soil Property Tests

Several types of mud are used for comparison in this research, including: Tamar Estuary (experiments tam, cos, isis), Weston-Super-Mare (wsm), Combwich (cmw) and Dibden Bay (dbd and did). Tamar Estuary clay was chosen as the main test soil, since its behaviour in situ and in the lab has been documented by researchers at the University of Plymouth and at the Plymouth Marine Labs, and since it was to be used by other researchers in the COSINUS project (eg. Lintern 2000). Dibden Bay mud came to be used as a result of a contract between ESSO Petroleum and the Department of Engineering Science, in which ESSO required information about the nature of flocculated mud near the cooling intake valves of its Dibden Bay Petroleum refinery (Sills and Lintern 2001). Combwich and Weston-Super-Mare muds were chosen since many studies had previously been made on these muds in Oxford.

Analyses have been performed to determine the organic content, the grain size distribution, and the particle density of the muds (Table 3.1). Cone penetration liquid limit and plastic limit tests have also been performed to determine the engineering properties of the soil, and the resulting plasticity indices are shown in Figure 3.1.

X-ray diffraction and mineralogical tests have been conducted on Tamar, Weston-super-Mare and Dibden Bay muds. These reveal that for the clay fraction all three of these soils are dominated by illite (Figure 3.2). Kaolinite and chlorite are also important components of the fine fraction. The results of the XRD for Tamar mud in this study are slightly at odds

Table 3.1 Results of soil property tests.

Soil	Type	D_{50} (：m)	%clay	LL	PL	PI	s.g.	%Org
Tamar	Silty clay	22	23%	88%	64.1%	23.9%	2.67	20%
Combwich	Silty clay	-	40%	62-73%	28-32%	30-40%	2.66	2-5%
WestonSM	Silty clay	-	15%	53%	23%	30%	2.65	NA
Dibden	Clayey silt	2-3	97%	65%	35%	30%	2.47	7.2%

with those reported by (Stephens *et al.* 1992), who report significant quantities of montmorillonite near the town of Calstock, where the mud for this research was sampled. In addition to illite, kaolinite and chlorite, Dibden Bay mud is characterised by a high proportion of randomly interstratified illite and smectite. The major elements for all three muds are quartz, aluminium oxide and pyrite. Dibden Bay and Weston-super-Mare muds also have a relatively high proportion of calcite. This may indicate the existence of grossular garnet (Ca-Al ($3CaO\text{-}Al_2O_3\text{-}3SiO_2$)) as the dominant accessory mineral.

Automated sediment size analysis was carried out on Tamar and Dibden Bay muds (the two main muds studied) by means of two pieces of apparatus- The initial measurements were made with a CILAS 920 laser particle sizer at the Department of Geography, University of Oxford, and later measurements were made using a Sedigraph 5100 x-ray particle sizer. Results of the size analysis are presented in Table 3.1. For both methods the samples were dispersed in a dilute aqueous solution of Sodium-Hexametaphosphate in a sonic bath for approximately 10 minutes, and again immediately prior to measuring for approximately 30 seconds. Due to restrictions on this equipment it was necessary to remove the coarse fraction above 355 ：m using a wet sieving technique.

For Tamar mud, the median particle size is approximately 22 ：m, 10% of the particles are smaller than 3.3 ：m and 90% of the particles are smaller than 66.6 ：m. Dibden Bay mud showed a variety of primary particle diameters in different tests, however in tests where extra care was taken in dispersing the sediments (including the removal of organic material) the median diameter was consistently around 2-3 ：m (the grainsize distribution is shown along with the floc distribution in a later chapter. Grainsize distributions are not readily available for Weston-super-Mare mud, however Munachen (in prep) performed extensive classification tests on this sediment and found it to be relatively well graded consisting of 18% sand, 67% silt and 15% clay. Combwich sediment has been classified as a silty clay.

Organic content analyses were conducted according to Head (1992), using the hydrogen

peroxide decomposition method. An average of three subsamples of Tamar mud is reported in Table 3.1 as 20% organic matter by weight. These values are higher for Tamar mud than the weight loss due to ignition values previously reported for samples from a nearby site (Stephens *et al.* 1992), and those shown in Figure 3.2b (L.O.I.) but in keeping with the values of 15 - 20% determined by other COSINUS project participants (Bill Roberts, HR Wallingford, personal communication). Organic contents for Combwich and Dibden Bay muds are 2 to 5% and 7.2 % respectively (Gilliane Sills, personal communication), and those for Weston-super-Mare are thought to be similarly low.

3.2 Experimental Information

Slurry deposited versus slowly sedimented experiments

As the experiments reported within this thesis have been funded through a variety of contracts, they have been conducted in a variety of manners. Table 3.2 presents the experiment names associated with each mud type and the specific behaviours examined in each suite of experiments. Much more detail is given for each of the measurements made in Table 3.3. It is important to point out (as has been done in Chapter 2) that some of these experiments were conducted by depositing a slurry of known concentration into a settling column (these are termed slurry experiments), whereas the majority made use of the automated sedimentation system (slowly deposited experiments).

Of the slurry experiments, isis experiments were generally prepared to make measurements of resistance to erosion, and tam experiments were generally set up to test the bender element apparatus. This thesis also makes use of exp slurry experiments, which used Tamar mud and were conducted by Murphy (2001) and dib slurry experiments conducted by Sills (2001). Other slowly deposited muds XRCI, reported in later chapters have been taken from Sills and Thomas (1984). A hydraulic gradient was applied to the beds to extend the stress levels in the slowly deposited experiments cos16, wsm1 and cmw1, and in all the dbd experiments.

Setting up the experiments

Table 3.2 Types of experiments

experiment name - mud type	number and type of experiments	investigations
cos - Tamar	16 flocculated	flocculation, consolidation, shear wave.
tam - Tamar	5 slurry	consolidation, shear wave, erosion.
isis - Tamar	6 slurry	consolidation, erosion
dbd, dib - Dibden	4 flocculated (dbd) 2 slurry (dib)	flocculation, consolidation, shear wave, shear vane.
cmw - Combwich	1 flocculated	consolidation, shear wave
wsm - Weston-super-Mare.	1 flocculated 1 slurry	consolidation, shear wave

All experiments required that mud was mixed with water. In all cases seawater was manufactured with deaired and deionised water and Tesco brand sea salt. The seawater contained approximately 10 ppt by weight salt. Densities of the starting slurries (g/cm^3) were measured using a Paar density meter for the less dense slurries, or by gravimetric methods for the more dense slurries. For slurry experiments the mud was mixed for a period of several hours before being added to the column. For slowly deposited experiments the slurry was also mixed beforehand, and was kept stirred during the experiment in the overhead mixer. In preliminary experiments the mud was sieved first at 63 μm, in an attempt to retain mainly cohesive material. However, it was decided that this would obliterate the natural properties of the sample (structure and salinity). Instead, for the experiments reported here, only obvious large items (shells, sticks, pebbles etc.) were removed by hand so that they did not block the sedimentation system. There were, in fact, very few of these large items.

Often two slowly sedimented experiments were running concurrently, and sometimes three experiments were running. Alongside these longer term experiments, there may have been slurry experiments underway. This led to complications since there was only one x-ray device, one signal generator for the bender elements and two cameras. In addition, since one computer was used to operate all of the apparatus there was a restriction on the number

of system timers that could be used accurately from the CMOS clock under Windows. As a result measurements often had to be made in a staggered fashion. The pore pressure and floc measurements are made from the start of the experiments. Shear wave measurements were made some hours to days later, once the sediment had reached the bender elements, but the connections to the signal generator had to be swapped from one experiment to another throughout the experiments. It was felt that it was important to leave the cameras in place (focussing on the same point) during sedimentation, and since taking x-ray measurements would have meant moving the cameras there are few experiments where x-ray measurements are available during sedimentation. Experiments cos4, cos13 and cos17 were conducted one at a time, allowing both cameras and the x-ray to operate simultaneously, and providing information about the development of the beds during sedimentation.

Variation in sedimentation rate

Figure 3.3 illustrates the range of sedimentation rates and bed heights tested for slowly sedimented experiments. There are too many experiments to create a clear plot containing all of the experimental information. Generally though, the experiments cos16, wsm1 and cmw1 were deposited most quickly, dbd experiments had middle to high sedimentation rates, and the remaining cos experiments (not all shown) were spread throughout the range. Comparisons between the bed heights, sedimentation rates and settlement rates are made in Chapter 5, where the bed heights are more appropriately plotted a few experiments per figure. Table 3.3 outlines the conditions under which the tests were made. Slurry experiments are highlighted with shading. The table includes, amongst other things, the sedimentation height achieved (or start height in slurry experiments), the average rate of sedimentation, the height achieved by the bed under self-weight consolidation and the height achieved after the application of a hydraulic gradient.

3.3 Units and conversions

This work follows closely after work that has previously been conducted at Oxford. Therefore, in most cases, the decision has been made to use the dimensional units that are

most frequently published from the Oxford work. However, concepts (and sometimes data) have been borrowed from other scientific fields, most notably chemical engineering. The measure of concentration is often reported in different units from one scientific field to the next. Normally, in this thesis, concentration is reported as g/l for the flocculated suspensions, and as bulk density (Mg/m^3) or void ratio (dimensionless) for the beds. Chemical engineers often use the porosity, or its inverse, the solids volume fraction. In order to make it easier for the reader, conversion charts have been given in Figure 3.4. These use bulk density as a basis from which to convert to other units. The conversions are slightly different for each of the mud types because of the difference in the specific gravity of the solids (G_s) of the muds. However Tamar ($G_s = 2.67$), Weston-super-Mare ($G_s = 2.65$) and Combwich ($G_s = 2.66$) have such similar G_s values that they may accurately be converted using the chart in Figure 3.4a. Dibden Bay mud, with a much lower G_s ($G_s = 2.47$) may be converted using the chart in Figure 3.4b.

Table 3.3 Details of the experimental conditions and types of measurements made. Slurry experiments have a shaded background.

Name	initial density	expt. time (h)	sedn. time (h)	sedn. rate (mm/day)	sedn. or initial height (m)	self weight height (m)	hydraulic gradient height (m)	floc images (no.)	bed images (no.)	density profiles (no.)	pore pressure (y/n)	shear wave tests (y/n)	erosion test (y/n)	notes
cos1	1.018		-	9.8	0.126	0.109	-	46	3	7	y	n	n	images of shear layers
cos2	1.246		320.0	3.8	-		-	none	n	4	n	y	paddle	paddle mixer images
cos3	1.246		320.0	4.1	0.054	0.048	-	10	7	4	n	2	paddle	paddle mixer images
cos4	1.090		336.0	12.9	0.180	0.18 ?	-	64	91	-	4	2	-	bed profile images
cos5			1344.4	3.9	0.220	-	-	488	50	2	1	1	49	bed profile images
cos6	1.090		360.0	7.0	0.105	0.102	-	153	-	3	cos6c	-	68	streamer images
cos7	1.090		235.3	11.6	0.114	0.109	-	108	55	2	1		y	
cos8	1.011		207.5	22.6	0.195	0.195	-	389	-	cos8a	-	-	-	-
cos9	1.118		360.0	2.5	0.038	-	-	467	200		-	-	-	-
cos10	1.118		78	21.5	0.070	-	-	12	202	n	n	n	n	-
cos11	1.12		69.4	41.2	0.119	0.096	-	20	1	1			-	image of shear layers
cos12	1.120		na	5.9	0.057	na	-	540	-	1	logged	1	-	abondoned after 7 days
cos13	-		137.6	35.8	0.205	0.197	-	-	-	7	7	-	-	-
cos14	-		-	-	-	-	-	160						-
cos15	-		-	-	-	-	-	165						-
cos16	1.052		17.0	515.4	0.375	0.206	0.153	8	659	8	logged	3	-	4 floc movies void ratio analysis
isis1	1.137		168.0	slurry	0.201	0.115	-	-	-	2	-	-	11	worms
isis2	1.164		312.0	slurry	0.188	0.122	-	-	-	-	-	-	100	-
isis3	1.164		456.0	slurry	0.197	-	-	-	-	yes	-	1	5	density during erosion
isis4	1.164		768	slurry	0.190	-	-	-	-	4				-
isis5	1.080		120	slurry	0.182	0.138	-	-	-				1	-

Name	initial density	expt. time (h)	sedn. time (h)	sedn. rate (mm/day)	sedn. or initial height (m)	self weight height (m)	hydraulic gradient height (m)	floc images (no.)	bed images (no.)	density profiles (no.)	pore pressure (y/n)	shear wave tests (y/n)	erosion test (y/n)	notes
isis6	1.162		1392	slurry	0.196	0.136	-	-	-	-	-	-	6	erosion images poor
isis7	1.11		720	slurry	0.262	-	-	-	211	-	-	-	-	quality column image
tam1	-		-	slurry	-	-	-	-	-	2	-	-	-	-
tam2	-		-	slurry	-	-	-	-	-		-	-	-	-
tam3	1.131		360	slurry	0.123	0.122	-	-	-	8	-	-	10	images of bed surface
tam4	-		-	slurry	-	-	-	-	-	-	-	y	-	shear wave time lapse
tam5	1.113		1032.0	slurry	0.205	-	-	-	163	y	-	y	-	worms
cmw1	1.052		14.8	789.0	0.485	0.216	0.142	-	867	12	logged	n	-	-
wsm1	1.052		17.0	408.5	0.270	0.133	0.100	-	195	8	logged	n	-	
wsm2	-		-	slurry	-	-	-	-	-	-	logged	y	-	-
dbd1	-		311.1	17.1	0.221	0.200	0.130	-	-	-	-	-	-	-
dbd2	-		807.0	6.2	0.209	0.177	0.137	-	-	-	-	-	-	-
dbd3	-		456.3	9.4	0.179	0.156	0.108	-	-	-	-	-	-	-

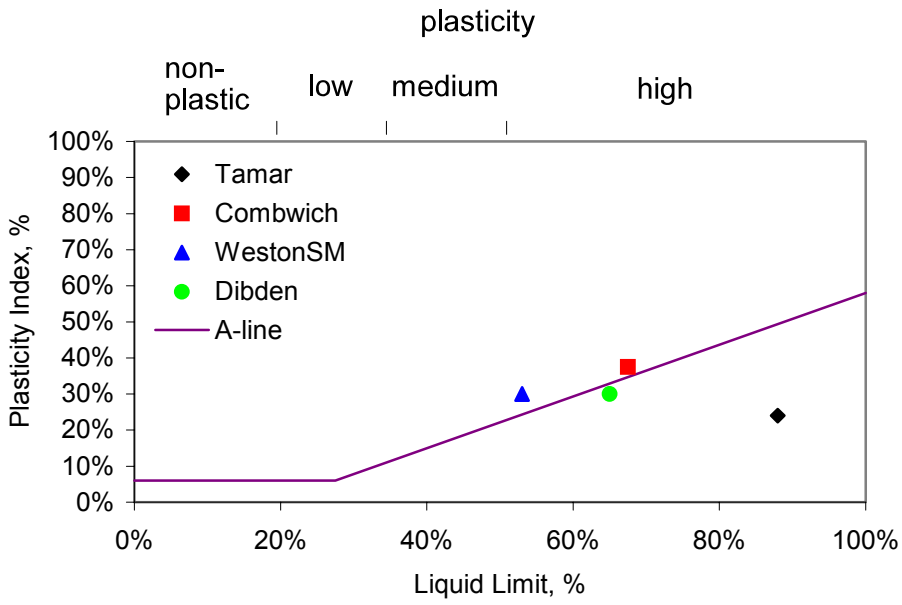

Figure 3.1 Results of Atterberg limit tests.

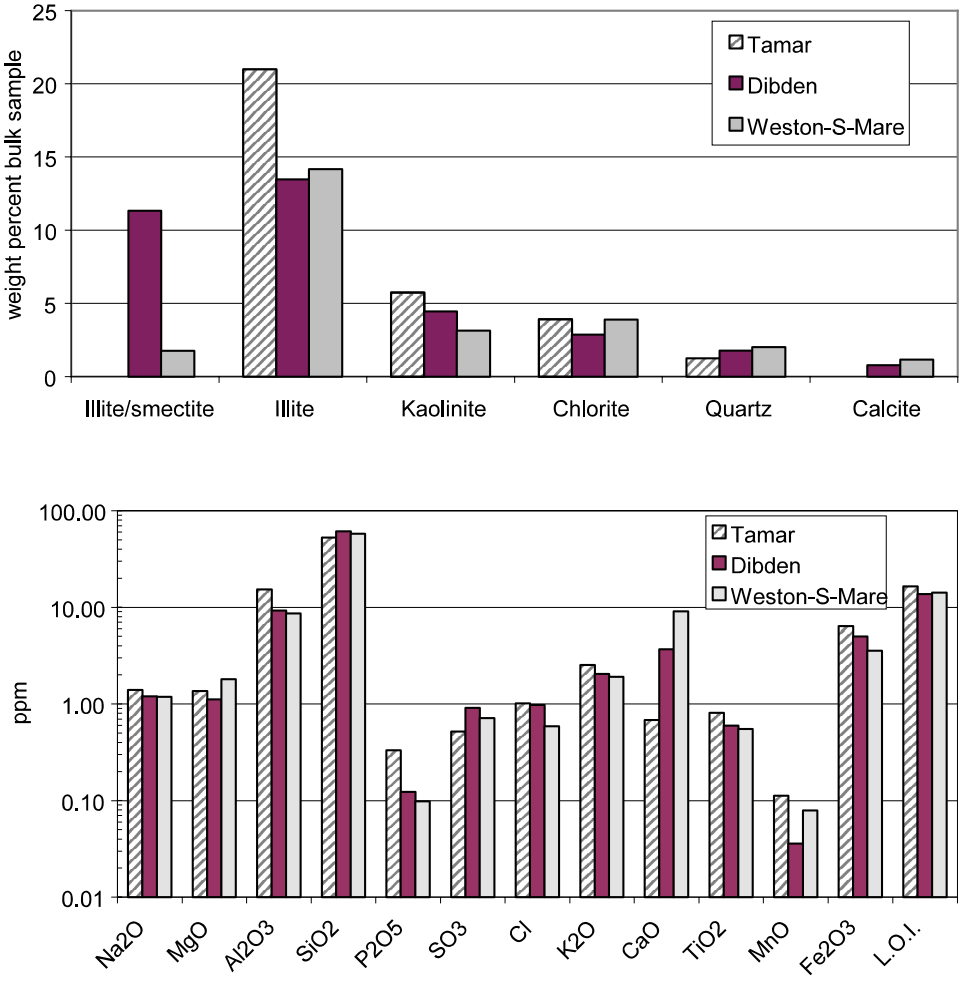

Figure 3.2 a. Clay types and b. elemental analysis for Tamar, Dibden Bay and Weston-super-Mare muds. Percent loss on ignition (L.O.I.) also shown in b.

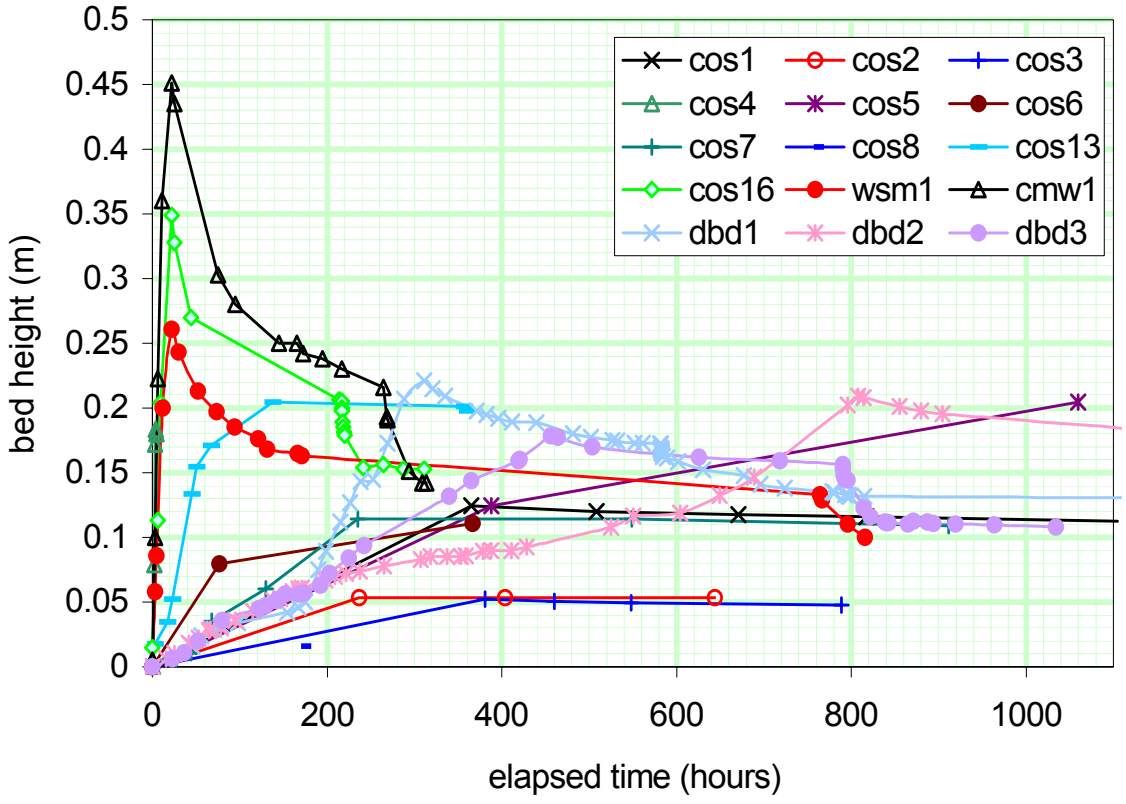

Figure 3.3 Bed heights during sedimentation and consolidation for all experiments.

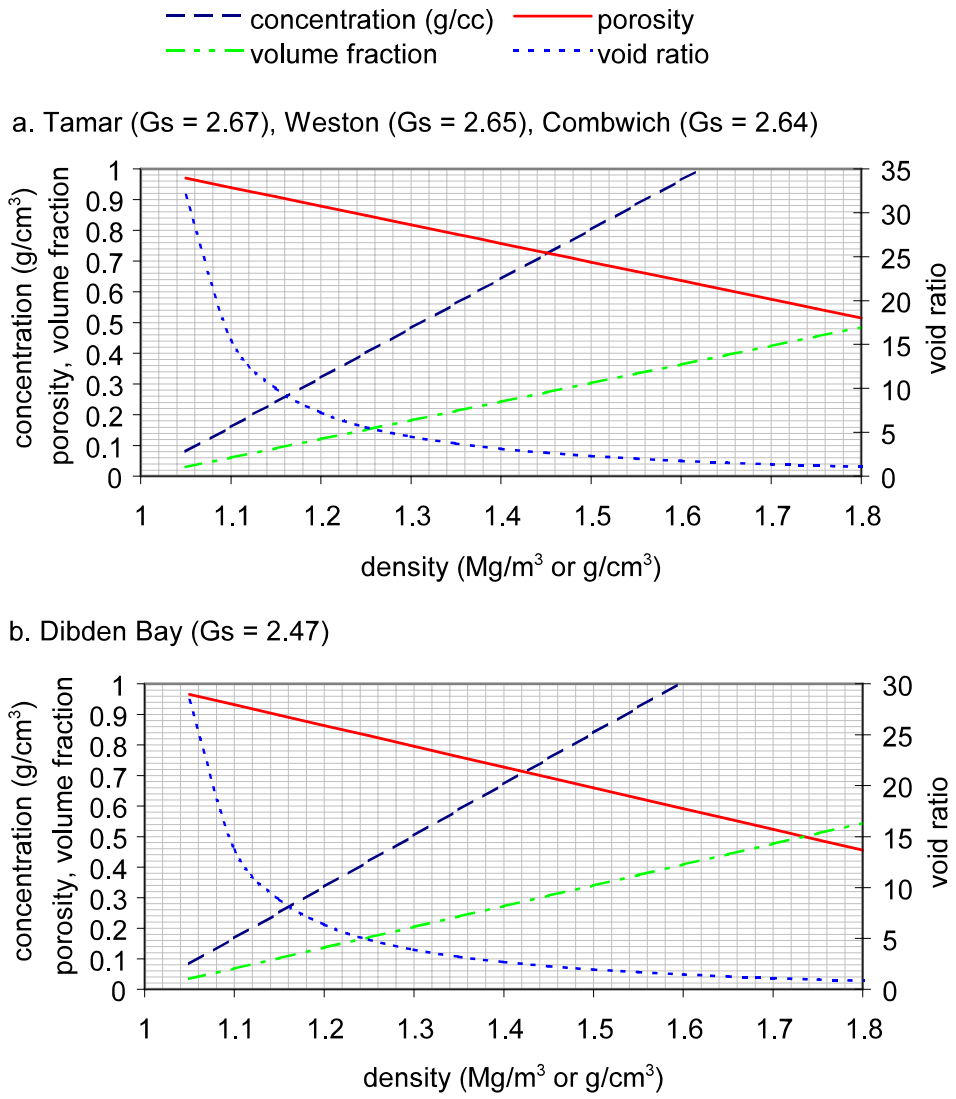

Figure 3.4 Conversion charts for various measures of concentration.

Chapter 4 Flocculation Characteristics

4.1 Introduction

This chapter describes the general floc properties and behaviours. Floc images have been converted into useful measures such as floc size, shape, orientation, and excess density. The development of flocs under increasing shear forces and concentration is examined. The data shown in this chapter are used in the forthcoming chapters to show how floc properties extend into the bed.

Flocs measured in laboratories, or *in situ*, usually show a wide range of characteristics within a single sample for any given parameter (see for example Dyer 1985; Manning 2001). Because of this enormous variability, it is ineffective to describe the properties of the raw data. A number of techniques are used in the literature to extract the most useful floc data. These include: plotting all of the data as it is initially calculated, fitting a best fit curve based on the set of data, fitting a curve based on theory or past experience, binning the data into subsets and then analysing these subsets

In addition to these, several other statistical techniques are introduced in this chapter to produce meaningful floc measurements from inherently highly variable data. These techniques are described below.

4.2 Overall floc characteristics

Size and shape

Photographic negatives of typical floc images are shown in Figure 4.1. Flocs come in a variety of shapes. A high proportion are elongated with the major axis generally 1.1 to 2.0 times the length of the minor axis (Figure 4.1c). Less often they are in the form of stringers, that is they are very much elongated in their major length relative to their minor length (Figure 4.1b). The main floc is nearly always located at the bottom of these stringers, and a tail, probably consisting of biological exopolymer, contains smaller flocs. This variability in shape makes it difficult to define a floc size. Thus flocs are often reported in terms of their equivalent spherical diameters (ESDs), that is the diameter of the

sphere which contains the same volume as the floc image. This measure allows the determination of the volumetric relationships between flocs, and also allows calculations of density to be made. This method of standardising the sizes to a sphere, of course, leads to difficulties when interpreting the hydrodynamic properties of flocs. However it allows comparisons to be made with many other papers which use ESD, and it was agreed that it is the most appropriate method for reporting floc size for the COSINUS research[8]. The words 'floc size' and ESD are used interchangeably throughout this thesis.

One method to present floc sizes is to examine their distribution. Figure 4.2 shows floc size distributions on a familiar grainsize distribution chart for experiment dbd3, on Dibden Bay mud. For various reasons, described in Chapter 2, the imaging and analysis methods do not account for flocs smaller than around 25 μm, and this explains the cutoff at the lower end of the figure. However, flocs sizes smaller than this are not likely to contribute greatly to estuarine sedimentation masses. It is apparent that as the experiment progresses in time the floc sizes become larger, that is the distribution shifts towards the right for all floc sizes. As well as becoming larger overall, their distribution changes so that a higher percentage are contained within the larger floc sizes- The 70^{th} to 90^{th} percentiles increase relatively more than the smaller floc sizes.

This plot also shows the distribution of the disaggregated Dibden mud with organic material removed, as measured with Sedigraph 5100 x-ray particle sizer. It is seen that, except for the region between 95% and 100%, the flocs are significantly larger than the primary particles. A second particle size analysis undertaken without the removal of organic content gave a similar size (around 3 μm) for the median particle diameter. For points less than 50%, the points lay below the distribution shown for the non organic material- ie. there were fewer small particles in the material with organic matter included, as might be expected since organic material helps to bind particles. For percentages greater than 50%, the organic material had a slightly smaller grainsize than the non organic

[8]This decision was made at the meeting of the EU MAST 3 COSINUS participants in Copenhagen, 1999.

material. For the purposes of this thesis the grainsize analyses of the primary particles, including organic material and not including organic material, are relatively similar and the small particle sizes, as compared to those in the experiment clearly indicate that flocculation is taking place in the experiment.

Orientation, eccentricity and sphericity

Three interesting measures of the floc properties are orientation, eccentricity and sphericity. Orientation refers to the direction of the long axis in degrees from the horizontal, 0° represents a horizontal direction and 90° represents a vertical direction. Flocs usually orient themselves with the long axis in a vertical direction, and less often with the long axis in any other direction. Figure 4.3, as an example, shows a summation of the floc orientations for 10 random images in experiment cos17. The angles have been binned at 15 degree intervals. In this case there are nearly twice as many flocs oriented vertically (bins centred at 90° and -90°) than those oriented horizontally (centred at 15° and -15°). Single images have similar distributions of floc orientations, though with more variation. For flocs with equal major and minor axis lengths (ie. rounded) flocs, Matlab records the orientation as zero. A large number of flocs that fit this category, of no orientation, have been removed from this figure, since their presence would falsely indicate that many flocs are horizontally oriented.

Figure 4.4a shows the relationship between ESD and floc orientation for experiment cos17. The round flocs have not been removed from this figure, and therefore contribute to the data at 0°. This figure serves to show the difficulty of plotting a large number of measurements for this inherently variable data and sets the stage to introduce the statistical method of kernal density estimation or kde.

Probability density calculations provide a method of showing the density of the datapoints on a XY scattergraph. Thus, in a large set of data it provides a method to look at where the probability levels are for the points, and to allows the less probable points to be disregarded. The data from Figure 4.4a is replotted in Figure 4.4b, after having applied the

kde calculations. Matlab is used as the front end for applying these techniques with a user interface designed by Beardah and Baxter of The Nottingham Trent University, which has been modified for this research. This, and all of the following kde plots are calculated using a bivariate normal probability density function, with a grid interval of 1/64th of the difference between the maximum and minimum data points (on both axes). Figure 4.4b is a smoothed 2D surface plot, which represents all of the data using differential shading. The figure shows the probability density at the 10^{th}, 30^{th}, 50^{th} and 70^{th}, 90^{th} and 95^{th} percentiles. That is, 10 percent of the data points are contained in the innermost region and 95 percent of the datapoints are located in the outermost region.

Figure 4.4a shows that the flocs exist at all sizes throughout the orientations (or vice versa), and indicates that the larger flocs are likely to exist in areas surrounding -90° to +90° and 0°. Figure 4.4b provides more information about the data. First, it tells us that 50 percent of the datapoints lie below a size of 100 μm. It also reveals that these smaller flocs have a similar distribution to the large flocs (surrounding -90° to +90° and 0°), except that they are more dense at 90° and -90° than they are at 0.

This can be compared to a similar plot for all of the floc measurements in experiment dbd3, which used Dibden Bay rather than Tamar mud (Figure 4.5). Again, the kde probability plot in Figure 4.5 shows that a majority of the flocs lie in the areas surrounding 0° and ±90°. In this case, the smaller flocs are distributed rather evenly around these points. However, the larger flocs quite clearly do not exist at 0°, indicating that the large flocs have a mainly vertical orientation in the Dibden Bay experiment. Since the sedimentation rates are similar for the two experiments, the difference in floc orientations must be a property of the mud.

The floc eccentricity, as calculated by Matlab, is the ratio of the distance between the foci of the ellipse and its major axis length. For eccentricity, 0 and 1 are degenerate cases; an ellipse whose eccentricity is 0 is actually a circle, while an ellipse whose eccentricity is 1 is a line segment. Sphericity is the minor axis length divided by the major axis length. A

sphericity value of 1 represents rounded flocs, and as the flocs elongate the sphericity value approaches zero. Thus sphericity and eccentricity show the same features, but are inversely related. As pointed out earlier, the images in Figure 4.1 show that the flocs sometimes have elongated forms, the most extreme case shown in Figure 4.1b as a linear stringer.

Eccentricity data for the first 500 images of experiment dbd1 are shown in Figure 4.6. In this figure, some 5000 flocs have been binned into 40 distinct eccentricity levels. The resulting histogram is two-tailed. The largest number of flocs occurs in the bin surrounding 0. That is, a large number of the flocs are round. However, the majority of flocs, overall, are contained in the asymmetric peak from around 0.5 to 0.9. Very few flocs are found at lower eccentricities. This corresponds to the major axis of a floc being approximately 1.2 to 2 times longer than the minor axis. The large peaks at certain eccentricity bins in the histogram may be caused by the image analysis calculations which enhance common pixel configurations, but this remains under investigation.

Figure 4.7 shows the eccentricity data for experiment cos17 at the beginning (a) and throughout the experiment (b). In this case the vertical axis shows the fraction of flocs at each eccentricity level. The distributions are broadly similar in both plots. A slightly lower proportion of flocs are contributing to the peaks on the right hand side of the Figure 4.7 b, due to a doubling of round flocs in that same figure. That is, initially the flocs are slightly more elongated, but as the experiment progresses they become more rounded.

Figure 4.8 shows the relationship between ESD and eccentricity for the same dbd1 flocs that were shown in Figure 4.6. It seems from this figure that smaller flocs (around 50μm) may span the entire range of eccentricities, although larger flocs are more restricted to higher eccentricities. This is the same pattern in all experiments. As already discussed (Chapter 1), and shown later, larger flocs are expected to be less dense and weaker than small flocs. Therefore it seems reasonable that larger flocs are more likely to elongate due to viscosity (frictional) forces acting on them as they settle.

Effect of turbulence on floc size

Experiment cos5 examined the variability of floc properties under different sedimentation rates, and under turbulent conditions. The experiment consisted of a series of stages in which the mud concentration in the column was slowly increased and then, at the higher concentration, turbulence was added using (compressed) air bubbles discharged approximately half way up the column. The results are shown in Figure 4.9, which shows mean floc size against number concentration. The images under conditions of higher initial concentrations ( ) clearly show a larger mean floc size, as compared to those under more diluted concentrations (- and >). The changes in number concentration are less distinguishable in this figure. The effect of concentration on floc size is examined in the next section. Adding turbulence to the column ( ) apparently breaks apart the flocs, causing their equivalent diameters to decrease and their numbers to increase. Originally it was intended that adding turbulence to the column by this method would enhance flocculation, however the turbulence level was too great, and caused the flocs to tear apart.

4.3 Concentration

Sediment concentration is often considered to be the single most important physical property controlling flocculation. Higher concentrations lead to higher collision rates. These collisions may either enhance or destroy existent flocs, depending on the collision energy and floc strength.

Figure 4.10 shows the floc size distributions of mud particles in the column over the first 11 hours of sedimentation for experiment dbd1. The thin lines on the figure represent different percentile levels, that is the sizes at which a certain percent of the flocs are smaller. The thick line shows the mean ESD. These data have been averaged over twenty images to eliminate scatter. As the concentration of slurry in the column increases, the size of the flocs increase.

Figure 4.11 shows the floc size distribution for the entire duration of dbd3. The rate of sediment introduction into the column for this experiment was increased gradually over

time. This is shown as the top series of points (x) and right axis in the Figure. It is calculated by the volume of initial slurry (of known concentration) being introduced to the top of the column. The curves generated for concentration and floc sizes conveniently show good fits to the logarithm of time. Thus the various size percentiles give equations in the form:

$$size_{perc} = m \cdot \ln(time) + i \quad (4.1)$$

where $size_{perc}$ is the percentage of flocs below 'size', t is time, and i is a constant. Sedimentation rate versus time gives roughly the same form of equation. The ESD and sedimentation rate equations can be combined to give ESD_{perc} values at increasing sedimentation rates. These are plotted in Figure 4.12. A slice through the various percentiles at any given sedimentation rate provides the data needed to construct a floc size distribution curve at that sedimentation rate. This information could be particularly useful to estuarine or dredge disposal modelers, who often know the rate at which sediment is added to the estuary. Ultimately it is the floc sizes, and the development and destruction of flocs, which control estuarine sedimentation patterns, so such a correlation between input sedimentation rates and floc size distributions may be extremely useful. The importance of being able to predict particle size spectra for an estuary is emphasised by van Leussen (1988). This relationship would be unique for each mud and water type.

4.4 Settling velocity and hindered settling

Settling velocities are measured using one of two methods described in Chapter 2. Figure 4.13 shows settling velocities of the flocs plotted against their equivalent spherical diameters. These have been calculated for a number of random images by the first method, in which the flocs are selected by a user. Overall, in this figure, larger flocs have faster settling velocities. The large settling flocs displace water which carries small flocs upward (negative settling velocities in the figure). The fastest floc observed in the Dibden experiments (and happens to be shown in this figure) settled at up to 2950µm/s, or 255 m/day. By using an image sequence at one second intervals it would not be possible to measure flocs settling faster much than this, since they would pass through the field of

view too quickly. The majority of flocs settled at velocities between 0 and 600 μm/s, or 52 m/day. These are well within ranges observed in natural coastal areas of 2 to 360 m/day.

When automated settling velocity analysis is used a much larger number of images is processed, although the number of flocs tracked in each image might be less than in the GUI approach. Figure 4.14a is a randomly selected movie frame (binarised), overlayed by a quiver plot of the velocity vectors. By comparing the velocity vectors to the original movie, it is apparent that the tracking software has performed extremely well. There are a few exceptions worth pointing out. Generally in this movie the flocs are moving downward and leftward. The smaller flocs have a relatively larger left component than the larger flocs. Two velocity vectors (a and b) indicate upward movement. These are incorrect, and arise from (a) the floc becoming obscured during the movie as a larger floc passes over it and (b) a floc appearing from behind a larger floc at some time during the movie. The floc indicated by (c) is verging on the illuminated laser sheet, and is therefore very faint. At a point several frames into the movie the binarising method causes this very faint floc to appear as two, thus two velocity vectors. The erosion - dilation technique described in Chapter 2 failed to join these two halves together due to the large size of the apparent void separating the two halves. Fine-tuning of these particle tracking algorithms is beyond the scope of this thesis, and at any rate is not required since nearly all the floc velocities are represented accurately.

A plot showing all of the settling data throughout experiment dbd1 is shown in Figure 4.15a. It is not at all obvious, from the plots of ESD vs. settling velocity throughout an entire experiment that there is a relationship between the two. Any relationship, if it exists, is obscured by the high density of datapoints combined with the large variation inherent in floc data. The data has been replotted in Figure 4.15b, using the probability density method; this figure includes boundaries for the 30^{th}, 50^{th}, 70^{th}, 80^{th} and 90^{th} percentiles, from the inside out. It shows that the majority of data (within the 50^{th} percentile) lies in a small area with diameters less than 90 μm and the velocities in the range -20 to 100 μm/s, a feature which is not obvious in the top plot. This dense portion of the data has a shape

similar to that in Figure 4.13.

Overall there is a slight positive relationship between ESD and settling velocity. This is more apparent in Figure 4.13 then it is in Figure 4.15. It is often assumed that there is a power-law relationship between ESD and settling velocity, since this is the case for the Stokes settling equation:

$$w_f = \frac{D_f^2(\rho_f - \rho_w)g}{18\mu} \tag{4.2}$$

w_f is the floc settling velocity, D_f is the equivalent spherical diameter of the floc, ρ_f, and ρ_w are the densities of the floc and the water, and μ is the viscosity of the water. Figure 4.17 examines this for a set of dbd1 floc measurements, using both an exponential fit and a straight line fit. For these data it is not possible to assume that any particular type of curve fits this data better than any other, and in fact a linear fit gives a slightly better regression coefficient than an exponential one (though both are poor). Figure 4.16 presents the slope of a straight line relationship between ESD and settling velocity for each of the image sequences throughout the first 24 hours of experiment dbd1. The darker coloured points in the centre of the plot represent an average over 5 samples. A substantial majority of these slopes are positive indicating that there is a clear relationship between settling velocity and ESD at most times during this period, particularly in the very initial stages where the slopes are greatest. This relationship levels out somewhat as the concentration in the column increases. After the first day (not shown) the data becomes very highly scattered, although the interval averaged slopes remain positive.

This graph is probably showing the onset of hindered settling. In the initial stages of the experiment, when the column concentration is relatively low, the calculated straight line relationship between ESD and settling velocity give high slopes, that is large flocs settle considerably faster than small flocs. As the column concentration increases over the first 5 hours these slopes are reduced quite significantly indicating that there is, by this point, little difference between the settling rates of large and small flocs. The slope continues to reduce

throughout the first day. The increased scatter that occurs after the first day may be a consequence of the complete breakdown of this relationship, but it may also be due in some part to turbulence or of reduced visibility to the camera.

The observation that hindered settling is taking place is supported by a plot of settling velocity against time (Figure 4.18). Here again, the percentiles for settling velocity are shown. This is shown as a line plot, although the data is made up of distinct points, since it is much easier to follow than a scatter plot. The percentile lines show at first a slightly increasing settling velocity and then a decreasing velocity over the first day in experiment dbd1. Other experiments show the same pattern.

It is possible to calculate the interparticle distances between all particles, by using matrix operations on the centroid data. Figure 4.19 illustrates the use of Delaunay triangulation to represent the image as a series of triangles- the circles represent the floc centroids. Each floc has several lines linking it to its nearest neighbors. This type of analysis, unfortunately, does not account for the focal depth of an image which is less than 1mm. As a result the mean distances between flocs may be underestimated. Figure 4.20 examines the changes taking place in the settling velocities, interparticle distances and floc sizes during one of these hindered stages for experiment cos17. This experiment was carried out in several sedimentation stages, one of which was started just before 210 hours after the water had cleared from the previous sedimentation. A shift occurs suddenly in the settling velocity from 210 to 213 hours (Figure 4.20a). During this time the mean of the minimum distances between all the flocs in an image also decreases (Figure 4.20b). This is accompanied by a decrease in the mean floc size (Figure 4.20c), which it could be argued results from a higher number of collisions. Figure 4.20d examines this possibility, and indicates that the mean particle size does perhaps have a dependence on the mean minimum distance, measured from the centroids of each floc (not the distance between the floc surfaces).

Effect of floc shape on settling velocity

It might be expected that the settling velocity of a floc is affected by its shape or

'streamline' properties. Figures 4.21 and 4.22 show the floc eccentricities and orientations plotted against their settling velocity for experiment dbd3 on probability plots. As mentioned earlier the eccentricities lie either at 0 (round) or between 0.6 to 0.9. However the shape of the floc appears to have no influence whatsoever on settling velocity, which for all eccentricities is centred around 60 to 70 ：m/second.

It might also be expected that the floc orientation could affect settling velocity. Or, that the settling velocity might, in fact, alter the orientation of the floc. This is shown to be quite untrue in Figure 4.22, where the majority of the flocs are oriented vertically, but regardlesss of whether they are vertical or not the settling velocity remains centred, again, at about 60 to 70 ：m/sec.

The previous section paid attention to the calculation of settling velocity, since it is to be used for calculations in upcoming sections.

4.5 Excess Density

It is often convenient for modellers to use the concept of excess density, which is the difference between the floc bulk density and the water density (also referred to as differential density or density contrast). Generally excess density can be calculated by using the common Stokes' settling velocity equation (Equation 4.2). Excess density, D_e, is the bracketed term in this equation. This technique has been used by McCave (1975), Gibbs (1985a), Gibbs (1985b), Fennessy (1994), Al Ani (1991), Bache (1997), Manning (2001) and many other researchers. A number of assumptions must be made in order to use Stokes equation. First, it assumes that the particle is a solid - the equation in its original form used w_s rather than w_f. Theoretically and intuitively, at least, there are reasons to believe that highly porous flocs do not behave as solid material. Second, this equation leaves out the influence that floc shape might have. However, since no such influence is apparent in the data this assumption can be safely accepted. Third, the viscosity of the water is rarely known by researchers. It is usually taken to be unity, as it is in this thesis. Finally, Stokes derived this equation for use with particles of a Reynolds (Re) number of less than unity.

Very often this is not the case for flocs. A more detailed discussion of the use and misuse of this equation, along with examples from the current data, is presented next.

Primary particle density, ρ_p

Most often in the literature the density of the primary particle, ρ_p, is assumed to be equal to the dry density of the solid, ρ_s. However, Lee *et al.* (1996) point out that primary particles in a floc move together with bound water. Therefore ρ_p is a function of this bound water content and a lower limit can be calculated by the following equation:

$$\rho_p = \frac{1 + w_B}{1/\rho_s + w_B/\rho} \tag{4.3}$$

where w_B is the mass of bound water per mass of dried solid. The upper limit to ρ_p is the dried solid density ρ_s. Lee *et al.* provide no information on reasonable quantities for the ratio w_B. However a subsequent paper by Wu *et al.* (1998) gives a range of values for kaolin sludge of 0.5 to 5 $kg_{water}/kg_{drysolid}$.

In the current research, assuming a w_B of 5 $kg_{water}/kg_{drysolid}$, the lower limit for ρ_p would be calculated as 1.7 g/cm^3, whereas that for the upper limit (measured ρ_s) is 2.47 g/cm^3. This is a significant difference.

The bound water content for the current experiments is not known. Wu *et al.* (1998) point out that methods for determining the bound water content are highly inaccurate at low solids concentration (such as in the present experiments), so even if this quantity was measured its accuracy would be questionable. Therefore for this thesis the density and the porosity of the flocs are calculated using the known upper limit, ρ_s. This may have some (at least theoretical) error associated with it, but it is calculated from a certain upper limit of the primary particle density. Furthermore, this method is used in the majority of the literature on estuarine flocs and allows an uncomplicated comparison to those studies.

There are instances of particles composed of something more dense than the bulk solids

density. These may be mineral 'slivers', which not only settle faster than predicted by Stokes equation due to their density, but also due to their streamlined shapes. For instance, hornblende needles are known to occur in Tamar mud[9]. The contribution of these particles to the calculation of sedimentation properties may be safely ignored, since there are relatively few of them.

Permeability and S

The drag force on a highly-porous sphere is lower than that on a non-porous sphere, thus a correction factor S has been developed for Stokes' equation. Lee et al. (1996) and Wu and Lee (1998) investigate the calculation of permeability which is required for a subsequent calculation of S. Based on the work of Neale et al. (1973), and following the Brinkman model for a highly porous sphere moving through a medium under creeping flow, S is calculated as:

$$\Omega = \frac{2\beta^2[1 - \tanh\beta)/\beta]}{2\beta^2 + 3[1 - (\tanh\beta)/\beta]} \tag{4.4}$$

where

$$\beta = \frac{D_f}{2\sqrt{k}} \tag{4.5}$$

The floc permeability, k, can be calculated by a number of methods all using the primary particle size, D_p, and a function of porosity. So, this calculation also requires an estimate of the porosity. Unfortunately the calculation of porosity from the settling velocity can introduce its own errors, which will be carried through to calculation of the permeability.

Wu and Lee (1998) report that using S to correct the Stokes' equation is inadequate, since the available methods for the calculation of permeability, and thus of S, in creeping flow requires that the floc's Reynolds number is much less than 1. In fact, floc size and shape properties can cause the Reynolds number to be up to several tens, and the above correction

[9]Professor Keith Dyer, University of Plymouth, personal communication.

is not applied in this thesis.

Drag coefficient, C_D

When Re<1 the drag coefficient for a non-porous sphere, according to Stokes is governed by the relationship (Wu and Lee 1998):

$$C_D = 24 / \mathrm{Re} \tag{4.6}$$

For flocs whose Reynolds numbers are higher than unity a number of suggestions have been made which stray away from Stokes law. However Lee et al. (1996) report that, although seemingly erroneous, the results given by a form of Stoke's law (replacing 24 with another constant in the above equation) gives more reasonable results in some respects than more theoretical equations. In particular they report that, according to their computer models, fractal dimensions are appropriately reported, whereas effective density may be erroneous. In the absence of C_D values for flocs Winterwerp (1999) and references therein suggest the use of the equation:

$$C_D = \frac{24}{\mathrm{Re}}(1 + 0.15\,\mathrm{Re}^{0.687}) \tag{4.7}$$

However, as Winterwerp points out, this equation has been derived for non-cohesive sediment, for which it appears to match empirical data. Since highly-porous flocs are known to behave quite differently (at least in theory) this equation is also not utilised in the present work.

The discussion on how to correct for high Re numbers continues in the literature. Computer models have given highly variable results, often showing less reasonable values than the use of Stokes type relationships. To counteract the effects of high Re numbers Manning (2001) has used the Oseen Modification when Re>0.5 to correct the effective density for flocs in the Tamar Estuary:

The Re number is calculated with:

$$\mathrm{Re} = \frac{\rho_e D_f w}{u} \tag{4.8}$$

Where Δ_e is the effective density, D_f is the floc diameter, *w* is velocity and u is the molecular viscosity. If Re>0.5 then

$$\rho_e = \frac{\rho_e}{(1 + 0.1875\,\mathrm{Re})} \tag{4.9}$$

A review of the ongoing and complex debate about the effects of high Re numbers on highly-porous flocs is not suitable for this thesis. As much of this work, due to its funding and sampling area, was intended to parallel and compliment the work at Plymouth, the above modification has been applied to the present data at Re>0.5. Figure 4.25 shows the effect that this has on a sample set of data from experiment dbd3. This data comes from randomly selected images throughout the experiment. The 'incorrect' Stokes calculations for Re>0.5 are shown in the figure for comparison. Applying the Oseen correction to the flocs with higher Reynolds number, which incidently was most of the flocs, has caused the effective densities to decrease for those flocs and has also restricted the data to more closely approximate a log-log relationship. However, the general characteristics, and the calculated relationship, of the data in this plot are not altered a great deal. Again, it was decided that applying this correction, and thereby complicating the results, is not the best method forward for the present work. The large datasets available, however, would be useful for future examination of the questions raised above.

In order to calculate the excess density, Δ_e, of the floc Equation 4.1 is rearranged:

$$\rho_e = \rho_f - \rho_w = \frac{18 w_f \mu}{D^2 g} \tag{4.10}$$

This is slightly more complicated in the present experiments since the flocs are undergoing a two-phase flow. In this case the velocity of the fastest upward moving floc, and therefore approximate velocity of the water must be subtracted from the settling velocity of the floc being analysed. Since downward settling velocities are normally reported as positive the fastest upward moving floc, denoted w_{min}, is that with the lowest negative number. The equation is altered to:

$$\rho_e = \frac{18(w_f + |w_{\min}|)\mu}{D^2 g} \tag{4.11}$$

where w_{min}#0. A neutrally buoyant particle has an excess density of 0, whereas a spherical quartz particle has an excess density of 1600 kg/m^3. The effective densities of the flocs are plotted against their equivalent spherical diameters in Figure 4.23. In this figure, only a random selection of images from dbd3 has been selected for analysis. As has been confirmed in many other studies the effective densities of the flocs are noticeably reduced as they become larger. This has been mentioned previously, and is due to the ordered structure of the flocs. A kde plot of all of the images in the same experiment is shown in Figure 4.24. This also shows that, for the majority of flocs, the larger flocs are less dense than the smaller flocs, although once again, there is a large amount of variation.

4.6 Effects of salinity and pH

The effect of increased salinity on the floc structure was tested in experiments cos3, with a column water salinity of 0ppt and cos4, with a salinity of 10ppt. The higher salinity of experiment cos4 was expected to lead to larger flocs due to suppression of the electrical double layer. However, during the testing (and on subsequent investigations) it became apparent that the salt in the natural pore water of the mud slurry was being washed out into the mixing water, and the salinity of experiment cos3 was increasing. Flocculation is enhanced by increasing salinity up to a certain threshold, above which a further increase in salinity is believed to have no effect (eg. Krone 1962; Allersma *et al.* 1967). It is believed, in hindsight, that this threshold salinity was reached in experiment cos3. There is no method known that could flush the porewater salt from the soil without completely obliterating its natural marine properties. Therefore attempts to determine the effect of salinity were abandoned.

Experiments cos7 and cos8 used the same experimental setup, except that the settling column of cos8 was filled with water of a lower pH. This had the effect of making the flocs larger, between concentrations of 200 to 500 mg/l, than in the other experiments (Figure 4.26). This larger size, and absence of flocs in concentrations over 500 mg/l, may indicate that the larger flocs formed at low pH are weaker. This makes sense in flocculation theory, since below a certain pH (somewhere between 5.8 to 7.3) the negative charge on the plate

edge becomes positive. This promotes edge-face attraction, as the charges become opposite, resulting in an open card-house structure (Yariv and Cross 1979).

4.7 Conclusions

- Flocs in the lab closely resemble those seen *in situ*, in size, shape and settling velocity. The lab flocs are mainly elongated with the longer dimension oriented vertically. Some flocs appear as stringers.
- Flocculation efficiencies increase with increasing column concentration. This allows the flocs to become larger and initially to settle faster. The floc size distributions can be calculated for each of the different muds based only on column sediment concentration.
- Hindered settling is observed at a certain concentration.
- Effective density of the laboratory flocs match those of *in situ* flocs. Some theoretical equations specific to flocs (and not solid spheres) have been applied, although Stokes' law seems to give reasonable results which are comparable to other studies.
- Statistical techniques such as kernel density estimation allow important information to be extracted from large and highly variable floc data.

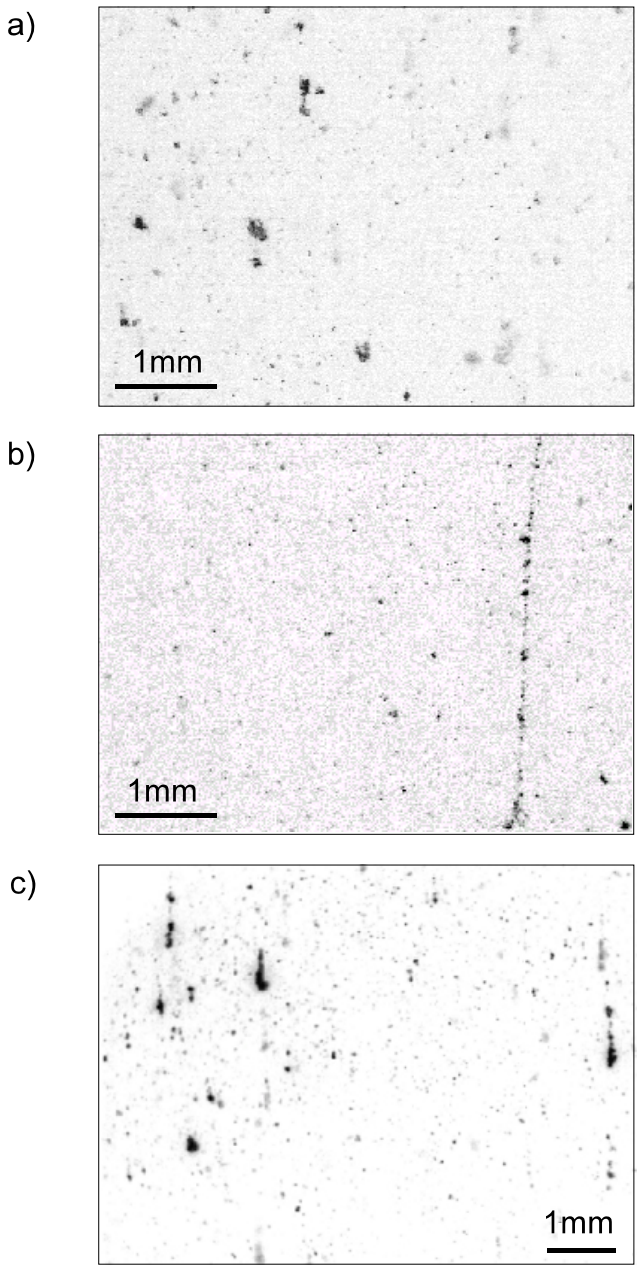

Figure 4.1 Typical images of flocs.

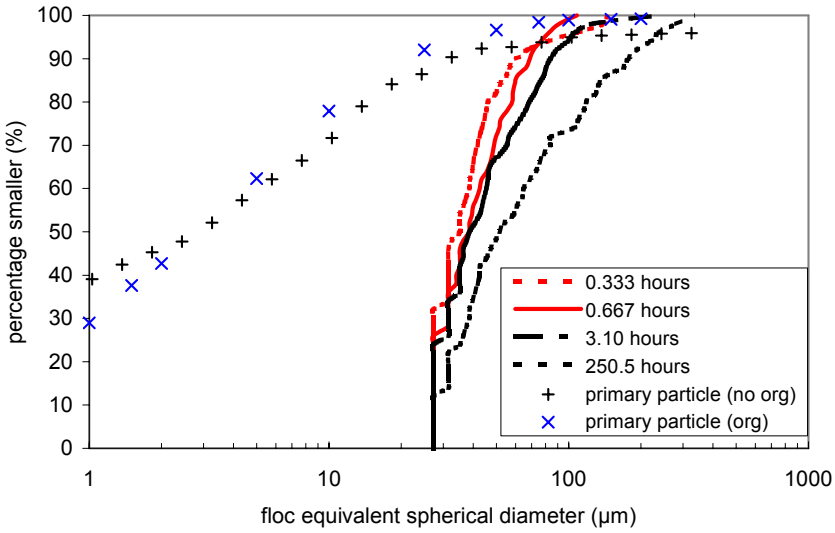

Figure 4.2 Development of floc size distributions throughout experiment dbd3, as concentrations in the column are increased. The vertical axis refers to the percentage of flocs below a given size.

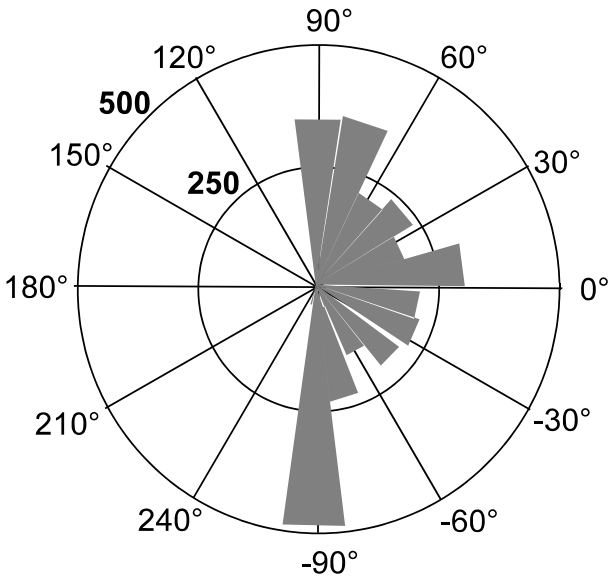

Figure 4.3 Floc orientations over 10 summed random images in experiment cos17. 0° is horizontal, 90° and -90° are vertical. The summed number of flocs is shown in bold.

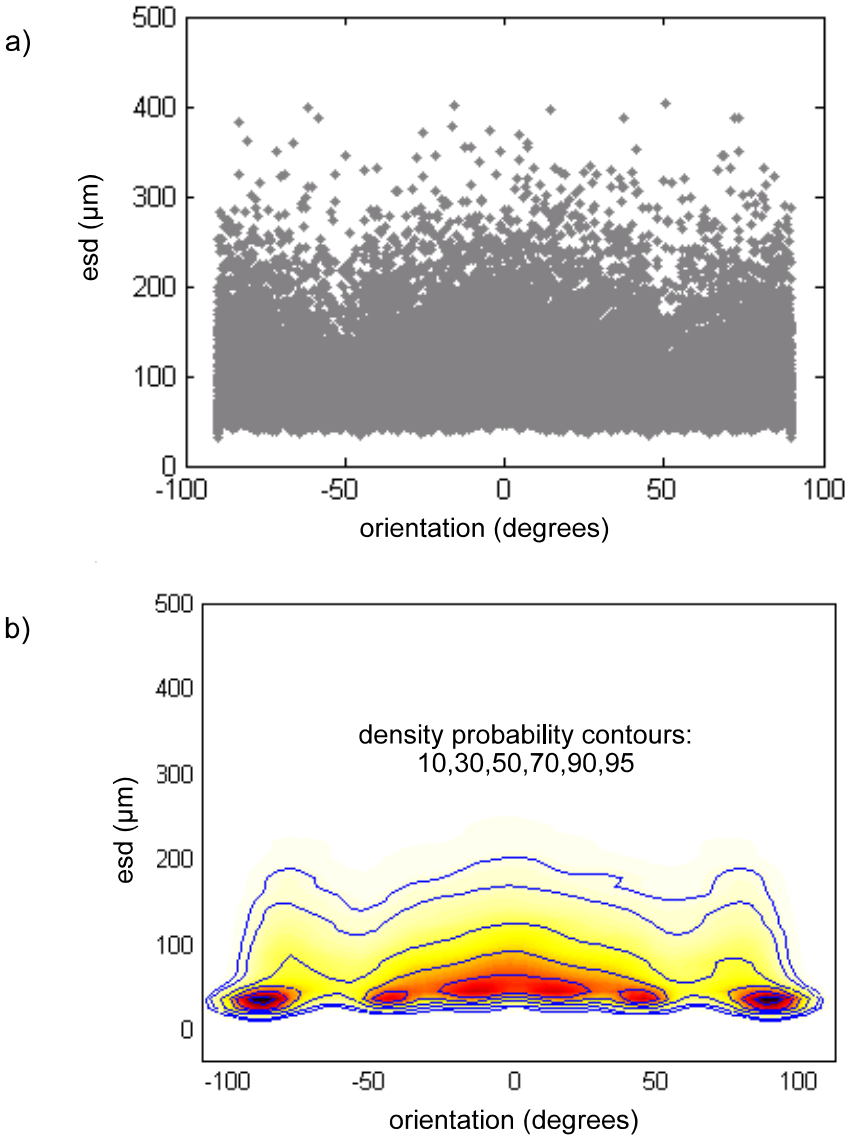

Figure 4.4 Esd vs orientation for experiment cos17. B. Probability density estimation for all flocs throughout the experiment. C. Probability density estimation for flocs at the start of the experiment.

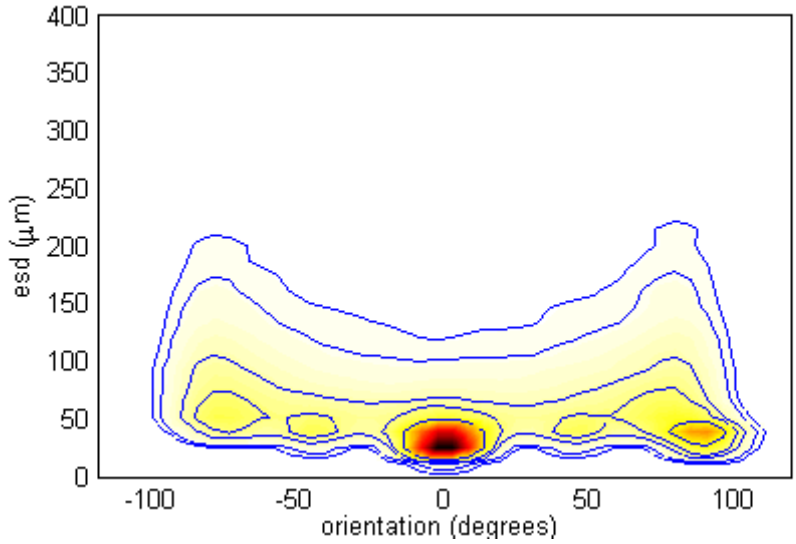

Figure 4.5 Floc orientations vs. ESD for experiment dbd3. The contours represent the density of the datapoints (several thousand in total).

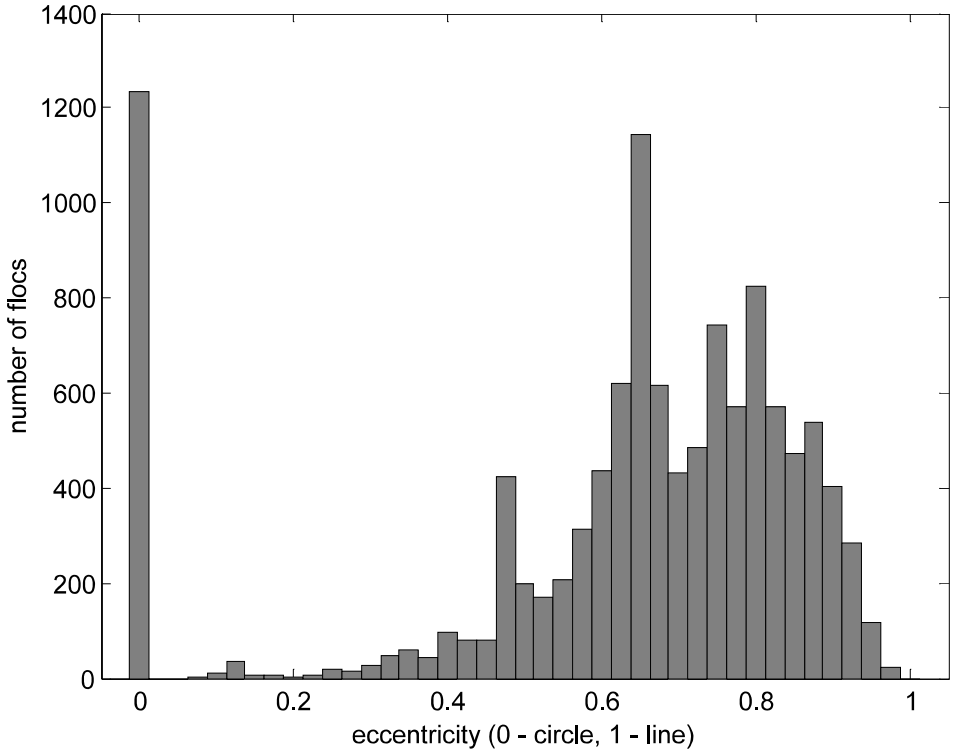

Figure 4.6 Histogram of floc eccentricities for the first 500 images in experiment dbd1.

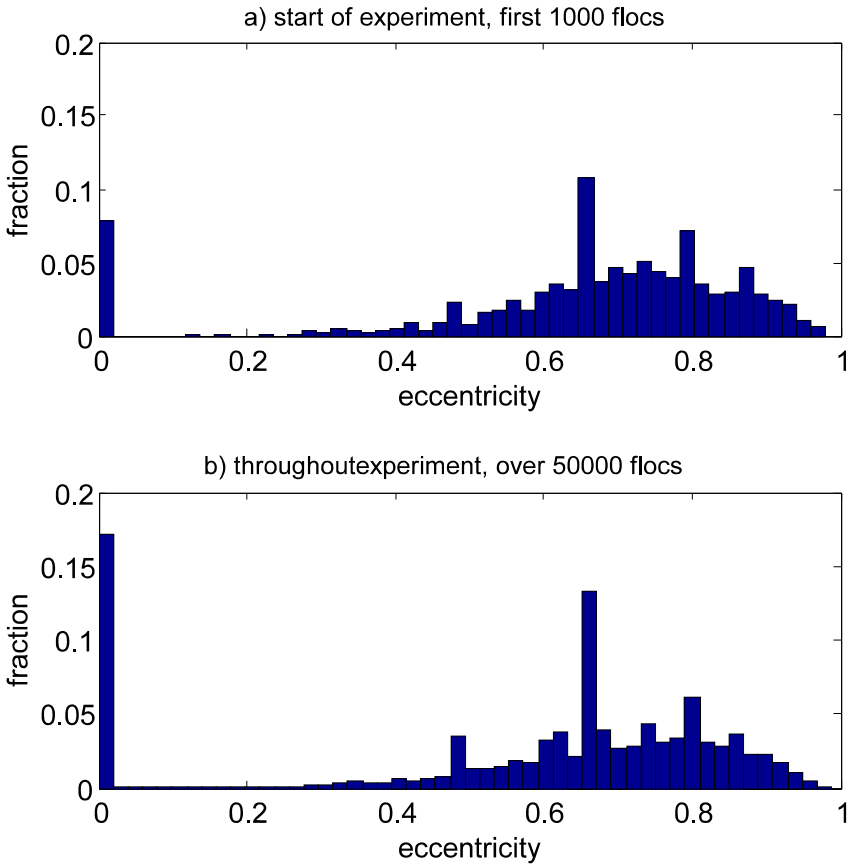

Figure 4.7 Distribution of floc eccentricities at a) start of experiment and b) throughout entire experiment.

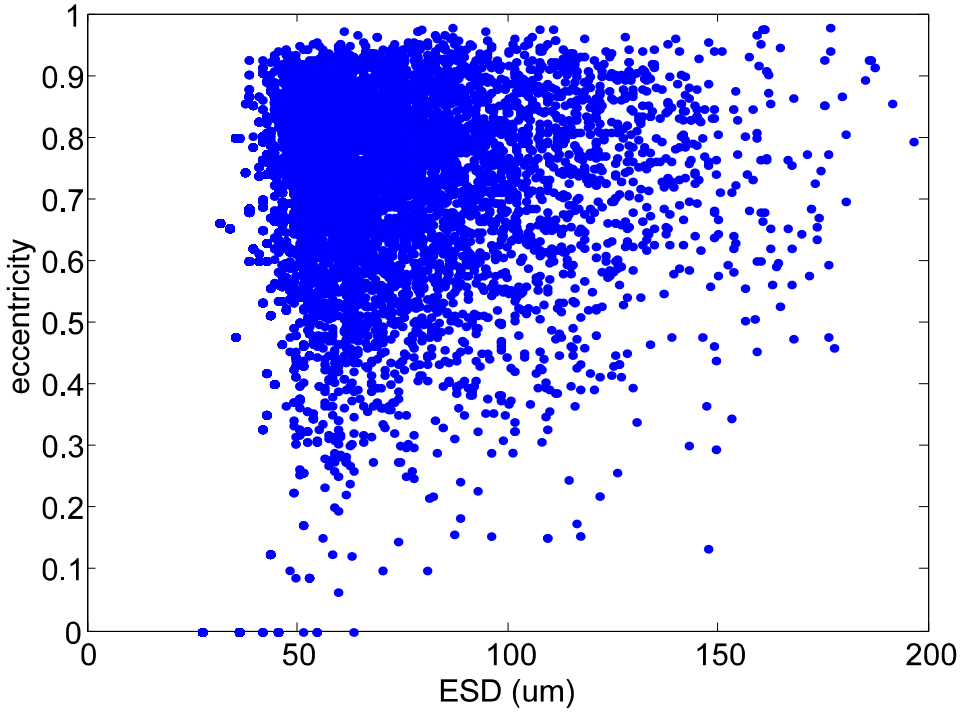

Figure 4.8 ESD vs. eccentricity for the first 500 images in experiment dbd1.

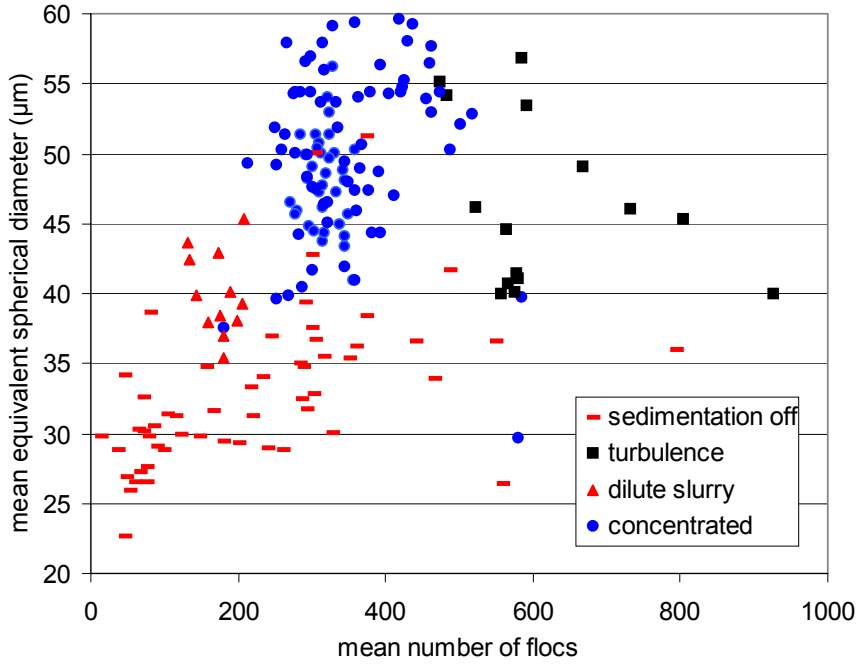

Figure 4.9 The effect of concentration and turbulence on floc sizes.

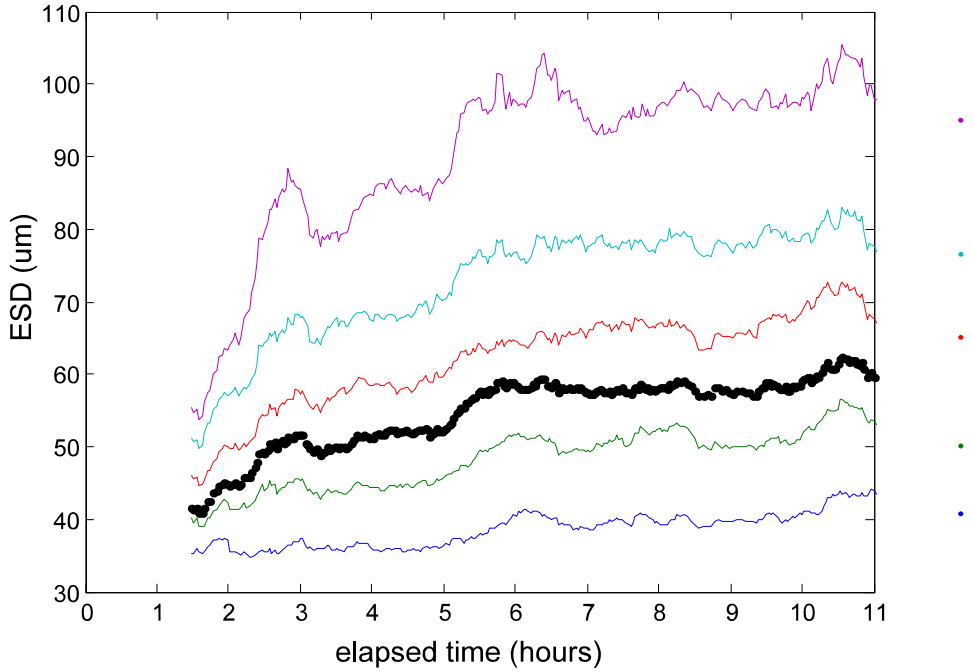

Figure 4.10 Development of floc size over first 11 hours of sedimentation for experiment dbd1. The thin lines, from bottom to top, show the 30th, 50th, 70th, 80th and 90th percentiles. The thick line is the mean ESD.

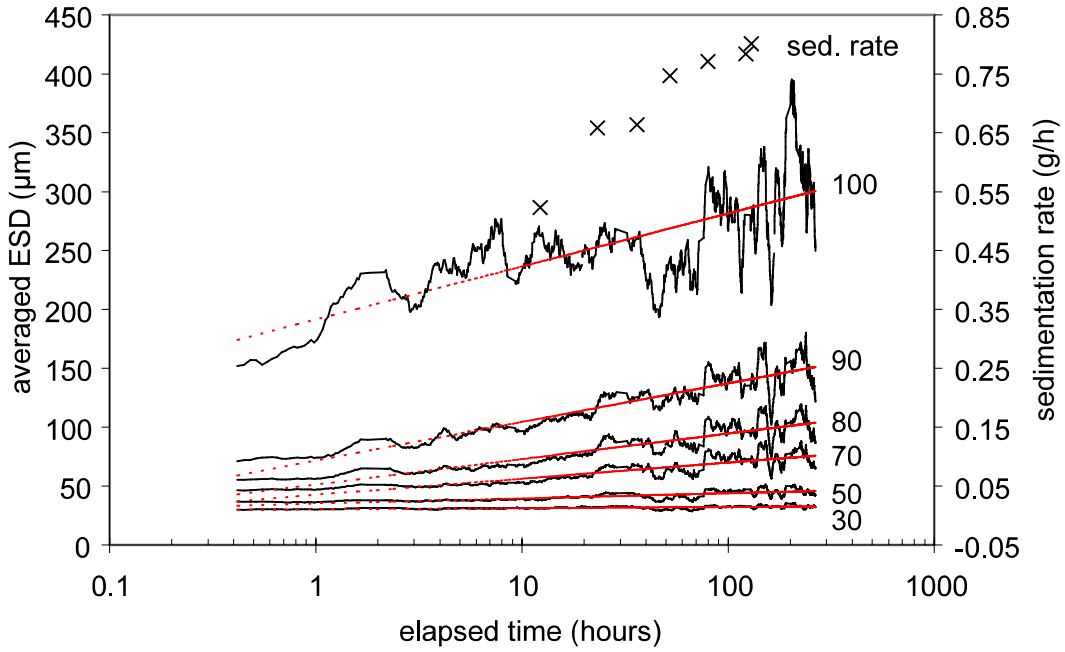

Figure 4.11 Time dependance of sedimentation rate, and of the 30th, 50th, 70th, 80th, 90th and 100th percentiles. To reduce scatter each datapoint is the mean of 20 images.

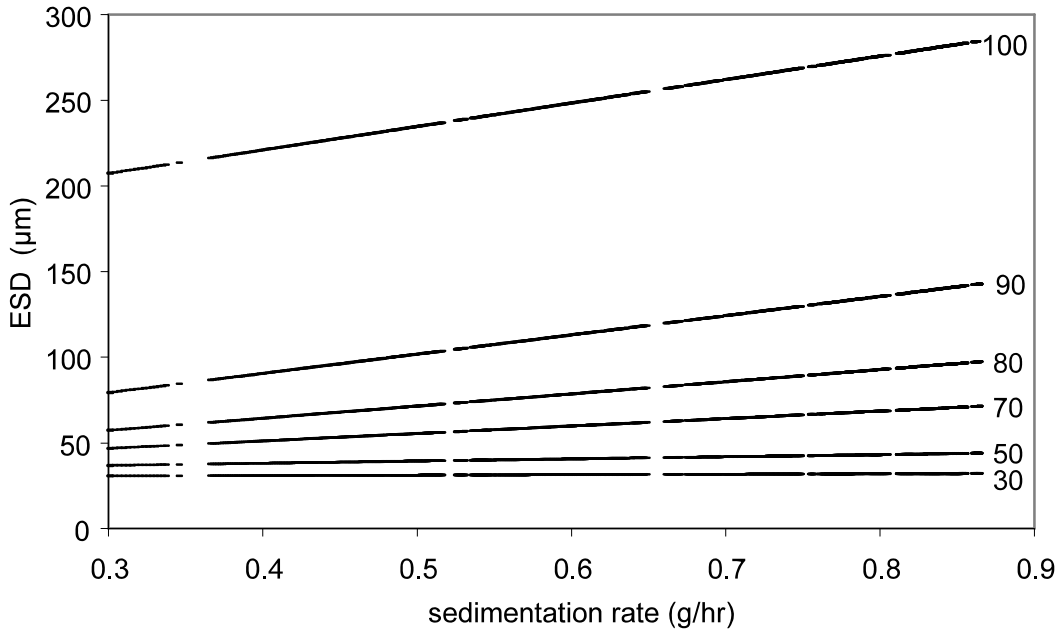

Figure 4.12 ESD vs. Sedimentation rate for 30th, 50th, 70th, 80th, 90th and 100th percentiles.

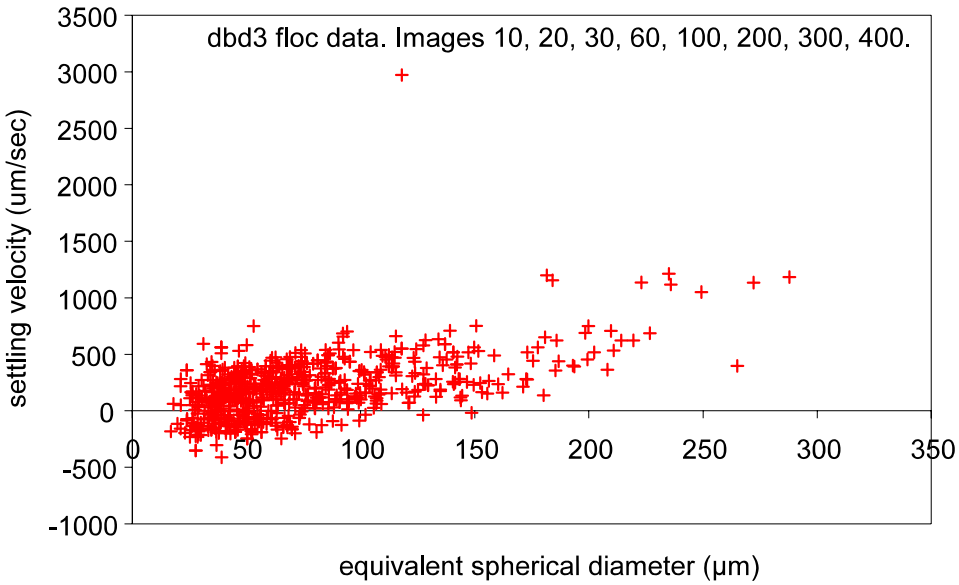

Figure 4.13 Equivalent spherical diameter vs. settling velocity for experiment dbd3. In the analysis each floc was selected by hand from random images.

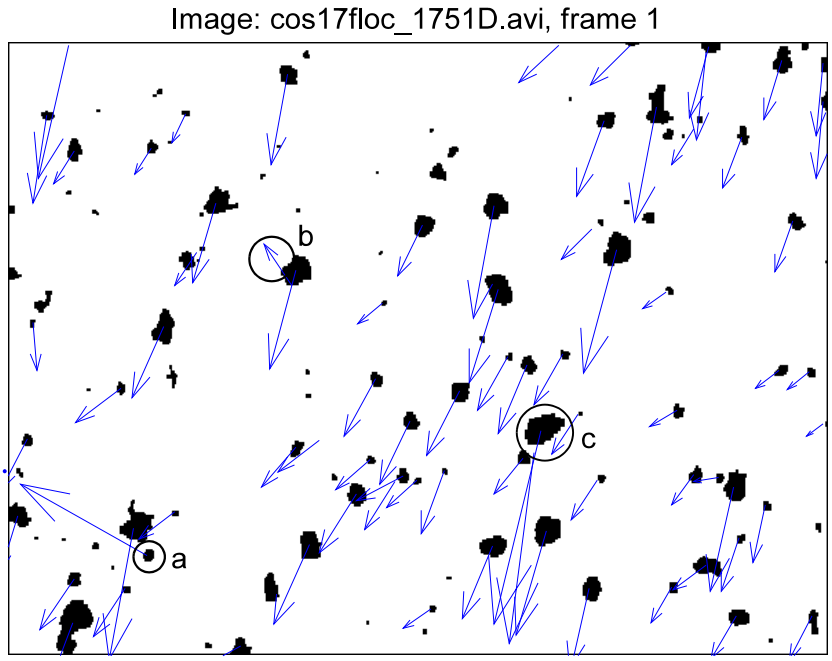

Figure 4.14 Result of automated tracking.

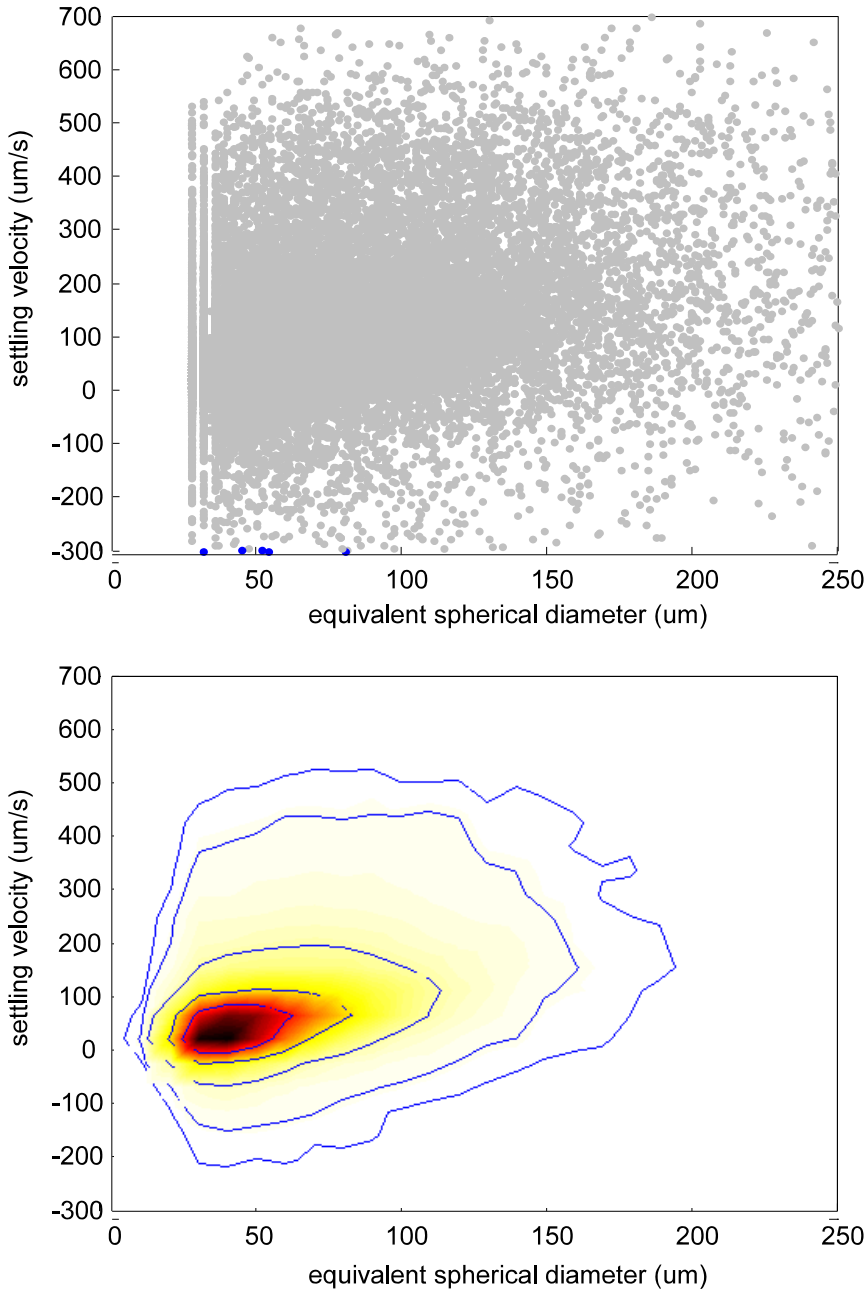

Figure 4.15 Equivalent spherical diameter vs. settling velocity for experiment dbd1. A shows floc velocities throughout the entire experiment calculated automatically. B shows the density of the datapoints in this plot, with 30th, 50th, 70th, 80th and 90th percentiles.

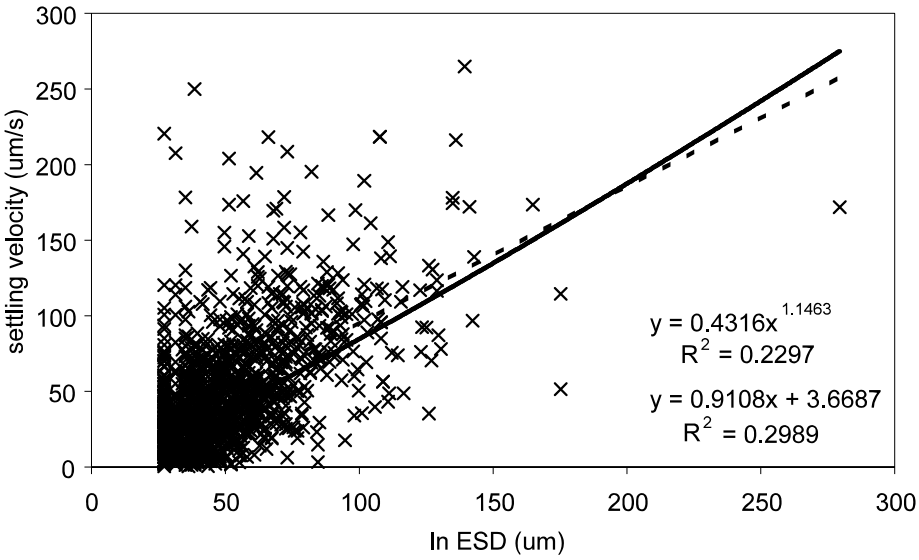

Figure 4.17 Exponential and linear fits to a set of dbd1 settling velocity data.

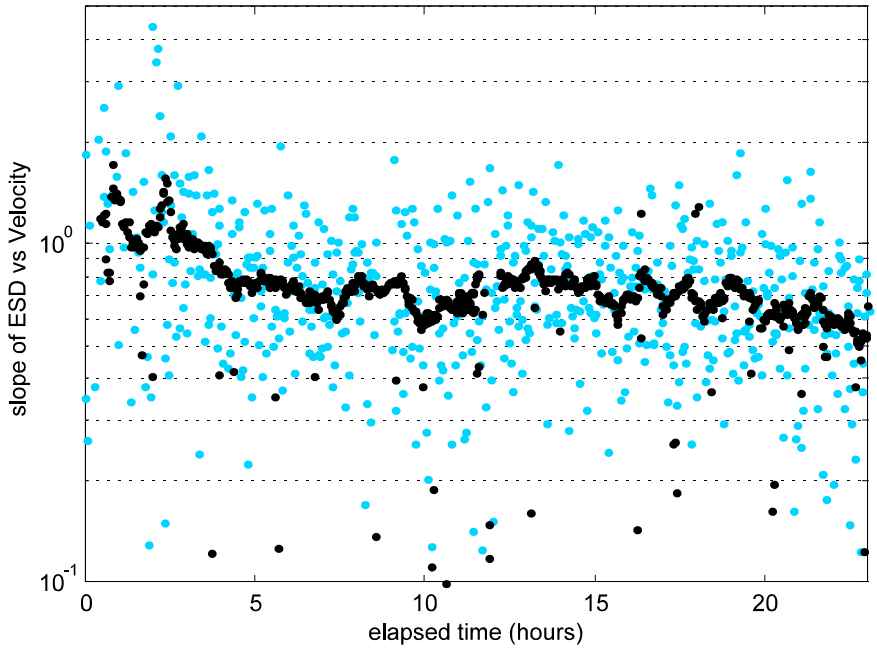

Figure 4.16 Slope calculated from a best fit straight line relationship between ESD and settling velocity during the first 24 hours of experiment dbd1. Darker points towards the centre represent an average over 5 samples.

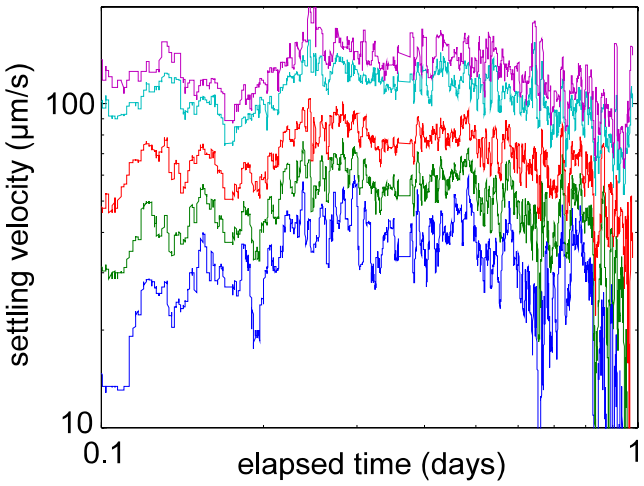

Figure 4.18 Settling velocity over the first day of experiment dbd1 showing the onset of hindered settling. Shown are percentiles (from bottom) 30, 50, 70, 90, 95.

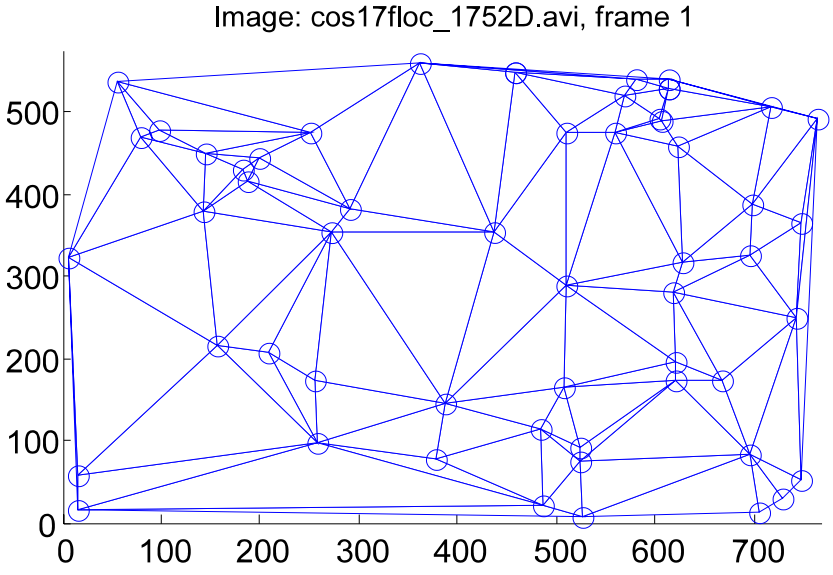

Figure 4.19 Delaunay triangulation, showing interfloc distances.

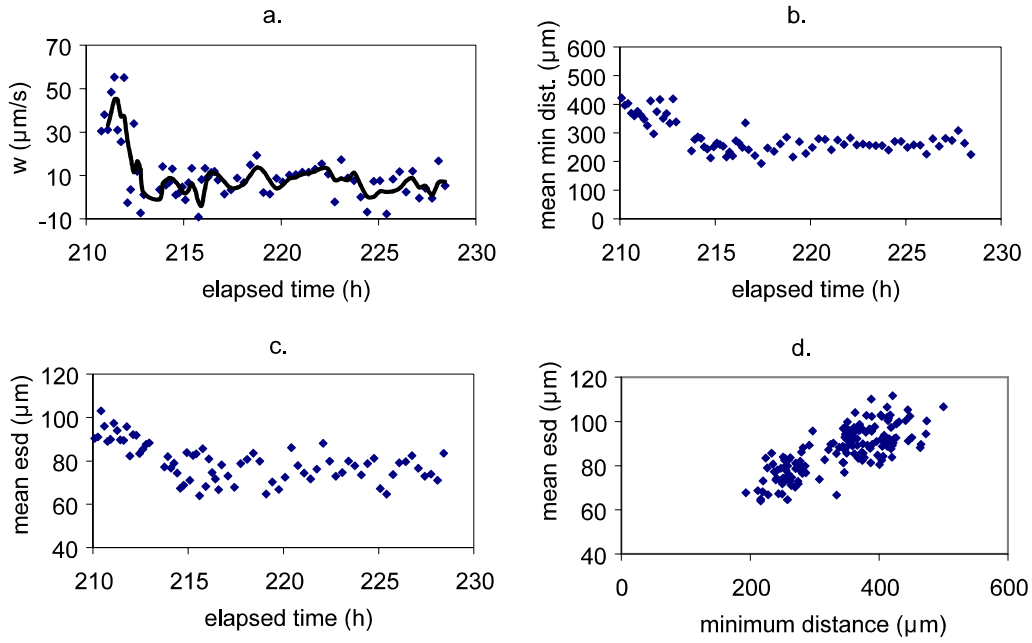

Figure 4.20 Onset of hindered settling, effect on settling velocity (a), minimum distance between flocs (b) and esd (c). Relationship between esd and minimum floc distance (d).

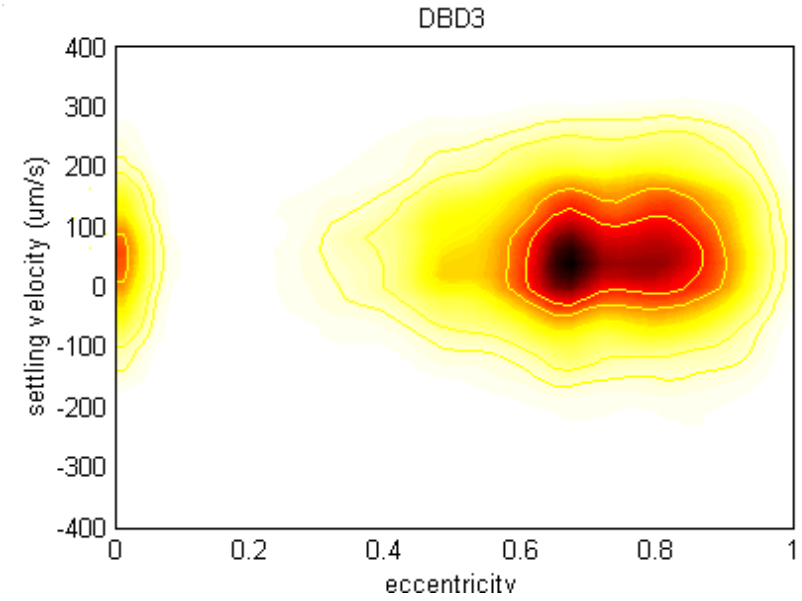

Figure 4.21 Floc eccentricity vs. settling velocity for experiment dbd3

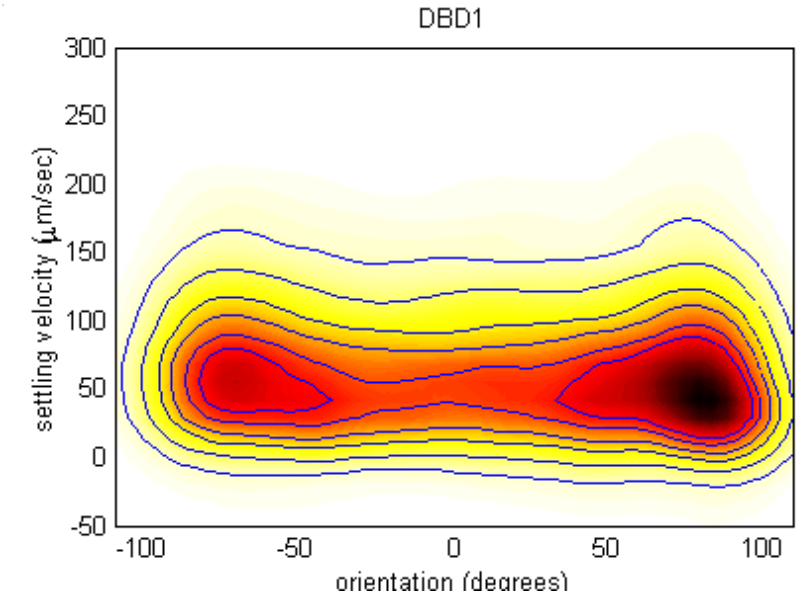

Figure 4.22 Floc orientation vs. settling velocity for experiment dbd1.

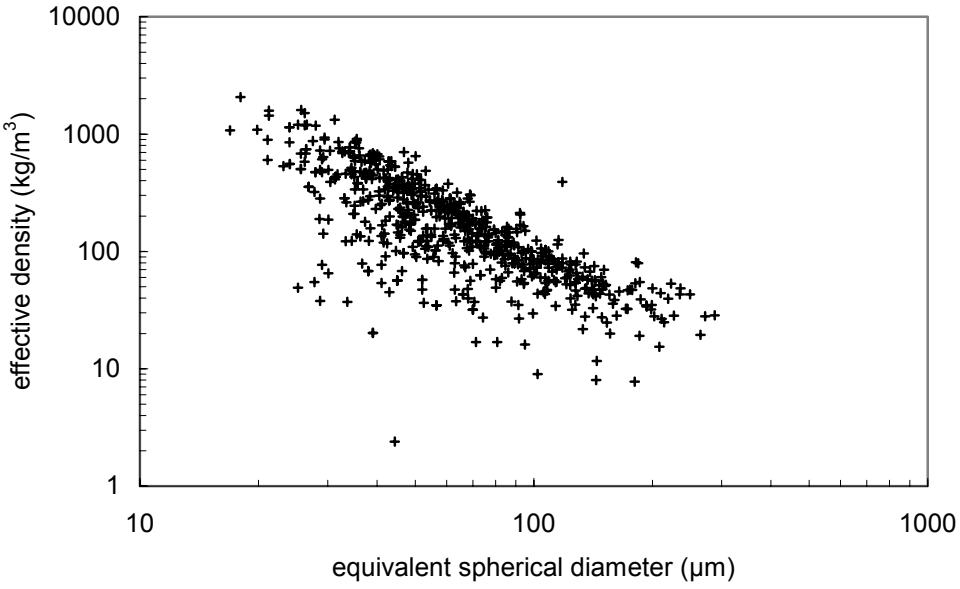

Figure 4.23 Effective density against size of flocs, calculated from a random selection of images for experiment dbd3.

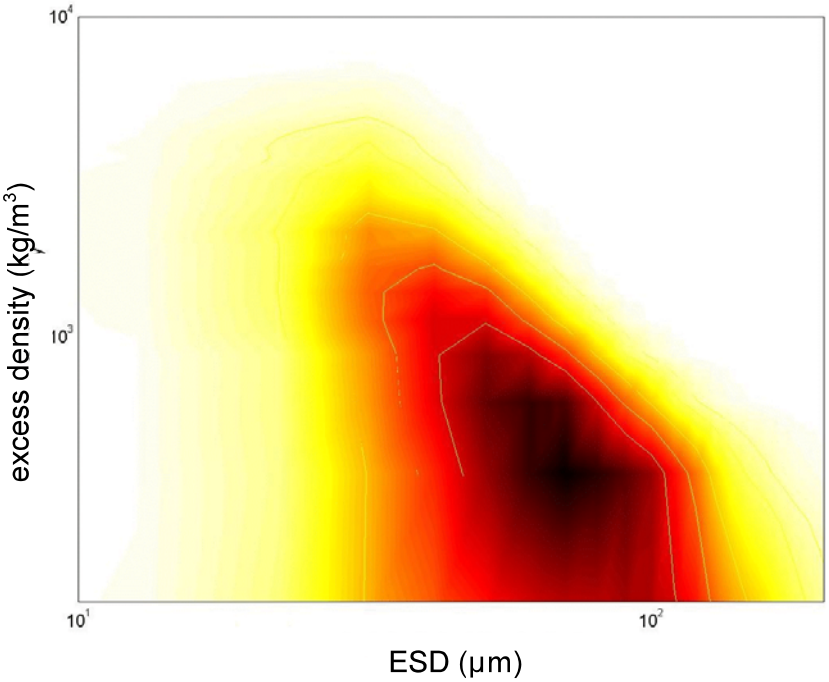

Figure 4.24 ESD versus excess density for all datapoints in experiment dbd3, shown as density probabilities.

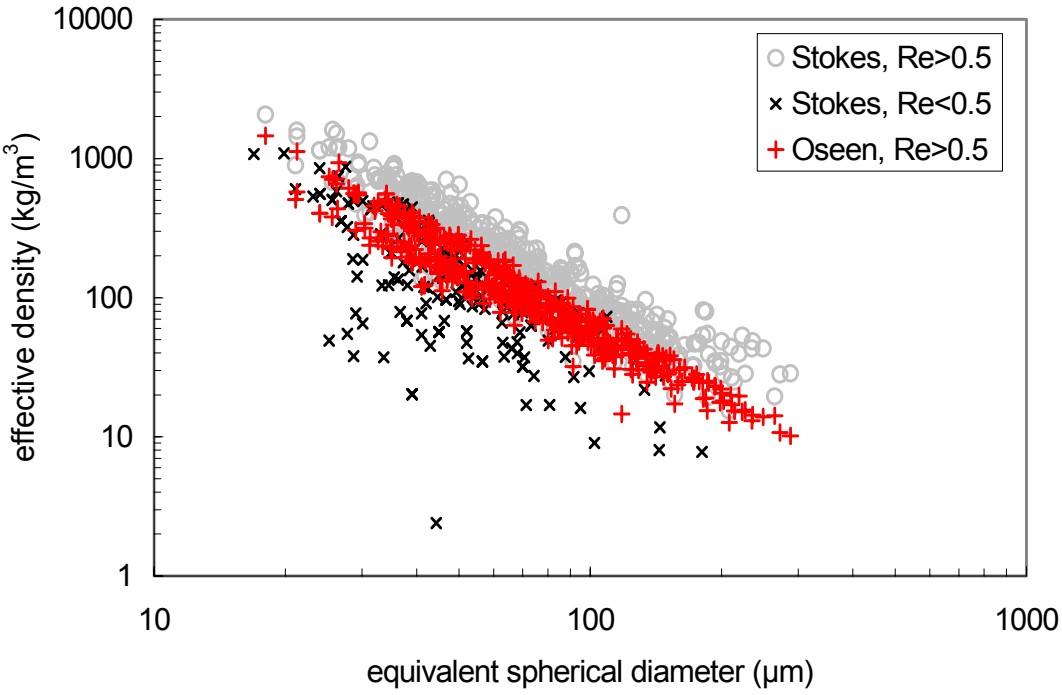

Figure 4.25 Calculation of effective density by using Stokes' equation, and by using the Oseen correction where Re>0.5

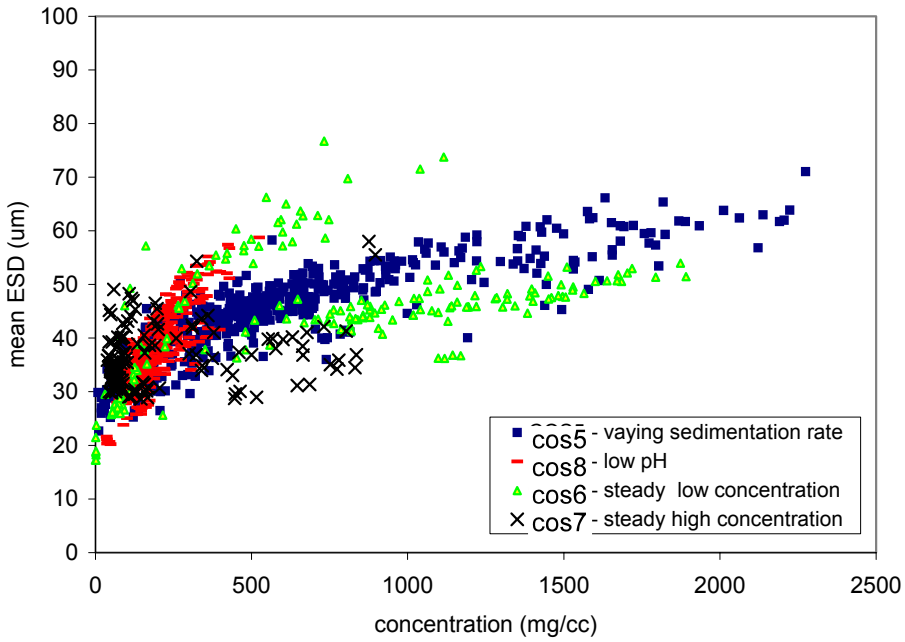

Figure 4.26 Variation in floc size versus concentration between experiments taken from randomly selected images.